DNA-mediated oxidation of transcription factor p53

Thesis by

Kathryn Nicole Schaefer

In Partial Fulfillment of the Requirements for the

Degree of Doctor of Philosophy

California Institute of Technology

Pasadena, California

2015

(Defended January 21, 2015)

ACKNOWLEDGEMENTS

I first and foremost thank Jackie Barton for allowing me to conduct my graduate research in her laboratory at the California Institute of Technology. I know that I had a lot to learn, and I had much room to grow, so thank you for your patience and helping to shape me into the significantly stronger person I am today.

I am also extremely grateful for my thesis committee for seeing me through this process. Doug Rees I thank for his unwavering positivity, support, and anecdotal stories about his experiences in academia that make you realize you aren't alone in your struggles. Harry Gray I thank for his continuous positivity. Harry not only made me feel like I could do great science, but that I did have creative and worthwhile ideas. I also have many thanks for Ray Deshaies for bringing a more biological perspective to my committee meetings, challenging questions, and new insights.

I have to sincerely thank Eric Stemp, the driving force that empowered me to continue on to graduate studies. I thank him for unwavering support, encouraging me to not be afraid of a challenge, pushing me outside of my comfort zone, and making me realize that the world wouldn't end if I did something wrong. Most of all, I have to thank him for being the person who saw my potential and adamantly wouldn't let me waste it, when I couldn't yet see it in myself.

My experience at Caltech would have not been the same without Mo Renta. Mo has always looked out for my well-being, constantly making sure that I knew that I was wanted here, that I deserved to be here, that I do not need to be distracted by my past, and that I can and will keep marching on. I also have many thanks for Alison Ross, our BMB coordinator, for her warmth and support.

Many thanks are due to the many amazing people in my life that have offered unconditional love and continual support throughout my time here at Caltech. I thank David Angel for constantly reminding me that there is a world outside of lab that is to be enjoyed, always being wholly understanding of the work I needed to do, and empowering me to continue when the going gets rough. Two of the most important people during my graduate experience at Caltech were Gwen Johnson and Taylor Lenton. These two ladies were the best housemates, friends, and support group anyone could ask for. Many thanks are deserved to our third housemate, Leia, my dog and source of unconditional love, joy, companionship, and sanity. Amanda Madison I thank for being my best friend, my second-half, and for always being able understand what I'm going through. I thank Felecia Hunt for her kindness and keen understanding of the undergraduate institution I came from, what a different world Caltech is, and how to make me feel included in my new community. I also sincerely thank Liz Shon for her patient ear, voice of reason, and unwavering support.

I thank my parents, Connie and Ron Schaefer, for always being there for me and excitedly supporting my education. Secretly I think Caltech was their plan for me all along, literally baptizing me into Caltech as a child when I fell into the lillypond. I also have immense gratitude for my second families, the Madisons and the Angels. I thank the Madisons for adopting me into their family and letting me know that there is nothing wrong with taking care of myself and finding happiness. I thank the Angels for their relentless support, positivity, and amazing home-cooked meals.

I sincerely thank all of my fellow Caltech labmates and friends, past and present, that have seen me through all stages of graduate life: Anna and Seth Arnold, Phil Bartels,

Lisa Beckmann, Kelsey Boyle, Adam Boynton, Marissa Buzzeo, Justin Charton, Russ Ernst, Ariel Furst, Wendy Geil, Joey Genereux, Mike Grodick, Chinny Idigo, Alexis Komor, Paul Lee, Sebastian Liska, Anna McConnell, Tim Mui, Natalie Muren, Liz O'Brien, Eric Olmon, Catrina Pheeney, Cindy Puckett, Christine Romano, Curtis Schneider, Helen Segal, Rebekah Silva, Pam Sontz, Alyson Weidman, and Brian Zeglis.

ABSTRACT

Transcription factor p53 is the most commonly altered gene in human cancer. As a redox-active protein in direct contact with DNA, p53 can directly sense oxidative stress through DNA-mediated charge transport. Electron hole transport occurs with a shallow distance dependence over long distances through the π-stacked DNA bases, leading to the oxidation and dissociation of DNA-bound p53. The extent of p53 dissociation depends upon the redox potential of the response element DNA in direct contact with each p53 monomer. The DNA sequence dependence of p53 oxidative dissociation was examined by electrophoretic mobility shift assays using radiolabeled oligonucleotides containing both synthetic and human p53 response elements with an appended anthraquinone photooxidant. Greater p53 dissociation is observed from DNA sequences containing low redox potential purine regions, particularly guanine triplets, within the p53 response element. Using denaturing polyacrylamide gel electrophoresis of irradiated anthraquinone-modified DNA, the DNA damage sites, which correspond to locations of preferred electron hole localization, were determined. The resulting DNA damage preferentially localizes to guanine doublets and triplets within the response element. Oxidative DNA damage is inhibited in the presence of p53, however, only at DNA sites within the response element, and therefore in direct contact with p53. From these data, predictions about the sensitivity of human p53-binding sites to oxidative stress, as well as possible biological implications, have been made. On the basis of our data, the guanine pattern within the purine region of each p53-binding site determines the response of p53 to DNA-mediated oxidation, yielding for some sequences the oxidative dissociation of

p53 from a distance and thereby providing another potential role for DNA charge transport chemistry within the cell.

To determine whether the change in p53 response element occupancy observed *in vitro* also correlates *in cellulo*, chromatin immunoprecipition (ChIP) and quantitative PCR (qPCR) were used to directly quantify p53 binding to certain response elements in HCT116N cells. The HCT116N cells containing a wild type p53 were treated with the photooxidant $[Rh(phi)2bpy]^{3+}$, Nutlin-3 to upregulate p53, and subsequently irradiated to induce oxidative genomic stress. To covalently tether p53 interacting with DNA, the cells were fixed with disuccinimidyl glutarate and formaldehyde. The nuclei of the harvested cells were isolated, sonicated, and immunoprecipitated using magnetic beads conjugated with a monoclonal p53 antibody. The purified immounoprecipiated DNA was then quantified via qPCR and genomic sequencing. Overall, the ChIP results were significantly varied over ten experimental trials, but one trend is observed overall: greater variation of p53 occupancy is observed in response elements from which oxidative dissociation would be expected, while significantly less change in p53 occupancy occurs for response elements from which oxidative dissociation would not be anticipated.

The chemical oxidation of transcription factor p53 via DNA CT was also investigated with respect to the protein at the amino acid level. Transcription factor p53 plays a critical role in the cellular response to stress stimuli, which may be modulated through the redox modulation of conserved cysteine residues within the DNA-binding domain. Residues within p53 that enable oxidative dissociation are herein investigated. Of the 8 mutants studied by electrophoretic mobility shift assay (EMSA), only the C275S mutation significantly decreased the protein affinity (K_D) for the Gadd45 response

element. EMSA assays of p53 oxidative dissociation promoted by photoexcitation of anthraquinone-tethered Gadd45 oligonucleotides were used to determine the influence of p53 mutations on oxidative dissociation; mutation to C275S severely attenuates oxidative dissociation while C277S substantially attenuates dissociation. Differential thiol labeling was used to determine the oxidation states of cysteine residues within p53 after DNA-mediated oxidation. Reduced cysteines were iodoacetamide labeled, while oxidized cysteines participating in disulfide bonds were $^{13}C_2D_2$-iodoacetamide labeled. Intensities of respective iodoacetamide-modified peptide fragments were analyzed using a QTRAP 6500 LC-MS/MS system, quantified with Skyline, and directly compared. A distinct shift in peptide labeling toward $^{13}C_2D_2$-iodoacetamide labeled cysteines is observed in oxidized samples as compared to the respective controls. All of the observable cysteine residues trend toward the heavy label under conditions of DNA CT, indicating the formation of multiple disulfide bonds potentially among the C124, C135, C141, C182, C275, and C277. Based on these data it is proposed that disulfide formation involving C275 is critical for inducing oxidative dissociation of p53 from DNA.

TABLE OF CONTENTS

LIST OF FIGURES

CHAPTER 1

CHAPTER 2

CHAPTER 3

CHAPTER 4

LIST OF TABLES

CHAPTER 2

CHAPTER 3

CHAPTER 4

LIST OF APPENDICIES

APPENDIX: CHAPTER 3

APPENDIX: CHAPTER 4

CHAPTER 1

Biological contexts of DNA-mediated charge transport

The vast majority of intracellular deoxyribonucleic acid (DNA), the molecule that houses the information necessary for life as we know it, is stored within the nucleus of eukaryotic cells as chromatin. The chromatin is composed of double stranded DNA wrapped around histone proteins, condensing the DNA in an ordered manner that allows for accessibility of the genetic material when needed. Serving as the primary library of information in the central dogma of life, the genetic information stored within DNA is transcribed into single stranded ribonucleic acid (RNA), which is then translated into a corresponding string of amino acids to ultimately function as a protein.[1] Proteins are the catalytic and structural workhorses of the cell, and all of the information to make these proteins is housed in the DNA. With three DNA bases creating a single codon to which a specific amino acid is ascribed, the four DNA bases can therefore be arranged as 64 unique 3-base combinations. However, with only 21 naturally occurring amino acids, the DNA genetic code allows for redundancy.

DNA exists intracellularly in its physiologically relevant B-form structure. B-form DNA conforms to a 20 Å wide right-handed double helical structure, with the bases stacked centrally along the helical access (grey), with the negatively charged sugar-phosphate backbone circling the exterior (black), as represented in Figure 1.1.[2] Such B-form DNA is comprised of two antiparallel single strands of DNA that associate through the formation of specific hydrogen bonds among four distinct bases: adenine pairing with thymine via two hydrogen bonds, and guanine pairing with cytosine via three hydrogen bonds.[3] The bases pair so that a two-membered ring purine, G or A, always interacts with the corresponding a one-membered ring pyrimidine, C or T, such that the width of this molecule is consistently uniform.[2,3] Chemical structures of the individual bases are

FIGURE 1.1 — Structural representation of double stranded B-form DNA. Top: The DNA bases are represented in a space filling model (gray) and the sugar phosphate backbone as a ribbon model (black), highlighting the intimae stacking of the bases. Middle: Looking down the helical axis of B-form DNA, (center) the extensive degree of overlap among the base-paired core is depicted (right, yellow), and the structural similarity of the stacking to graphene (left, yellow), a known charge-conducting substance. Bottom: Stick representations of the four canonical DNA bases, where the purine adenine pairs with the pyrimidine thymine via two hydrogen bonds, and the purine guanine pairs with the pyrimidine cytosine via three hydrogen bonds.

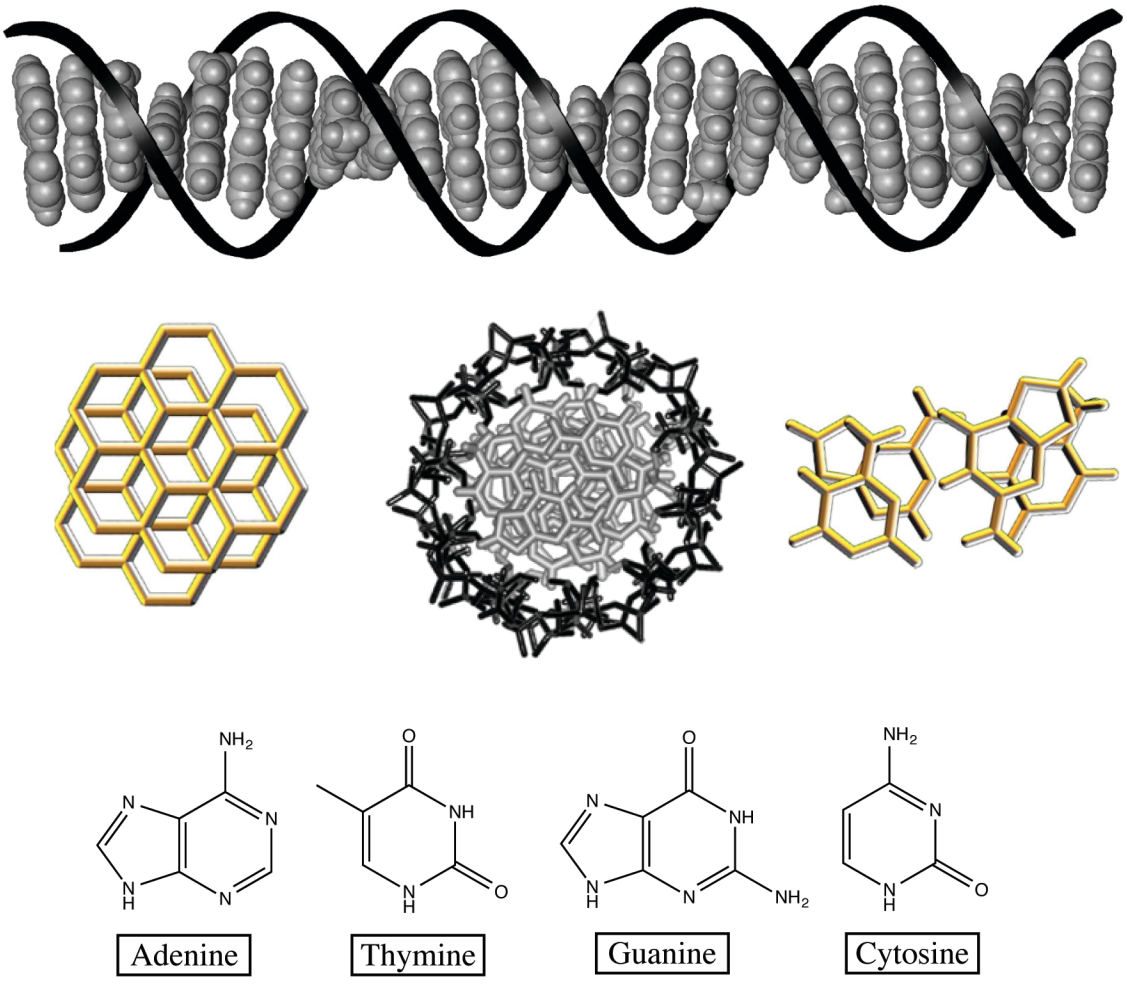

depicted at the bottom of Figure 1.1. Due to the base pairing geometry orienting the two strands not directly opposite of one another, the DNA double helix contains a wider major groove and a narrower minor groove. The major groove is 22 Å wide and allows access to the bases, and is known to act as sequence-specific binding sites for many transcriptions factors. The minor groove is much more narrow at 12 Å, making base access and sequence specific protein binding more difficult from this location.[2]

Of greatest interest to the research conducted in the Barton laboratory is the ability of DNA to act as a molecular wire. The potential for conductivity through DNA was first suggested in 1962, when structural characterization determined that the interplanar spacing of the aromatic bases in B-form DNA is similar to the spacing between individual sheets of graphite, a known conductive material. This similarity of DNA to stacked graphite sheets could therefore form a conductive path of overlapping π-orbitals extending parallel to the helical axis, as depicted in Figure 1.1.[4] This property of DNA mediated charge transport (CT) was tested using many platforms and illustrated in ground state electrical experiments, where it was found that well stacked DNA has the same conductivity as charge traveling perpendicular to sheets of graphite.[5] It was also found that the graphite-like stacked bases of DNA also allow for the conduction of both electrons and electron holes along the helical axes.[6]

Long range DNA damage

The properties of DNA with respect to its conductive ability have been probed in solution through the use of tethered oxidants and electrochemically through attaching DNA to electrode surfaces. From the numerous investigations conducted it has been

determined that DNA is able to conduct both electrons and electron holes along the helical axis.[6] DNA must be double stranded for this conductivity to occur, whereby single stranded, poorly stacked, oligonucleotide counterparts are unable to convey CT. The transport of charge in double stranded DNA is also extraordinarily sensitive to the integrity of the DNA base stack. Perturbations such as a single DNA mismatch, an abasic site, or an oxidatively damaged base adduct severely attenuate CT.[6-10] However, nicks in the DNA sugar-phosphate backbone do not attenuate CT, confirming that the conductive nature is dependent upon the base-stacking and does not involve the backbone.[10] We have also exploited this property in electronic devices to detect base mismatches, base lesions, and to characterize DNA-binding proteins.[11-15] These investigations have determined that DNA CT occurs with a shallow distance dependence, meaning that charge can be conducted over long molecular distances with low resistance. By using a variety of distally bound photooxidants, we have also measured effective CT through DNA over a distance of 20 nm; much longer distances for CT are expected given the very shallow distance dependence observed.[9,12,13] Through *in vitro* experiments we have also found that oxidative damage to DNA can occur from a distance due to the migration of electron holes through the DNA base stack, as depicted in Figure 1.2.[6-9]

The Barton laboratory has focused our studies on the properties, usefulness, and biological implications of long-range charge transport (CT) through DNA. With respect to the research conducted herein, the focus has been on the biological context of DNA-mediated oxidation. The eukaryotic genome incurs thousands of oxidative events daily and may arise from such sources as ionizing radiation, exogenous chemicals, and metabolic side products. But how does the DNA respond to these oxidative events?

FIGURE 1.2 — *In vitro* DNA-mediated charge transport experimental construct. Synthetic oligonucleotide conjugated with a Rh or Ru photooxidant (red) that then intercalated into the double stranded DNA (blue). Photoexcitation (hν) of the tethered and intercalated photooxidant abstracts an electron from the DNA, creating an electron hole which than equilibrates among the π-stacked bases. Guanine doublets (yellow) within the DNA sequence are efficient electron hole traps due to their low redox potential, leading to oxidative DNA lesions at these locations. Oxidative lesions have been observed over 200 Å from the DNA bound photooxidant *in vitro,* depicted as the white flare at the far right of the oligonucleotide.[9]

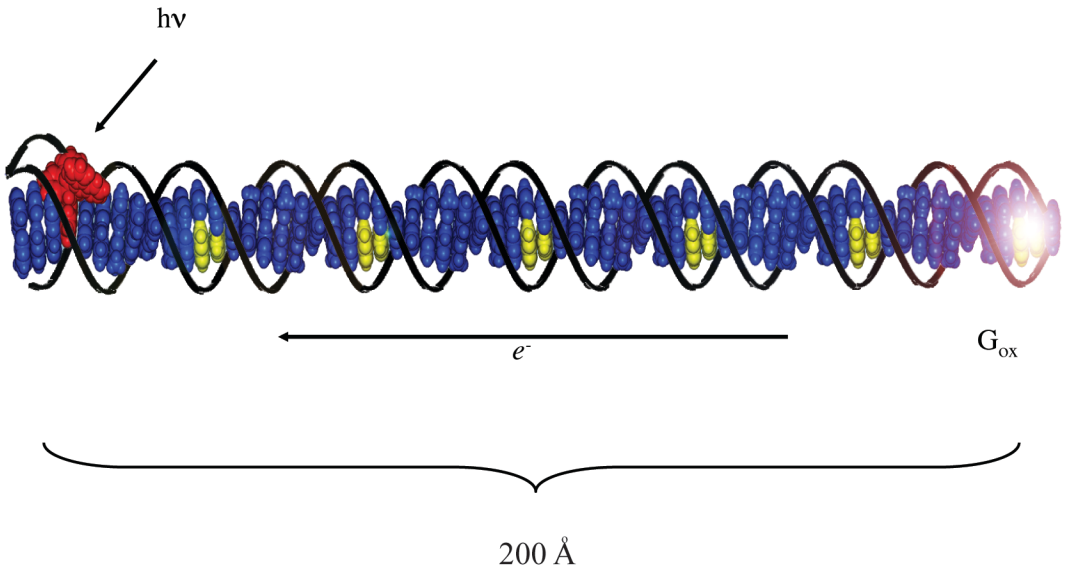

Research in the Barton lab and other groups has found, based on DNA CT, that once oxidized, the electron hole within the DNA can equilibrate among the bases and localize to sites of low redox potential.[9,16,17]

The redox potentials of the individual bases are key in determining the location to which electron holes will localize in oxidized DNA. The one-electron oxidation potentials for the bases are as follows: C(1.7 V), T(1.6 V), A (1.42 V), and G (1.29 V).[16] With the lowest redox potential of the four canonical bases, guanine is the most easily oxidizable. Guanine doublets and triplets are even more readily oxidizable than single guanine residues, and guanine oxidation at the 5′ end of such sites has become a known hallmark of one-electron oxidation of DNA.[17] As shown in Figure 1.2., *in vitro* photooxidation of a long oligonucleotide shows that the electron hole preferentially localizes to guanine doublet sites over 200 Å away from the DNA tethered photooxidant.[9] Given the ease of electron hole migration through DNA, we expect holes to localize to DNA sites of lowest reduction potential: particularly guanine doublets and triplets.[17] Guanine radicals can yield a myriad of mutagenic lesions as a result of reacting with water or dioxygen.[18]

Long range DNA CT in the presence of DNA-bound proteins

One avenue of research within the Barton lab has been to explore how DNA CT may be used *in vivo*. In accordance with the central dogma, DNA is primarily useless if it cannot be transcribed and subsequently translated, indicating that histone proteins or transcriptional proteins are continually within close proximity of DNA.[1] One can imagine that proteins intimately involved with DNA may be able to couple into the CT

pathway of DNA and potentially utilize this property as a means of cellular signaling. In certain cases, DNA-bound proteins may react with the base radicals to form covalent adducts.[19] If the DNA-bound proteins are also redox active, they may be able to modulate their activity upon oxidation, and not become covalently attached to the DNA. While most studies conducted thus far have used synthetic oligonucleotides tested *in vitro*, we have also seen been able to observe that long-range oxidative damage can occur in chromatin and in the nucleus of HeLa cells.[20-22]

One example of a protein that affects the DNA CT properties is the TATA binding protein. The main function of the TATA protein kinking the DNA is to destabilize the bases to allow for other transcriptional machinery to access a transcriptional start site.[23] However, the kink made by the binding of TATA protein to the DNA is so severe that charge transport is attenuated and can be detected electrochemically.

Another transcription factor formerly studied in the Barton group includes SoxR, which is an *E. coli* stress response protein that contains a [2Fe2S] cluster.[24] SoxR is a transcriptional regulator for the SoxS gene pathway, and the activation of SoxR only occurs once the protein is oxidized. Since the SoxR protein has similar binding affinities for its response element in the apo, reduced, and oxidized forms, binding of SoxR to DNA is not the source of its oxidation. However, it appears that only the SoxS downstream products are activated in the presence of oxidized SoxR and the DNA mediated oxidation of SoxR leads to a conformational change that elicits the transcription of downstream SoxS.[25] Experiments *in vitro* have shown that SoxR can be oxidized from

a distance through DNA CT, leading ultimately to the transcriptional activation of SoxS.[25]

Even more complex DNA-protein interactions have been studied and a model has been proposed whereby DNA CT plays an integral biological role in DNA damage, sensing for the first step of DNA damage repair.[26] This DNA-mediated genomic repair process is made possible by the prevalence of [4Fe-4S] clusters in base excision repair enzymes, such as MutY, EndoIII, and DinG.[27, 28] More recently, [4Fe-4S] clusters have been found in the full range of DNA-processing enzymes, suggesting a general role for DNA CT within the cell in long range signaling of genomic integrity.[8,26] In this model, the proteins communicate to one another through electron injection to the DNA. If the proteins can communicate, that means the intervening region between the two proteins has been scanned and is free of damage; in this case, the proteins can dissociate and move on to investigate another location within the genome. If DNA damage is located between the two proteins, the scan cannot be completed due to the attenuation of CT, and both of the proteins remain bound within the local area. The proteins may then process around that general region to find and repair the site of damage.[8,26]

DNA CT recognition by proteins does not necessarily require an iron-sulfur cofactor; other redox-active moieties within a protein can participate as well. Cysteine residues can be oxidized to form disulfide bonds at physiological redox potentials. As shown both by *in vitro* photooxidation and electrochemical experiments, thiols incorporated into the DNA backbone can be oxidized to disulfides at a distance through long range DNA CT.[29,30] Cysteine redox chemistry is often harnessed *in vivo* by DNA-

bound proteins as a redox switch in regulation; DNA CT chemistry would offer the ability to carry out such reactions from a distance *in vivo*.

Transcription factor p53

Transcription factor p53 was initially thought to be an oncogene, due to its marked upregulation in numerous human cancers. It was however determined that p53 is a transcription factor whose mutation leads to a predisposition to cancer. Therefore, p53 is a tumor suppressor and not itself an oncogene. Human transcription factor p53 transduces a variety of cellular stresses into transcriptional responses. The pivotal role which p53 plays in human cells classifies this protein as a tumor suppressor. Intracellularly, p53 has a short half life due to its negative regulator murine double minute 2 (MDM2), which is an E3 ubiquitin ligase that sequesters p53 and targets it for proteolytic degradation through multiubiquitination. When some cellular stress signal is sensed, such as oxidative stress, hypoxia, or oncogene activation, p53 is activated and escapes MDM2 control. This increases intracellular p53 levels leading to the regulation of p53 target genes or other protein-protein interactions. Overall, many of the pathways in which p53 is involved revolve around decisions of cellular fate, including responses like apoptosis, senescence, cell cycle arrest, or DNA repair (Figure 1.3).[31-36]

The importance of p53 integrity for proper biological function is highlighted by the fact that mutations in this protein are observed in over half of all human cancers. The most common type of mutations observed in human cancers involving mutant p53 are point mutations, resulting in a single amino acid substitution within the protein.[37] Such mutations may cause improper protein folding, disruption of integral protein-protein interactions, or alteration of protein-DNA contacts.[38] Of the known p53 point mutations

FIGURE 1.3 — The p53 response to cellular stress. The p53-MDM2 feedback loop is the primary means of intracellular p53 regulation. Activating signals (top) inhibit the p53-MDM2 interaction, leading to increased intracellular p53 concentrations and the subsequent activation and repression of various transcriptional targets. Under physiologically normal levels of cellular stress, p53 tends to promote repair processes. However, in the case of severe cellular stress, in which repair attempts may be futile, cellular senescence and apoptosis are preferentially promoted.[40]

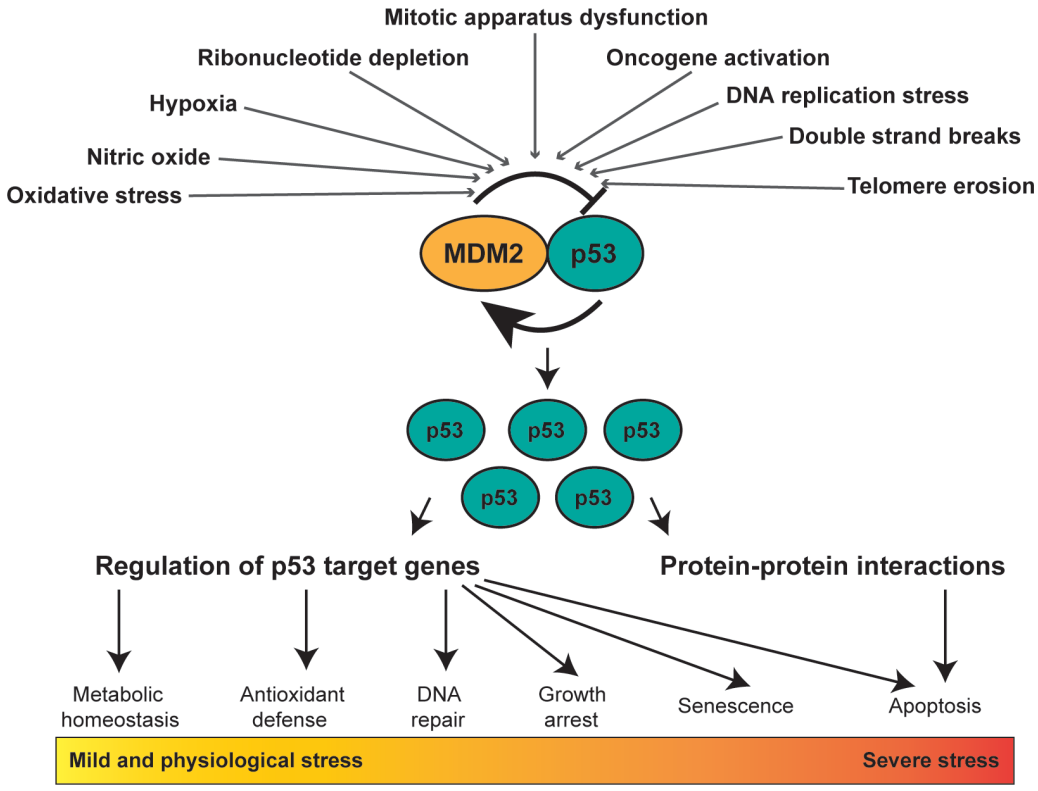

FIGURE 1.4 — Frequency of point mutations within p53 observed in human cancers. The top chart represents the percent of point mutations as observed in human cancers (n=24,210) per individual codon. Of the cancer relevant mutations observed, over 80% of these occur within the conserved DNA-binding domain. The structural domains of p53 are depicted below the plot. p53 contains an N-terminal trans activation domain (TAD), followed by a proline rich domain (PRD), the highly conserved and structured DNA binding domain (DBD), followed by the tetramerization domain (TD) and the C-terminal domain (CTD).[37]

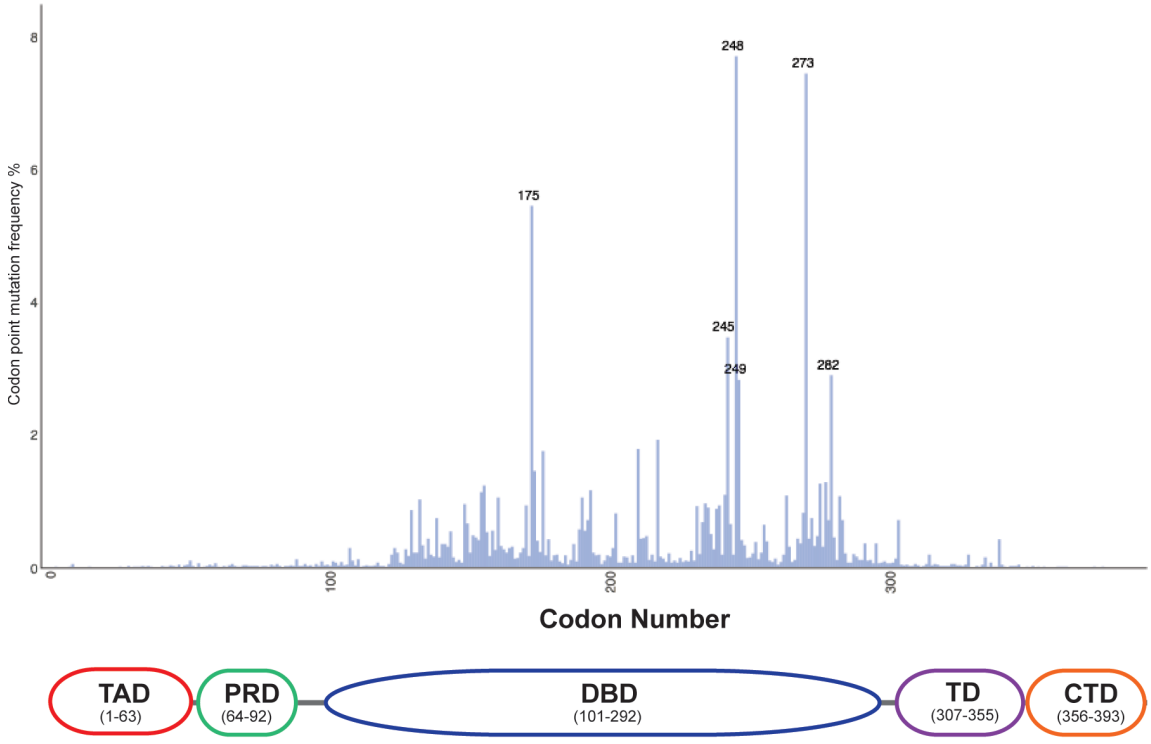

observed in human cancer, the majority of these mutations occur within the DNA-binding domain, as seen in Figure 1.4.[38,39] This finding strongly suggests that the proper function of the DNA binding domain is of the utmost importance for proper p53 function. Human p53 is the most highly researched human transcription factor due to its association with cancer.

Structure of p53

At 393 amino acid residues long, human p53 contains many highly conserved residues within the DNA binding domain. Human p53 is comprised of a loosely structured amino-terminal transactivation domain (TAD—residues 1-63) containing two transactivation subdomains (TADI—residues 1–42, TADII—residues 43–63), to which many different post translational modifications can be appended. The TAD is followed by a proline-rich domain (PRD—residues 64–92), which is a common feature in many transcription factors. Following the PRD is a flexible and unstructured region that leads into the highly structured and evolutionarily conserved core of the protein, the DNA-binding domain (DBD—residues 102–292). The DBD is followed by the tetramerization domain (TD—residues 307–355), which allows for the protein to assemble as a tetramer when binding response element DNA. The TD contains a flexible linker region (residues 307–315) as well as a nuclear localization signal domain (residues 316-325). The p53 protein is then terminated with an unstructured basic C-terminal domain (CTD—residues 356–393).[40] This general landscape of the p53 domains is depicted in Figure 1.4. Corresponding point mutation frequencies at each codon of p53 as observed in human

cancers is also listed, demonstrating that the majority of cancer relevant mutations occur within the DNA binding domain of the protein.[37]

Transcription Factor p53 binds to its response element as a tetramer. The DNA sequence to which p53 was found to recognize and bind is comprised of two copies of the 10 base pair half site motif 5′-RRRCWWGYYY-3′, separated by 0-13 base pairs, with R representing a purine, Y representing a pyrimidine, and W being either an adenine or thymine.[41] Each monomer of p53 also contains one Zn^{2+} that appears necessary for structural integrity, allowing for response element binding. p53 makes several direct contacts with bases within the major groove of the response element, as well as direct backbone contacts and several water-mediated contacts. As depicted in Figure 1.4, the p53 DNA binding domain assembles to the response element as a tetramer.[42,43] Within each p53 monomer, three cysteine residues (C176, C238, and C242) and one histidine (H179) coordinate a zinc ion that is believed to be structurally necessary for DNA binding.[38,42-44] Located close to the Zn^{2+}, but not participating in metal binding, is C182. Closer to the DNA-p53 interface are the remaining conserved residues of interest: C124, C135, C141, C275, and C277. Nestled into the major groove, C277 is capable of forming a hydrogen bond within the purine region of the p53 response element quarter site.[42,43] C275 is located 7.0 Å away from C277, from sulfur atom to sulfur atom. Residues C124, C135, and C141 are found clustered deeper inside the core of the DNA binding domain, with C275 7.0 Å angstroms away from C135. Chen and coworkers have reported these residues as reduced in their structural characterizations of the p53 DNA binding site; however, disulfide formation is plausible based on the proximity of these residues with respect to one another.[42,43]

FIGURE 1.5 — Crystallographic representation of the p53 DNA-binding domain. Structural representation of p53 binding as a tetramer (blue and purple) to a full response element. The spherical representation of DNA and surface representation of p53 (top) display the tight interaction between the p53 monomers and the response element DNA. Looking down the helical axis of the stick figure DNA (bottom) one can see the symmetry of the DNA-bound p53 tetramer and how deepy it binds into the DNA major groove. Images based on PMID: 3KMD crystal structure.[42]

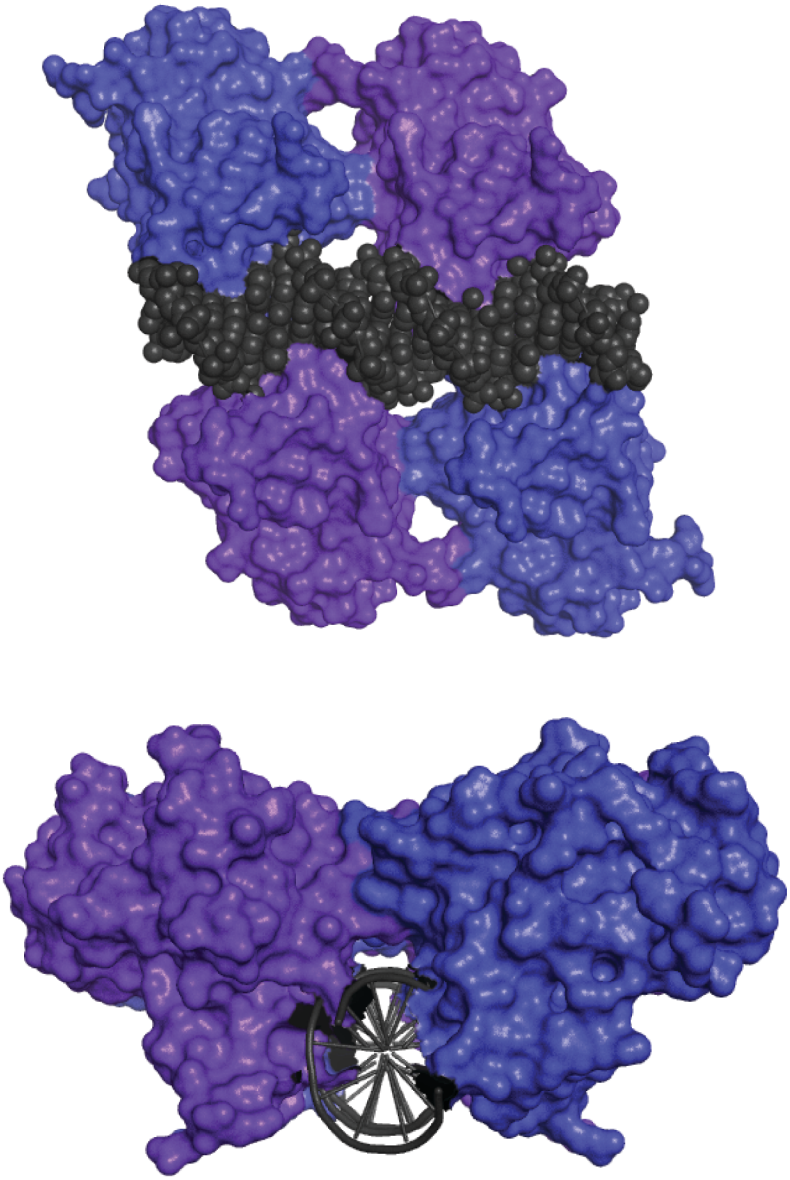

Transcriptional activity of p53

Most commonly, p53 serves as a transcription factor in the promotion of RNA polymerase II transcribed genes. Some of the most noteworthy and important genes under direct p53 regulation include genes playing roles in cell cycle arrest (*p21, 14-3-3*), apoptosis (*pig, Bax, puma, noxa*), scenescence (*pai-1*), and autophagy (*dram*).[45] Interestingly, p53 also promotes its negative regulator MDM2 and itself, p53. The majority of p53 response elements cluster within noncoding regions of the genes they regulate; it has been found that they can be located nearly anywhere within the target gene locus.[46] Response elements for p53 are most commonly found in the upstream promoter regions from the target gene transcription start site, within about 300 base pairs. A general trend appears and response elements tend to decrease in transactivation potential as they increase in distance from the transcription start site.[46] In several cases, p53 response elements have also been found in early intronic sequences of the target genes, as well as within exons.[46]

Once p53 binds its designated response elements, histone modifications within the region are necessary to relax the chromatin and enable general transcription machinery accessibility. In response to DNA damage, p53 is involved in the recruitment of the histone variant H2A.Z, an event which is required for full activation of p21.[47] The relationship of p53 with its most well-studied HATs, p300 and CBP, is fairly complex.[48] Once the local chromatin has been modified and remodeled, components of the preinititation complex may then be recruited or somehow altered to allow for the initiation of transcription.[49] TFIID is recruited to the promoter's TATA region to nucleate the formation of the PIC, followed by TFIIB, and finally by the assembly of the

other transcription initiation factors (TFIIF , TFIIE, TFIIH) complexed with unphosphorylated RNAPII.[50,51] However, for many genes, such as p21, it is clear that the levels of p53 bound are not the sole determinant of the ensuing transcriptional response.[52-55]

Repression of certain genes by p53 has been proposed to occur in several different ways. One suggestion is that the binding of p53 to certain response elements recruits corepressors to the site and results in overall downregulation. Another idea is that p53 can secondarily inhibit expression of certain genes by promoting the activation of certain repressor proteins. p53 may also bind to its response element and occupy the site so that other transcriptional activators cannot gain access. Lastly, it is thought that p53 may also repress genes that do not contain a p53 response element through protein-protein interactions that inhibit the promotion of those genes.[48]

Other roles of p53

There are many post-translational modifications that affect p53 and how it functions within the cell. It has been observed that upon DNA damage, p53 is phosphorylated on its NTD, and such damage-inducible phosphorylation then enhances p300/CBP-mediated acetylation and methylation of lysine and arginine residues of the CTD. Arginine methylation has also been observed in the tetramerization domain. Interestingly, unlike the MDM2 ubiquitination leading to p53 degradation, mono-ubiquitination of k320 appears to be for transcriptional regulation.[56,57]

Although p53 primarily serves as a transcription factor in response to cellular stress, many other roles of p53 have been investigated. Such roles have been found to

include transcriptional repression, translational regulation, recognition of DNA double strand breaks, as well as playing a role in homologous recombination and enabling a transcription-independent apoptotic response.[58-61] The C-terminal domain of p53 has also been suggested in specifically recognizing and binding to unique and biologically relevant DNA structures such as single-stranded DNA over hangs, hemicatenated DNA, minicircular DNA, and supercoiled DNA.[62-66]

Focus of this thesis

Much research has focused on the transcriptional role that p53 play through its recognition and binding of response element sites. However, with each new study, the network of roles played by p53 just becomes more and more complex. One facet of this research that has gone uninvestigated by other laboratories is determining if and how p53 can directly sense DNA damage, seeing that it is known that p53 is activated in this case. What also is not greatly known is how p53 selects binding to one response element over another. Also, many researchers focus on p53 recruitment, activation, and modification, but there is little understanding of what the deciding factor is and how p53 then returns to a signal-off state. Specifically we ask how p53 senses oxidative genomic stress and whether p53 senses it directly. The following work described in this thesis are investigations on the direct sensing of genomic oxidative stress by p53, and how it may accordingly respond. While p53 is generally known to sense oxidative stress as one of its inputs, its function as a redox-active DNA-binding protein remains to be fully elucidated.

REFERENCES

1. Crick, F. H. C. (1970) Central dogma of molecular biology. *Nature 227*, 561-563.

2. Wing, R., Drew, H., Takano, T., Broka, C., Tanaka, S., Itakura, K., and Dickerson, R. E. (1980) Crystal structure analysis of a complete turn of B-DNA. *Nature 287*, 755-758.

3. Watson, J.D., and Crick, F.H.C. (1953) A Structure for Deoxyribose Nucleic Acid. *Nature 171*, 737-738.

4. Eley, D. D., and Spivey, D. I. (1962) Semiconductivity of organic substances. Part 9 - Nucleic acid in the dry state. *Trans. Faraday Soc. 58*, 411-415.

5. Guo, X., Gorodetsky, A. A., Hone, J., Barton, J. K., and Nuckolls, C. (2008) Conductivity of a single DNA duplex bridging a carbon nanotube gap. *Nat. Nanotechnol. 3,* 163-167.

6. Delaney, S., and Barton, J. K. (2003) Charge transport in DNA duplex/quadruplex conjugates. *J. Org. Chem. 68*, 6475-6483.

7. Genereux, J., Boal, A., and Barton, J. K. (2010) DNA-mediated charge transport in redox sensing and signaling. *J. Am. Chem. Soc. 132,* 891-905.

8. Hall, D., Holmlin, R., and Barton, J. K. (1996) Oxidative DNA damage through long-range electron transfer. *Nature 382*, 731-735.

9. Núñez, M. E., Hall, D. B., and Barton, J. K. (1999) Long-range oxidative damage to DNA: Effects of distance and sequence. *Chem. Biol. 6*, 85-97.

10. Liu, T., and Barton, J. K. (2005) DNA electrochemistry through the base pairs not the sugar-phosphate backbone. *J. Am. Chem. Soc. 127*, 10160-10161.

11. Kelley, S. O., Holmlin, R. E., Stemp, E. D. A., and Barton, J. K. (1997) Photoinduced electron-transfer in ethidium-modified DNA duplexes: dependence on distance and base stacking. *J. Am. Chem. Soc. 119*, 9861-9870.

12. Boon, E., Ceres, D., Drummond, T., Hill, M., and Barton, J. K. (2000) Mutation detection by electrocatalysis at DNA-modified electrodes. *Nat. Biotechnol. 18*, 1096-1100.

13. Boon, E., Salas, J., and Barton, J. K. (2002) An electrical probe of protein-DNA interactions on DNA-modified surfaces. *Nat. Biotechnol. 20*, 282-286.

14. Henderson, P. T., Jones, D., Hampikian, G., Kan, Y. Z., and Schuster, G. B. (1999) Long-distance charge transport in duplex DNA: the phonon-assisted polaron-like hopping mechanism. *Proc. Natl. Acad. Sci. U.S.A. 96*, 8353-8358.

15. Slinker, J., Muren, N., Renfew, S. E., and Barton, J. K. (2011) DNA charge transport over 34 nm. *Nat. Chem. 3*, 228-233.

16. Steenken, S., and Jovanovic, S. (1997) How easily oxidizable is DNA? One-electron reduction potentials of adenosine and guanosine radicals in aqueous solution. *J. Am. Chem. Soc. 119*, 617-618.

17. Sugiyama, H., and Saito, I. (1996) Theoretical studies of GG-specific photoclevage of DNA via electron transfer: significant lowering of ionization potential and 5′ localization of HOMO of stacked GG bases from b-form DNA. *J. Am. Chem. Soc. 118*, 7063-7068.

18. Burrows, C. J. (2009) Surviving an oxygen atmosphere: DNA damage and repair. *ACS Symp. Ser. 2009*, 147-156.

19. Kurbanyan, K., Nguyen, K., To, P., Rivas, E., Lueras, A., Kosinski, C., Steryo, M., Gonzalez, A., Mah, D., and Stemp, E. D. A. (2003) DNA-protein cross-linking via guanine oxidation: Dependence upon protein and photosensitizer. *Biochemistry 42*, 10269-10281.

20. Núñez, M. E., Holmquist, G. P., and Barton, J. K. (2001) Evidence for DNA charge transport in the nucleus. *Biochemistry 40*, 12465-12471.

21. Núñez, M. E., Noyes, K. T., and Barton, J. K. (2002) Oxidative charge transport through DNA in nucleosome core particles. *Chem. Biol. 9*, 403-415.

22. Merino, E. J., Boal, A. K., and Barton, J. K. (2008) Biological contexts for DNA charge transport chemistry. *Curr. Opin. Chem. Biol. 12*, 229-237.

23. Gorodetsky, A. A., Ebrahim, A., and Barton, J. K. (2008) Electrical detection of TATA binding protein at DNA-modified microelectrodes. *J. Am. Chem. Soc. 130*, 2924-2925.

24. Lee, P., Demple, B., and Barton, J. (2009) DNA-mediated redox signaling for transcriptional activation of SoxR. *Proc. Natl. Acad. Sci. U.S.A. 106*, 13164-13168.

25. Amábile-Cuevas, C. F., and Demple, B. (1991) Molecular characterization of the soxRS genes of Escherichia coli: Two genes control a superoxide stress regulon. *Nucleic Acids Res. 19*, 4479-4484.

26. Sontz, P. A., Muren, N. B., and Barton, J. K. (2012) DNA charge transport for sensing and signaling. *Acc. Chem. Res. 45*, 1792-1800.

27. Grodick, M. A., Segal, H. M., Zwang, T. J., and Barton, J. K. (2014) DNA-mediated signaling by proteins with 4Fe-4S clusters is necessary for genomic integrity. *J. Am. Chem. Soc. 136*, 6470-6478.

28. Sontz, P. A., Mui, T. P., Fuss, J. O., Tainer, J. A., and Barton, J. K. (2012) DNA charge transport as a first step in coordinating the detection of lesions by repair proteins. *Proc. Natl. Acad. Sci. U.S.A. 109*, 1856-1861.

29. Takada, T., and Barton, J. K. (2005) DNA charge transport leading to disulfide bond formation. *J. Am. Chem. Soc. 127*, 12204-12205.

30. Gorodetsky, A. A., and Barton, J. K. (2007) DNA-mediated electrochemistry of disulfides on graphite. *J. Am. Chem. Soc. 129*, 6074-6075.

31. Vogelstein, B., Lane, D., and Levine, A. J. (2000) Surfing the p53 network. *Nature 408,* 307-310.

32. Vousden, K. H., and Lu, X. (2002) Live or let die: the cell's response to p53. *Nat. Rev. Cancer 2*, 594-604.

33. Prives, C., and Hall, P. A. (1999) The p53 pathway. *J. Pathol. 187*, 112−126.

34. Brooks, C. L., and Gu, W. (2006) p53 Ubiquitination: Mdm2 and beyond. *Mol. Cell 21*, 307−315.

35. el-Deiry, W. S., Tokino, T., Velculescu, V. E., Levy, D. B., Parsons, R., Trent, J. M., Lin, D., Mercer, W. E., Kinzler, K. W., and Vogelstein, B. (1993) WAF1, a potential mediator of p53 tumor suppression. *Cell 75*, 817−825.

36. Kastan, M., Zhan, Q., El-Deiry, W. S., Carrier, F., Jacks, T., Walsh, W. V., Plunkett, B. S., Vogelstein, B., and Fornace, A. (1992) A mammalian cell cycle checkpoint pathway utilizing p53 and GADD45 is defective in ataxia-telangiectasia. *Cell 71*, 587-597.

37. Petitjean, A., Mathe, E., Kato, S., Ishioka, C., Tavtigian, S. V., Hainaut, P., and Olivier, M. (2007) Impact of mutant p53 functional properties on TP53 mutation patterns and tumor phenotype: lessons from recent developments in the IARC TP53 database. *Hum. Mutat. 28*, 622-629. Version R17.

38. Joerger, A. C., and Fersht, A. R. (2007*)* Structure-function-rescue: the diverse nature of common p53 cancer mutants. *Oncogene 26*, 2226-2242.

39. Paveletich, N. P., Chambers, K. A., and Pabo, C. O. (1993) The DNA-binding domain of p53 contains the four conserved regions and the major mutation hot spots. *Genes Dev. 7*, 2256-2564.

40. Levine, A., and Oren, M. (2009) The first 30 years of p53: growing ever more complex. *Nat. Rev. Cancer 9*, 749-758.

41. el-Deiry, W., Kern, S., Pietenpol, J., Kinzler, K., and Vogelstein, B. (1992) Definition of a consensus binding site for p53. *Nat. Genet. 1*, 45-59.

42. Cho, Y., Gorina, S., Jeffrey, P. D., and Pavletich, N. P. (1994) Crystal-structure of a p53 tumor-suppressor DNA complex: Understanding tumorigenic mutations. *Science 265*, 346-354.

43. Chen, Y., Dey, R., and Chen, L. (2010) Crystal structure of the p53 core domain bound to a full consensus site as a self-assembled tetramer. *Structure 18*, 246-256.

44. Chen, Y., Zhang, X., Dantas Machado, A. C., Ding, Y., Chen, Z., Qin, P. Z., Rohs, R., and Chen, L. (2013) Structure of p53 binding to the BAX response element reveals DNA unwinding and compression to accommodate base-pair insertion *Nucleic Acids Research*, *41*, 8368-8376.

45. Beckerman, R., and Prives, C. (2010) Transcriptional Regulation by p53. *Cold Spring Harb. Perspect. Biol. 2*, 1-19.

46. Riley, T., Sontag, E., Chen, P., and Levine, A. (2008) Transcriptional control of human p53-regulated genes. *Nat. Rev. Mol. Cell Biol. 9,* 402-412.

47. Gévry, N., Chan, H. M., Laflamme, L., Livingston, D. M., and Gaudreau, L. (2007) p21 transcription is regulated by differential localization of histone H2A.Z. *Genes Develop. 21*, 1869-1881.

48. Grossman, S. R. (2001) p300/CBP/p53 interaction and regulation of the p53 response. *Eur. J. Biochem. FEBS 268*, 2773-2778.

49. Li, B., Carey, M., and Workman, J. L. (2007) The role of chromatin during transcription. *Cell 128*, 707-719.

50. Orphanides, G., Lagrange, T., and Reinberg, D. (1996) The general transcription factors of RNA polymerase II. *Genes Develop. 10*, 2657-2683.

51. Woychik, N. A., and Hampsey, M. (2002) The RNA polymerase II machinery: structure illuminates function. *Cell 108,* 453-463.

52. Espinosa, J. M., Verdun, R. E., and Emerson, B. M. (2003) p53 functions through stress- and promoter-specific recruitment of transcription initiation components before and after DNA damage. *Mol. Cell. 12*, 1015-1027.

53. Donner, A. J., Szostek, S., Hoover, J. M., and Espinosa, J. M. (2007) CDK8 is a stimulus-specific positive coregulator of p53 target genes. *Mol. Cell 27*, 121-133.

54. Mattia, M., Gottifredi, V., McKinney, K., and Prives C. (2007) p53-Dependent p21 mRNA elongation is impaired when DNA replication is stalled. *Mol. Cell Biol. 27*, 1309-1320.

55. Hill, R., Leidal, A. M., Madureira, P. A., Gillis, L. D., Waisman, D. M., Chiu, A., and Lee, P. W. (2008) Chromium-mediated apoptosis: involvement of DNA-dependent protein kinase (DNA-PK) and differential induction of p53 target genes. *DNA Repair 7*, 1484-1499.

56. Lambert, P. F., Kashanchi, F., Radonovich, M. F., Shiekhattar, R., and Brady, J. N. (1998) Phosphorylation of p53 serine 15 increases interaction with CBP. *J. Biol. Chem. 273*, 33048-33053.

57. Sakaguchi, K., Herrera, J. E., Saito, S., Miki, T., Bustin, M., Vassilev, A., Anderson, C. W., and Appella, E. (1998) DNA damage activates p53 through a phosphorylation-acetylation cascade. *Genes Dev. 12*, 2831-2841.

58. Ho, J., and Benchimol S. (2003) Transcriptional repression mediated by the p53 tumour suppressor. *Cell Death Differentiation 10,* 404-408.

59. Ewen, M. E., and Miller, S. J. (1996) p53 and translational control. *Biochim Biophys Acta 1242*, 181-184.

60. Bertrand, P., Saintigny, Y., and Lopez, B. S. (2004) p53's double life: transactivation-independent repression of homologous recombination. *Trends Genet 20*, 235-243.

61. Vaseva, A. V., and Moll, U. M. (2009) The mitochondrial p53 pathway. *Biochim. Biophys. Acta 1787*, 414-420.

62. Mazur, S. J., Sakaguchi, K., Appella, E., Wang, X. W., Harris, C. C., and Bohr, V. A. (1999) Preferential binding of tumor suppressor p53 to positively or negatively supercoiled DNA involves the C-terminal domain. *J. Mol. Biol. 292*, 241-249.

63. Zotchev, S.B., Protopopova, M., and Selivanova, G. (2000) p53 C-terminal interaction with DNA ends and gaps has opposing effect on specific DNA binding by the core. *Nucleic Acids Res. 28*, 4005-4012.

64. Gohler, T., Reimann, M., Cherny, D., Walter, K., Warnecke, G., Kim, E., and Deppert, W. (2002) Specific interaction of p53 with target binding sites is determined by DNA conformation and is regulated by the C-terminal domain. *J. Biol. Chem. 277*, 41192-41203.

65. McKinney, K., and Prives, C. (2002) Efficient specific DNA binding by p53 requires both its central and C-terminal domains as revealed by studies with high-mobility group 1 protein. *Mol. Cell Biol. 22,* 6797-6808.

66. Stros, M., Muselikova-Polanska, E., Pospisilova, S., and Strauss, F. (2004) High-affinity binding of tumor-suppressor protein p53 and HMGB1 to hemicatenated DNA loops. *Biochemistry 43*, 7215-7225.

CHAPTER 2

Oxidative dissociation of p53 is dependent upon response element DNA

Adapted from Schaefer, K. N. and Barton, J. K. (2014) *Biochemistry* 53, 3467−3475.

INTRODUCTION

Human transcription factor p53 is warmly referred to as the guardian of the genome, since it plays a critical role in sensing cellular stress and appropriating an according response. Thus far, nearly 150 genes have been identified and validated as being under the direct regulation of this transcription factor.[1,2] For a gene to be regulated by p53 it must contain a p53 response element within the upstream regulatory region of the gene under regulatory control, typically several hundred base pairs 5′ of the transcriptional start site.[1,2] When p53 binds to a given response element, depending on the gene in question, gene expression may either be activated or repressed; however, a recent computational analysis suggests that p53 is solely a gene activator.[2,3] It is through N-terminal phosphorylation of cytoplasmic p53 that it is activated, causing it to be transported to the nucleus, and function as a transcription factor.[4] Much research on p53 has focused on determining its transcriptional targets and untangling the intricate interplay of the protein signaling networks in which it is involved. Although much work has been done to elucidate how p53 actively regulates genes, much still needs to be learned about how p53 selectively choses which genes to promote and how these corresponding signals are again turned off at the according time.

As a transcription factor, human p53 is known to bind to specific genomic locations to regulate expression of certain genes. The p53 response element was experimentally determined through immunoprecipitation and genetic mapping of DNA fragments bound to p53.[5] From the cumulative results of 18 distinct binding sites, the p53 response element was determined. The DNA sequence to which p53 was found to recognize and bind is composed of two copies of the 10 base pair half site motif

5′-RRRCWWGYYY-3′, separated by 0-13 base pairs, with R representing a purine, Y representing a pyrimidine, and W being either an adenine or a thymine.[5] Each half site of the p53 response element has striking internal symmetry, and the entire response element is composed of four 5′-RRRCW-3′ quarter sites of alternating direction.[5] The determined p53 response element was consistent with *in vivo* and *in vitro* studies of the time, suggesting that p53 is able to assemble into a homotetramer.[6,7] Structural analysis via crystallography has also confirmed that p53 self assembles as a tetramer on response element DNA, with each monomer of the p53 tetramer occupying an individual 5′-RRRCW-3′ quarter site.[8] Interestingly, the construct of this response elements allows for hundreds of different distinct DNA sequences simultaneously conforming to this pattern. The determination of the p53 response element led to an explosion of research seeking to determine the genes which p53 regulates as a transcription factor and the physiological impact cellular activity.

In response to DNA-mediated oxidation, p53 bound to its response element DNA has been observed to relinquish its binding to DNA. Investigations of the oxidative dissociation of p53 via DNA charge transport (CT) has led to the study of several synthetic and natural p53 response elements *in vitro*. Oligonucleotide constructs were therefore designed to containin a p53 response element, flanked 5′ end with a 12 base pair linker, to which an anthraquinone (AQ) photooxidant is covalently appended.[9] Excitation of AQ via irradiation abstracts and electron from the DNA, leaving an electron hole among the bases.[10,11] The electron hole then equilibrates along the π-stacked helical axis and is able to oxidize DNA-bound p53, which leads to its dissociation, as depicted in Figure 2.1. It has been found that the oxidative dissociation of p53 in this system is

FIGURE 2.1 — DNA-mediated oxidation of p53 *in vitro.* Schematic illustration of DNA-mediated CT to promote oxidation and dissociation of DNA-bound p53 (green). Distally tethered to oligonucleotide, AQ serves as the photooxidant to selectively oxidize DNA. Upon photoexcitation, the AQ abstracts an electron from the DNA, leaving an electron hole in the DNA duplex that can equilibrate through the DNA to p53, resulting in protein oxidation. The DNA-mediated oxidation of p53 induces a change of p53, resulting in its dissociation, potentially through a conformational change by disulfide formation within the protein.

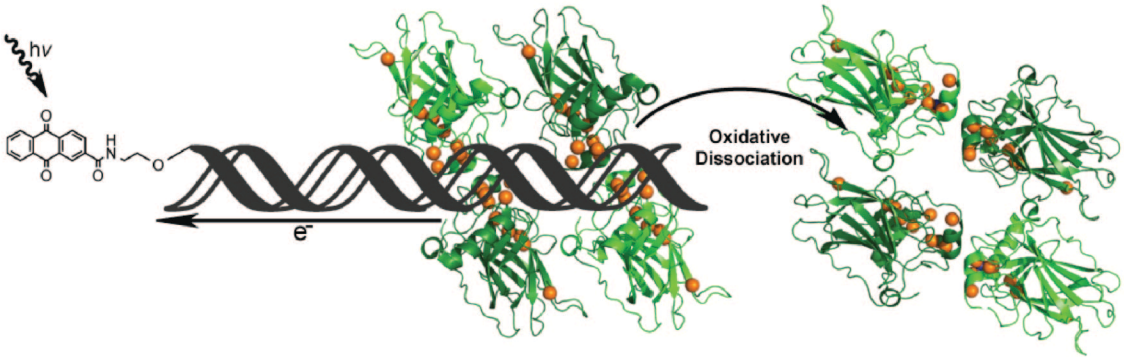

indeed DNA-mediated, since the insertion of a DNA mismatch between the AQ and the p53 response element ablates p53 dissociation.[9] Two human p53 response elements were also studied using the aforementioned construct. The first human p53 response element investigated was cyclin-dependent kinase inhibitor p21 (p21), which is activated by p53 binding and is known to block cell cycle progression out of G1.[12] The second human p53 response element investigated was Gadd45, which is also activated by p53 and is involved in the repair of DNA damage.[12] Apart from being undoubtedly controlled by p53, these two response elements were ideal to study, since they contain the same overall GC% and both sequences for p21 and Gadd45 fully conform to the response element constraints.[5,12] The binding affinities of reduced p53 are also comparable for both p21 and Gadd45, as determined through electrophoretic mobility shift assays (EMSA).[9] DNA-mediated oxidative dissociation of p53 as studied by EMSA determined that p53 readily dissociates from the Gadd45 response element but remains bound to the p21 response element under the same experimental conditions.[9]

The only difference between these two response elements is the order in which the DNA bases are arranged, urging that the DNA sequence of the response elements exert a level of control over p53 in its response to oxidative DNA CT. Interestingly, this sequence selectivity with regard to p53 dissociation as observed *in vitro* appears to correlate with sensical biological regulation of p53 under conditions of severe oxidative genomic stress. Since Gadd45 is involved in DNA repair, dissociation of p53 in response to severe genomic oxidation will lead to an overall downregulation, causing the cell to relinquish futile repair processes.[9] Concurrently, p21 promotes G1 cell cycle arrest, and

continued activation by p53 under severe oxidative genomic stress may lead to cellular senescence and possibly apoptosis.[9]

Due to the contrasting p53 responses from the Gadd45 and p21 response elements, we set out to determine how the p53 response element can dictate whether or not DNA-bound p53 will respond to DNA-mediated oxidation. Our goal is to understand the basis for the DNA sequence selectivity associated with the oxidative dissociation of p53. To investigate this property, we constructed a variety of synthetic response element constructs to tune the one-electron oxidation potentials within the response element, while simultaneously conforming to the response element constraints. Since guanine has the lowest one-electron oxidation potential of all the bases, it serves as an efficient electron hole trap and reactivity correspondingly increases for a guanine doublets and triples, a known hallmark of one-electron DNA oxidation.[13,14] Once the oxidative dissociation of p53 in response to DNA CT was determined on the synthetic response elements, naturally occurring human response elements were then investigated in the same manner. From the information learned herein, we were able to explore how the sequence context may play a role in p53 regulation more generally, enabling us to make predications about the response of p53 to oxidative DNA CT bound to other human response elements.

MATERIALS AND METHODS

Oligonucleotide synthesis and purification. Oligonucleotides were synthesized on an ABI 3400 DNA synthesizer using standard solid phase phosphoramidite chemistry. Light control sequences (LC) not containing a photooxidant were synthesized with the

dimethoxytrityl (DMT) group intact. Cleavage of the oligonucleotide from the resin and deprotection were conducted by incubation in NH_4OH overnight at 60 °C, and subsequently dried *in vacuo*. The oligonucleotides were purified by reversed phase C-18 HPLC (2% to 32% acetonitrile against 50 mM ammonium acetate over 30 min) with the main peak collected and dried *in vacuo*. DMT removal was conducted by a 15 min incubation of the sample solvated in 80% acetic acid. This reaction was then quenched by the addition of 200 proof ethanol and 3 M sodium acetate. Once dry, the oligonucleotides were subjected to reversed phase HPLC once more (2% to 17% acetonitrile against 50 mM NH_4OAc over 30 min).

Oligonucleotides for the anthraquinone (AQ) photooxidant tethered stands were synthesized with the DMT group removed. An AQ derivative, carboxylic acid(2-hydroxyethyl)amide was converted to its respective phosphoramidite and incorporated onto the 5′ end of the sequence using a 15 min coupling on the ABI 3400 DNA synthesizer.[9-11] AQ-conjugated oligonucleotides were cleaved from the resin and deprotected as previously described. The AQ-DNA was purified by reversed phase HPLC (2% to 17% acetonitrile against 50 mM NH_4OAc over 30 min), collecting the peak with absorbance for both DNA at 260 nm and AQ at 365 nm. Oligonucleotides were column desalted (Sep-pak, Millipore), characterized by MALDI-TOF mass spectrometry (Applied Biosystems Voyager DE-PRO), and quantified by UV-visible spectroscopy (Beckman DU7400 spectrophotometer) at their respective ε_{260} values. Double stranded oligonucleotides were formed by thermal annealing of equimolar amounts of complementary single strand, heating at 90 °C for 5 min and cooling to ambient temperature in 5 mM sodium phosphate, 50 mM NaCl, pH 7.5.

Protein production. The p53′ protein used is a full-length human p53 containing three stabilizing mutations: M133L, V203A, and N268D.[15] The gene for p53′ was cloned from the quadruple mutant p53 plasmid N239Y/M133L/V203A/N268D.[15] PCR mutagenesis by overlap extension and gene splicing was used to restore N239 and the sequence was verified by Laragen.[16] The plasmids were propagated in DH5α cells grown on 2yt media (16 g tryptone, 10 g yeast extract, 5 g NaCl; per 1L) plates with 30 μg/ml kanamycin plates and isolated using a miniprep kit (Qiagen). The p53′ protein was overexpressed and purified as described previously.[17] The protein was overexpressed in BL21(DE3) cells 2yt media with kanamycin and grown at 37 °C to a volume of 6 L and an optical density at 600 nm of 0.6-0.8. The cells were induced by 1mM of IPTG and 0.1 mM of zinc sulphate and allowed to express for 16 hours at 22 °C. At this point the cells should be pelleted by centrifugation and frozen at -80 °C.

The cells then can be defrosted on ice and suspended in nickel column buffer (50 mM KPi, pH 8; 300 mM NaCl; 10mM imidazole; 15 mM β-mercapto-ethanol and one complete protease inhibitor 1 tablet per liter) and manually homogenized. The homogenized cells were then lysed via microfluidization. The lysate was then cleared by centrifugation and filtered through a 0.2 micron sterile filter unit. The protein was first purified by FPLC using a heparin column, using a linear gradient over 10 column volumes to a final concentration of nickel column elution buffer (50 mM KPi, pH 8; 500 mM NaCl; 10mM imidazole; 15 mM β-mercapto-ethanol and one complete protease inhibitor 1 tablet per liter). The isolated protein was digested overnight at 4 °C with TEV protease (Invitrogen) overnight to remove the appended His tag. The protein isolate was then purified once more using FPLC with a heparin column, from 25 mM phosphate, pH

7.5, and 10% glycerol to 25 mM phosphate, pH 7.5, 1.0 M NaCl, and 10% glycerol over 10 column volumes. Dithiothreitol was diluted to nanomolar levels with p53 buffer (20 mM Tris, 100 mM KCl, 0.2 mM EDTA, 20% glycerol, pH 8.0) before the protein was flash-frozen and stored at -80 °C.

5′ oligonucleotide radiolabeling. Single stranded oligonucleotides were 5′ labeled with ^{32}P-g-dATP (Perkin Elmer) as described.[18] Purification of the oligos via denaturing gel electrophoresis is essential prior to annealing. The purified samples were dried *in vacuo* and resuspended in 5 mM potassium phosphate, 50 mM NaCl, pH 7.5.

3′ oligonucleotide radiolabeling. 3′ radiolabeling was carried out for DNA strands conjugated with anthraquinone at the 5′ end. The AQ oligonucleotides were radiolabeled using ^{32}P-γ dTTP (MP Biomedicals) and Terminal Transferase (New England Biolabs). The samples were mixed at standard NEB protocol conditions, incubated for 2 h at 37 °C, and subsequently passed through two Micro Bio-Spin 6 columns at 3,000 RPM. Purification of the oligos via denaturing gel electrophoresis is essential prior to annealing, and does not affect the tethered AQ. Samples were purified as previously described and the dried purified samples were resuspended in 5 mM potassium phosphate, 50 mM NaCl, pH 7.5.[18]

Electrophoretic mobility assay of p53′. The p53′ protein was allowed to bind to the radiolabeled oligonucleotides with a 1:1 DNA:protein tetramer ratio (100 nM 1% 5′ radiolabeled duplex and 400 nM p53 monomer) in the presence of 5 μM competitor DNA (5′GGAAAAAAAAAAAAAAAAAACC-3′)(IDT), 0.1% NP-40 (Surfact-Amps NP-40, Thermo Scientific), and 0.1 mg/ml BSA (Fraction V, Sigma) in 20 mM Tris-HCl, pH 8.0, 20% glycerol, 100 mM KCl, and 0.2 mM EDTA. The concentration of p53′ used

was dependent upon the K_D of the protein for the natural response elements, ensuring a minimum of 80% DNA bound with p53. Samples were made at 4 °C and irradiated on ice for varying lengths of time using a solar simulator (ORIEL Instruments) with a 1000 W Me/Xe lamp, and internal and expternal UVB/UVC longpass filters to avoid direct DNA strand damage. The radioactivity of each sample was determined by scintillation counting (Beckman LS 5000TD) and normalized prior to loading onto a 10% TBE polyacrylamide gel (Bio-Rad), with the ideal intensity of 300,000 c.p.m. per hour of irradiation of each sample. Each gel was run in 0.5x TBE buffer at 4 °C and 50 V for 1.5 h. DNA from the gel was transferred to Amersham Hybond-N nucleotide blotting paper (GE Healthcare) by semi-dry electroblotter (Owl HEP-1) for 1 h at 175 mA in transfer buffer (25 mM Tris, HCl, 200 mM glycine, 10% methanol, pH 8.5). The blots were exposed to a blanked phosphorimaging screen (GE Healthcare), imaged by a STORM 820 scanning system (Molecular Dynamics), and analyzed using Image Quant, Excel, and Origin. All data were normalized to the corresponding unirradiated control, and the change in p53 binding was determined by monitoring the signal of free DNA over the total DNA signal per lane.

Assay of oxidative DNA damage. Samples were prepared from a stock solution containing 1 μM 100% ^{32}P-3′ labeled oligomer duplex on the AQ strand, 5 μM competitor DNA, 0.1% NP-40, and 0.1 mg/mL BSA in p53 buffer (20 mM Tris HCl, 100 mM KCl, 0.2 mM EDTA, 20% glycerol, pH 8.0), with the titration of p53′ ranging from 0 to 40 μM. DNA damage was induced by sample irradiation for 1 h while in an ice-water bath, using a solar simulator with internal and external UVB/UVC longpass filters. Irradiated samples were subsequently treated with a 10% piperidine (Sigma) solution

with 0.2 units of calf thymus DNA in water, and heated at 90 °C for 30 min to cleave damage sites. Piperidine was removed by drying samples *in vacuo,* suspending again in water, and drying *in vacuo* once more. The DNA was ethanol precipitated to ensure purity, although in retrospect this step caused the loss of our lower molecular weight DNA pieces. Scintilation counting was used to ensure that equivalent levels of radioactivity were used in each lane. The dry samples were resuspended in denaturing formamide loading buffer, heated for 2 min at 90 °C, then loaded per lane onto a pre-run 20% polyacrylamide gel and run at 90 watts for 3 h in 1x TBE buffer. Sequencing lanes were created by standard Maxam-Gilbert Sequencing reactions.[19] Gels were visualized by phosphorimagery and quantified using ImageQuant TL and Excel.

RESULTS

p53′-DNA electromobility gel shift assays with synthetic p53 response elements.

The protein used in all of the following experiments is a full-length human p53 containing three thermodynamically stabilizing mutations: M133L, V203A, and N268D.[15] This mutant protein is designated as p53′. The stabilizing mutations for p53′ were based on research from the Fersht laboratory for a stabilized yet active p53.[15] For the three mutations in use, preliminary experiments determined that p53′ maintained its capacity to respond to oxidative DNA CT by dissociation. Four synthetic DNA response elements were constructed and used for *in vitro* experiments to determine the influence of the guanine pattern in enabling oxidative dissociation of DNA-bound p53′ by DNA CT. The oligonucleotides were designed to contain the canonical p53 response element pattern comprised of two response element half sites with no linking bases between the

sites. As seen in Figure 2.2, the response element site site is flanked 5′ with a 12 base pair linker to which the anthraquinone photooxidant (AQ) is covalently appended, and a ^{32}P radiolabel for the visualization of the DNA is located on the 5′ end of the complementary strand. DNA-mediated oxidation of p53′ induces a change in protein affinity for response element DNA and promotes its dissociation, which we can monitor by EMSA.

The purine content of the four synthetic constructs range from containing no sequential guanine bases to four sets of guanine triplets, all while fully conforming to response element constraints. Relative reactivity of the bases to one-electron oxidation varies as follows: 5′-GGG > 5′-GG > 5′-GA > 5′-AA.[13,14] Dissociation constants for p53′ to these oligonucleotides lacking AQ are provided in Table 2.1. The change in p53′ binding upon photooxidation is determined as the fraction of free DNA signal over total DNA signal per lane, normalized to its respective un-irradiated control, with error bars reflecting the standard error of the mean obtained over a minimum of three replicates. All samples contained 100 nM of response element DNA and 400 nM of p53′ to ensure a 1:1 ratio of DNA to p53′ tetramer.

The degree of p53′ oxidative dissociation is found to vary according to the sequence of the oligonucleotide and is dependent upon photoexcited anthraquinone, as depicted in Figure 2.3. All constructs of light control DNA strands (LC), which are irradiated but do not contain an appended anthraquinone for oxidation, display negligible dissociation of p53′. Dissociation from all of the sequences displays a relatively linear trend with respect to irradiation time, with a maximum dissociation of p53′ observed after 30 min. Longer irradiation past 30 min did not significantly increase overall p53

FIGURE 2.2 — Oxidative dissociation of p53′ by EMSA from sequences with varied redox potentials. Top: The oligonucleotide construct for investigating the DNA-mediated oxidation of p53′ contains the p53 response element. Oxidative DNA CT is induced by irradiation of the appended anthraquinone photooxidant. The red asterisk of the complementary strand denotes the location of the ^{32}P label for visualization. Bottom: Representative autoradiogram of a p53′ EMSA of the synthetic GGG sequence. Light control samples do not have an anthraquinone photooxidant conjugated to the DNA, and the overall amount of DNA-bound p53′ changes minimally with irradiation. The anthraquinone samples contain the appended AQ photooxidant, and an increase in the amount of lower-molecular weight free DNA is observed with respect to irradiation time.

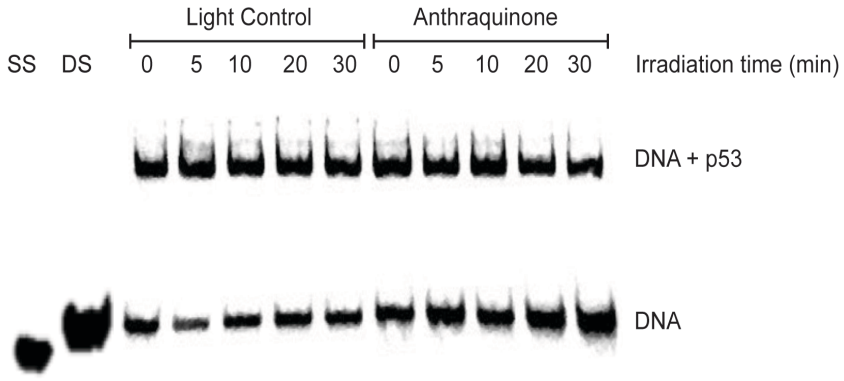

TABLE 2.1 — Oligonucleotide constructs for synthetic and natural p53 response elements studied by EMSA.

Construct Name	DNA Sequence (5′-3′)[a]	K_D (nM)[b]	GC %[c]	GG[d]	GGG[e]
AAA	AAATCAGCACTAAAACATGTCTAAACATGTCT	230 ± 40	30.0 %	-	-
AGG	AAATCAGCACTAAGGCATGTCTAGGCATGTCT	430 ± 110	50.0 %	2	-
GGG	AAATCAGCACTAGGGCATGTCTGGGCATGTCT	360 ± 70	60.0 %	-	2
GGG/GGG	AAATCAGCACTAGGGCATGCCCGGGCATGCCC	220 ± 40	80.0 %	-	4
CASP1	AAATCAGCACTAATAAAGACATGCATATGCATGCACA	610 ± 80	36.0 %	-	-
S100A2	AAATCAGCACTAGGGCATGTGTGGGCACGTTC	330 ± 20	65.0 %	-	2

a. Locations of altered purine nucleobases in direct p53 contact are underlined in the synthetic constructs.

b. Apparent K_D of p53´ was determined at 100 nM duplex, 5 μM dAdT, 0.1% NP-40, 0.1 mg/ml BSA in 20 mM TrisCl (pH 8.0), 20% glycerol, 100 mM KCl, and 0.2 mM EDTA and electrophoresed at 4 °C and 50 V on a 10% polyacrylamide gel in 0.5x TBE.

c. GC% of response element, not including 5′ linker.

d. Number of guanine doublets within the response element.

e. Number of guanine triplets within the response element.

FIGURE 2.3 — Oxidative dissociation of p53′ from synthetic p53 response elements. A plot quantifying the percent change in p53′-DNA binding with respect to irradiation time for the four different synthetic response elements compared to the LC. Sequence constructs are located in Table 2.1. The percent change in p53′ binding is determined as the free DNA signal over the total lane signal, normalized to the unirradiated control. Error bars reflect the standard error of the mean over a minimum of three replicates. Samples contained 100 nM duplex, 400 nM p53′ monomer, 5 µM dAdT, 0.1% NP-40, 0.1 mg/ml BSA in 20 mM TrisCl (pH 8.0), 20% glycerol, 100 mM KCl, and 0.2 mM EDTA.

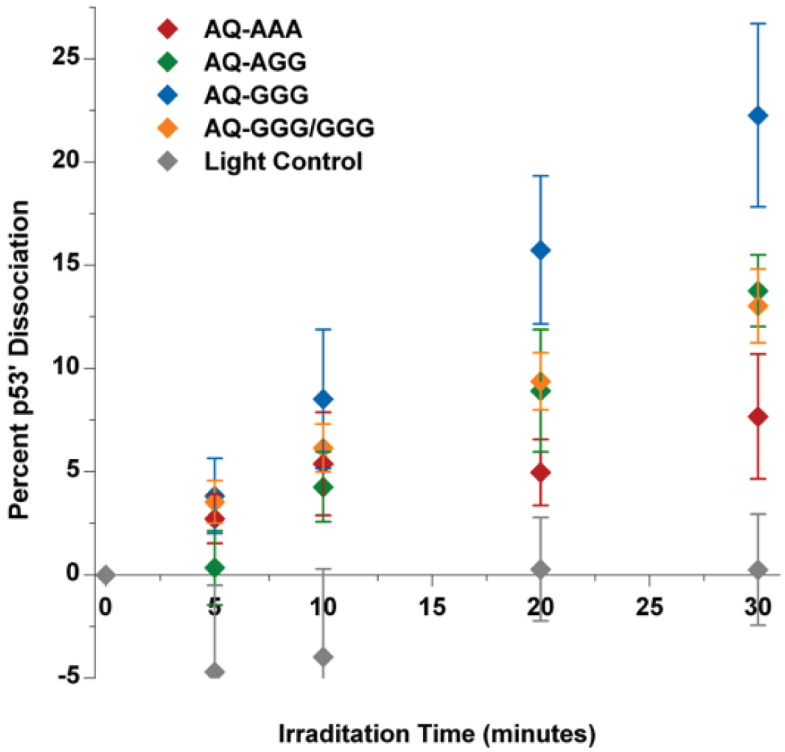

oxidative dissociation. The AQ-AAA sequence confers the least amount of oxidatively induced dissociation of p53′ with a maximum dissociation of 7.7%. The AQ-AGG and AQ GGG/GGG sequence both display similar extents of dissociation with a maximum of 13.8% and 13.0%, respectively. The DNA sequence that displayed the greatest amount of p53′ dissociation is AQ-GGG at 22.3%. Thus the highest levels of DNA CT oxidative dissociation of p53′ were observed from response elements with low redox potential guanine doublets and triplets.

p53′-DNA electromobility shift assays with human p53 response elements.

To determine whether the gel shift results obtained from the synthetic sequences are applicable to naturally occurring human p53 response elements, two human p53 response elements were also investigated: Caspase1A (CASP) and S100 calcium binding protein A2 (S100A2). DNA sequence constructs using their respective response elements and their relative dissociation constants are also shown in Table 2.1. Caspase1A is a cysteine-dependent aspartate-directed proteases and plays essential roles in apoptosis, necrosis, and inflammation.[20] This human p53 response element promotes the production of caspase when p53 is bound. The response element of Caspase1A is similar to the synthetic AAA sequence, with an adenine triplet within the purine region of the response element and no guanine doublets or triplets in either of the complementary strands.[20] Conversely, the S100A2 protein is intimately involved in cell cycle progression, cellular differentiation, and may function as a tumor suppressor.[21,22] When p53 is bound to this guanine-rich sequence, S100A2 protein production is promoted. The S100A2 response element is very similar to the synthetic GGG sequence, containing two guanine triplets

within the purine regions. The human response elements were constructed in the same manner as the synthetic sequences above, with an appended 5′-anthraquinone photooxidant, the same 12 base linker, and the complementary strand labeled with 5′ ^{32}P-ATP. The relative dissociation constant (K_D) for p53 with each sequence was determined by gel shift assay and quantified by ImageQuant and Excel, and located in Table 2.1.

Experiments were conducted at the protein concentration at which 80% of the radiolabeled oligonucleotides were bound with p53′, based upon their respective K_D values (500 nM for the S100A2 sequence and 800 nM for the Caspase1 sequence). As seen in Figure 2.3, the AQ-S100A2 sequence with two guanine triplets yields oxidative dissociation of bound p53′ at 14.0%, while the AQ-Caspase1 sequence yields significantly less oxidative dissociation, with a maximum of 6.4%. These sequences do not oxidize p53 linearly with irradiation, instead leveling out at earlier irradiation time points.

Comparison between natural and synthetic p53 response elements.

Figure 2.5 shows the direct comparison between synthetic and natural human sequences. We find that synthetic and natural response elements with varied oxidation potentials due to altered purine patterns within the p53 response element exhibit the following trend in increasing p53 oxidation: AQ-AAA, AQ-Caspase1A (red) < AQ-GGA, AQ-GGG/GGG, and AQ-S100A2 (blue) < AQ-GGG (green).

The AQ-Caspase1A sequence displays minimal dissociation of p53′ upon photooxidation, comparable to that seen with the synthetic AQ-AAA sequence. The high redox potential adenine triplet within the purine region does not allow for facile transfer of an electron hole from the DNA to the bound p53′. The AQ-S100A2 sequence, in

FIGURE 2.4 — Oxidative dissociation of p53′ from human response elements. A plot quantifying the percent change in p53′-DNA binding with respect to irradiation time for the natural human p53 response elements Caspase1A and S100A2. Sequence constructs are located in Table 2.1. The fraction of p53′ dissociation was determined as a ratio of the percent of bound DNA in the irradiated sample to that in the dark control. Error bars reflect the standard error of the mean obtained from a minimum of four trials. Samples contained 100 nM duplex, 500 nM p53 monomer for S100A2, and 800 nM for p53 monomer CASP, 5 µM dAdT, 0.1% NP-40, 0.1 mg/ml BSA in 20 mM TrisCl (pH 8), 20% glycerol, 100 mM KCl, and 0.2 mM EDTA.

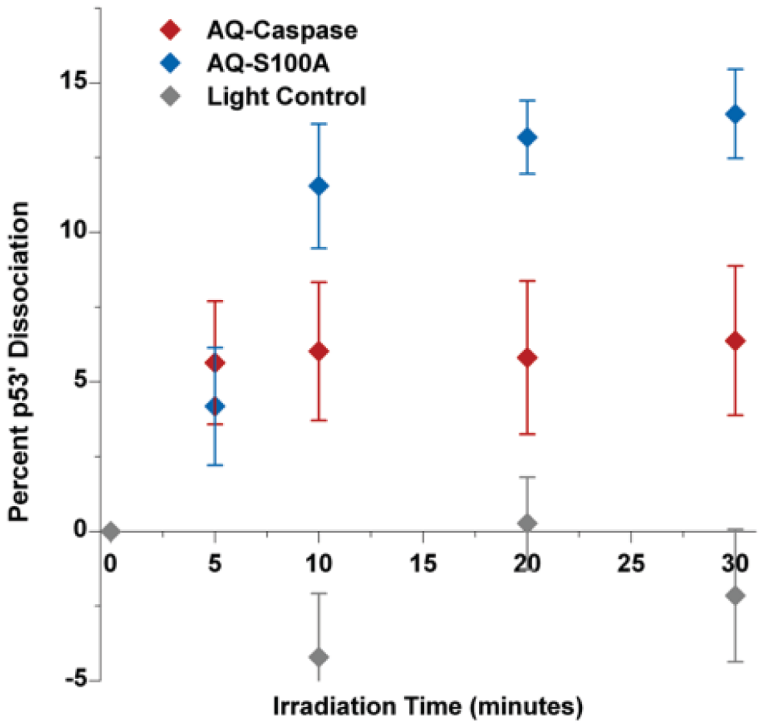

FIGURE 2.5 — Synthetic and human p53 response element EMSA comparison. Comparison of synthetic and natural human p53 response element DNA EMSA data. On the right in red, AQ-CASP1 and AQ-AAA display minimal oxidative dissociation even at long irradiation times. The sequences that allow for oxidative dissociation of p53′ (AQ-S100A2, AQ-AGG, and AQ-GGG/GGG) are compared on the left in blue. AQ-GGG in green displays the most oxidative dissociation of p53′.

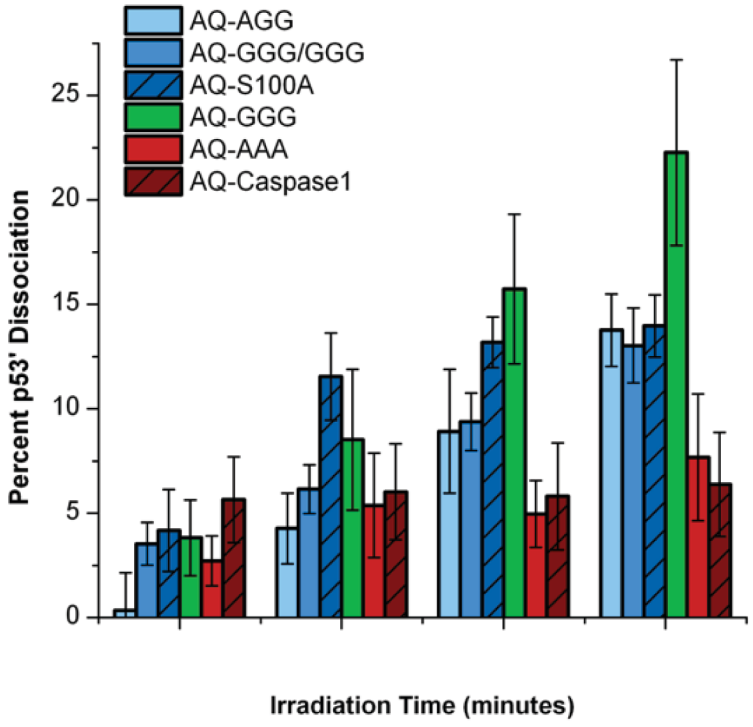

contrast, displays high levels of oxidative dissociation upon irradiation, similar to the AQ-AGG and AQ-GGG/GGG synthetic sequences at 30 minutes of irradiation. Therefore, even with different sequences the guanine pattern within the purine region of the response element allows for equivalent oxidative dissociation of p53′ with equivalent amounts of irradiation.

Long range oxidative damage with and without p53′ examined by denaturing polyacrylamide gels.

To determine the exact locations within the synthetic oligonucleotides to which the electron holes localize, denaturing polyacrylamide gels were used to determine sites of oxidative DNA damage. The oligonucleotides were 3′-^{32}P radiolabeled on the AQ strand for visualization, and treated with piperidine to cleave the DNA backbone at the site of oxidative damage.[19] When compared to Maxam-Gilbert sequencing lanes and the un-irradiated control, the locations of DNA oxidative damage induced by photooxidation are observed as bands on the denaturing polyacrylamide gel. The intensity of each piperidine cleavage site is measured in comparison to the total signal intensity of each lane. The p53′ protein was also titrated into the samples to assess how the protein inhibits DNA damage. The presence of p53′ inhibits DNA damage by transfer of the electron hole from the DNA to the protein, as shown in Figure 2.6 and Figure 2.7.

Oxidative damage is apparent primarily at the 5′-G of guanine doublets and triplets within the response elements, as expected thermodynamically. After an hour of irradiation for the AQ-AAA sequence, which lacks guanine repeats, oxidative damage is observed only at the single 5′-G located near the tethered oxidant; this guanine is not contained within the response element. Additionally, damage at this guanine is not

FIGURE 2.6 — Representative guanine oxidation gel shift assay analysis. The four 3′ radiolabled synthetic response element lane profiles are displayed at varying protein concentrations. The gels were analyzed using Imagequant, and each band was calculated as the percent of total lane signal. The dotted black line represents the unirradiated control. The concentration of p53′ in the irradiated samples is varied from 0 µM (red) to 40 µM (purple) p53′ monomer. Samples contained 1 µM AQ-Duplex, 5 µM dAdT, 0.1% NP-40, 0.1 mg/ml BSA in 20 mM TrisCl (pH 8), 20% glycerol, 100 mM KCl, and 0.2 mM EDTA.

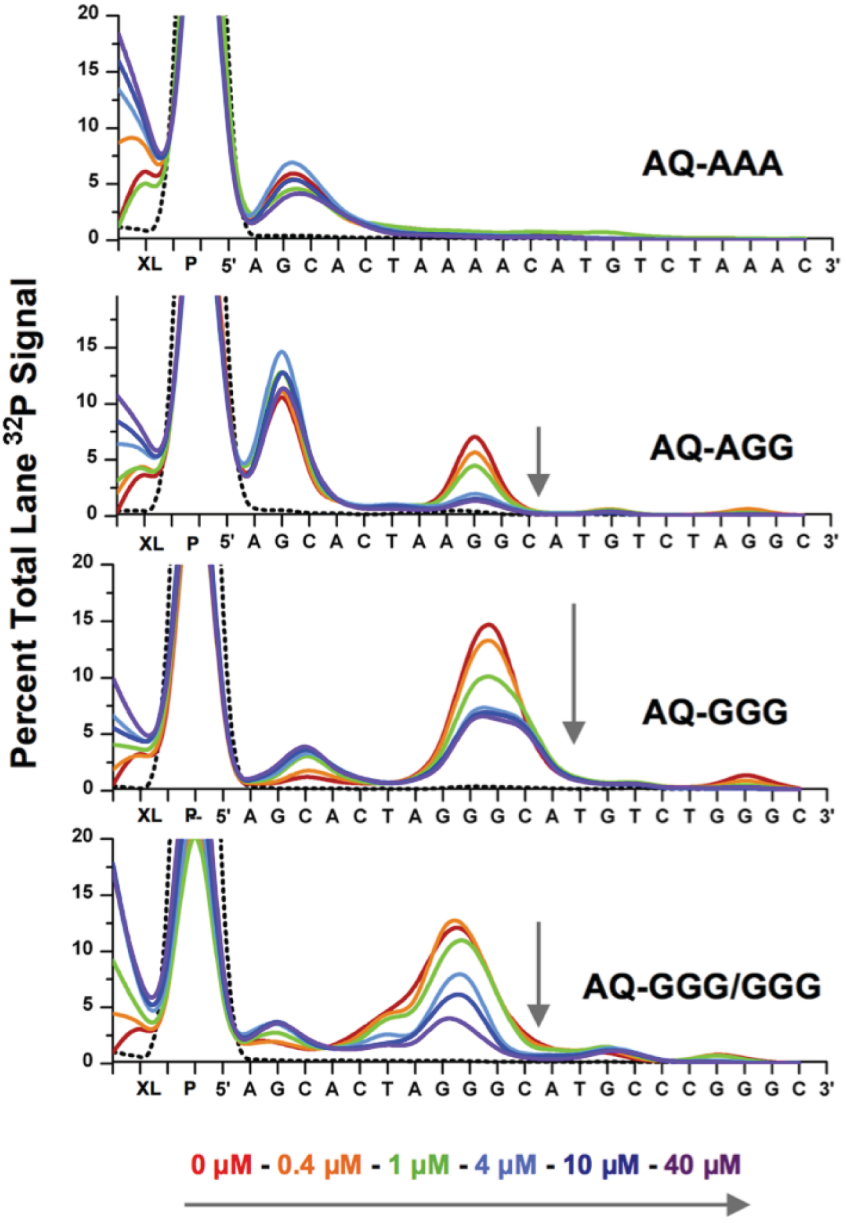

FIGURE 2.7 — Representative autoradiograms of the guanine oxidation gel shift assays. The AQ-conjugated synthetic response element oligonucleotides with a 3′ radiolabel. Lanes 1 and 2 are the Maxam-Gilbert sequencing lanes corresponding to pyrimidies (C/T) and purines (A/G). Individual bases are designated on the left along with the parent band (P) and the crosslinked bands (XL). The dark control in lane 3 was not irradiated and contained no p53′. The following lanes 4-9 are irradiated samples with varied concentrations of p53′ from 0 to 40 μM of p53′ monomer, respectively. Samples contained 1 μM AQ-Duplex, 5 μM dAdT, 0.1% NP-40, 0.1 mg/ml BSA in 20 mM TrisCl (pH 8), 20% glycerol, 100 mM KCl, and 0.2 mM EDTA. Ethanol precipitated samples were suspended in formamide loading dye and run on a pre-run 20% polyacrylamide denaturing gel at 90 watts for 3 h in 1x TBE buffer.

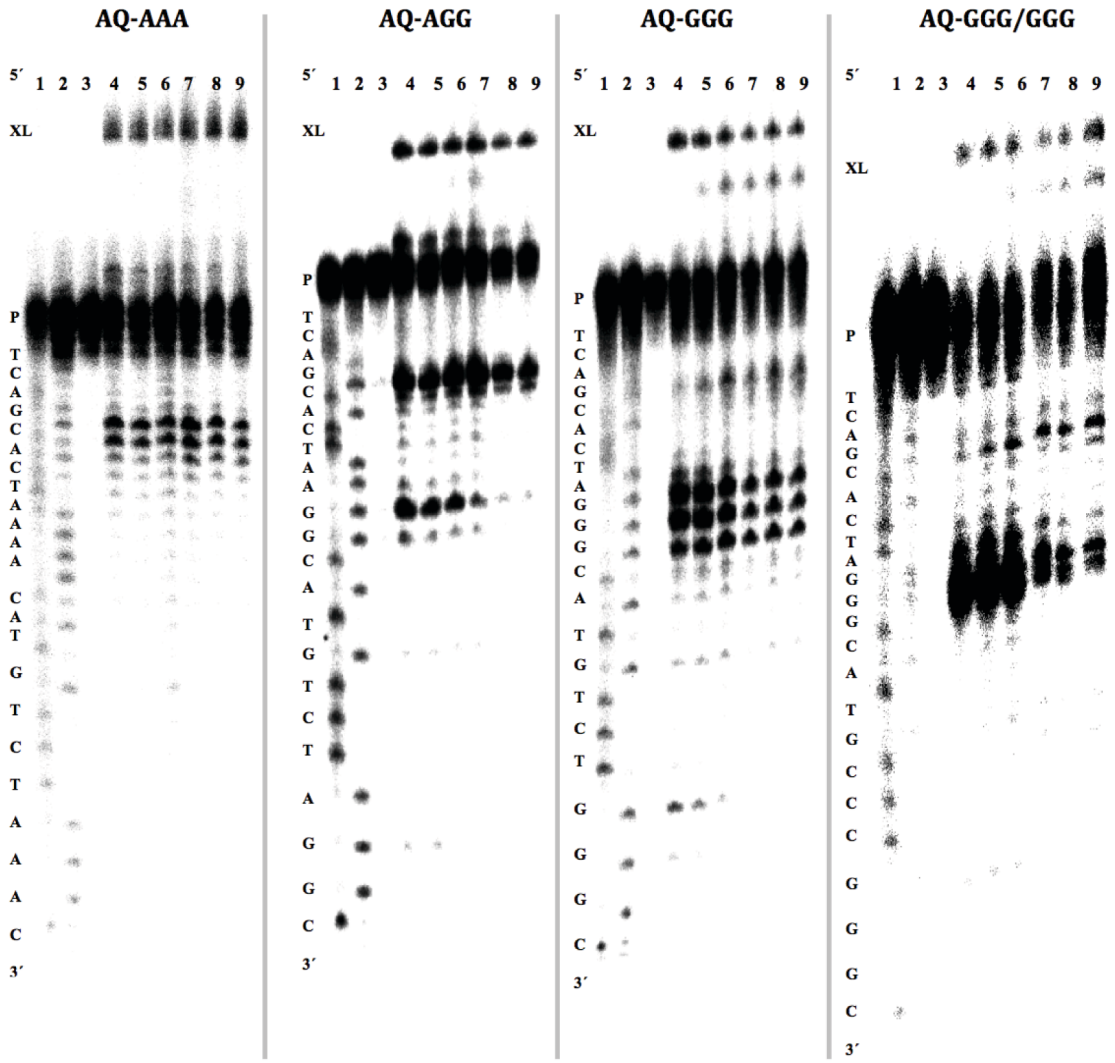

inhibited upon addition of p53′ at any concentration. The AQ-AGG sequence displays damage within the response element primarily at the 5′-GG location and at the single guanine located in the linker region, adjacent to the oxidant. Upon the addition of 10-fold excess p53′ tetramer, a full recovery of the damage within the response element guanine doublet is observed. In contrast, no recovery is observed at the single guanine in the linker region. Sequences AQ-GGG and AQ-GGG/GGG both displayed the majority of their oxidatively induced damage at the 5′-guanine triplet site within the response element, with no significant damage in the linker region. The addition of p53′ to both AQ-GGG and AQ-GGG/GGG mitigates DNA base damage within the response element. In these sequences the damage is not fully quenched by concentrations of p53′ up to 40 μM.

Damage was not readily observed at the purine regions near the 3′ end. Ethanol precipitation of the samples may have led to the loss of these low molecular weight products. In all of the sequences, some higher molecular weight products are also observed and can be attributed to the formation of covalently cross-linked products. Irradiation without the addition of p53′ gives one band which is indicative of a crosslink between the two DNA strands. The higher molecular weight bands are indicative of possible p53-DNA crosslinks.

DISCUSSION

Sequence dependence of p53′ dissociation.

Electron holes in DNA localize to regions of low redox potential, most notably guanine doublets and triplets. Specific sequences of oligonucleotides incorporating

guanine doublets and triplets into the purine regions of the response element site enabled the study of how the guanine pattern in p53 response element binding sites influences oxidative dissociation of p53. Sequences containing low redox potential guanine doublets and triplets enable oxidative dissociation of p53′; we refer to these as responsive sequences. Figure 2.2 shows maximum p53′ dissociation from the responsive sequences of AQ-GGG at 22.3%, followed by AQ-AGG, AQ-GGG/GGG around 13.0%. The AQ-AAA sequence confers minimal p53′ dissociation of 7.7%, and we categorize this as a non-responsive sequence.

Electron hole occupancy at a particular location can be described in the context of overall residence times. When equilibrating along the π-stacked DNA helical axis, an electron hole will spend more time at a low redox potential GGG site rather than a high redox potential AAA site. The finding that the AQ-GGG/GGG sequence did not yield the most oxidative dissociation of p53′ is noteworthy. In the double-stranded promoter site, the AQ-GGG sequence has two locations in which holes can reside, while the AQ-GGG/GGG has four. Effectively, the electron hole density in each GGG site of AQ-GGG/GGG is half of that of AQ-GGG, resulting in approximately half the p53′ dissociation as compared to AQ-GGG.

Importantly, the location of low redox potential sites should align with the p53-DNA major groove interface with the p53 DNA-binding domain to enable effective electron transfer. Thus, not all low potential sites within a response element are expected to transfer an electron hole to p53′, only those in close contact with the protein. It is known that CT in proteins decays exponentially with distance, highlighting the necessity for low reduction potential bases at the DNA-p53 interface for this process to occur. The

denaturing DNA damage gels of Figure 2.6 and Figure 2.7 illustrate the necessity both of proper p53 contact for electron hole transfer and of the redox potentials of purines in contact with p53 for conferring a sensitive response. As highlighted in the AQ-AAA and AQ-AGG sequences, damage does occur at the guanine in the linker region, but that damage is not inhibited by the addition p53′ at any concentration investigated. The inhibition of DNA damage in the presence of p53 is seen only at low redox potential sites in the p53 response element, and therefore in contact with p53′. Moreover, for oxidative dissociation of p53′ to occur, the bases in contact with p53′ must be able to initially trap the electron hole with an overall low redox potential. Thus the hole localization within the response element ultimately dictates the response the response element will confer for the oxidative dissociation of p53.

To establish whether natural p53 binding sites respond similarly to the synthetic ones, two sequences were studied. The natural sequences were found to behave similarly to their synthetic counterparts due to similar guanine patterns in the purine region of the response elements. Upon oxidation, p53′ dissociates from S100A2, which is similar to the responsive synthetic sequences due to the presence of two guanine triplets; S100A2 is thus classified as a responsive sequence. Since p53 promotes S100A2 expression when bound, oxidative stress would lead to p53 dissociation and subsequent downregulation of the gene, resulting in diminished tumor suppressor activity. In contrast, the CASP1 sequence is similar to the AQ-AAA synthetic sequence. Minimal dissociation of p53′ from CASP is observed upon irradiation, designating the CASP p53 response element as non-responsive. Thus, upon oxidation, p53 would be expected to remain mostly bound, leading to the continued promotion of CASP. The continual promotion CASP production

by p53 during times of oxidative genomic stress signals the cell to continue toward apoptosis.

Making predictions about natural p53 response elements under genomic oxidative stress.

We can also compare these results to our earlier work that demonstrated a contrasting oxidation response in p53 between recognition elements corresponding to Gadd45 (DNA repair) and p21 (cell cycle arrest), now known as CDKN1A.[9] These p53 binding sites contain identical G/C percentages but display different guanine patterns overall. The p53-bound Gadd45 sequence can be classified as responsive, yielding oxidative dissociation of p53. In contrast, little p53 oxidation was seen from the p21 sequence, characterizing this site at non-responsive. Figure 2.8 highlights the p53 residues that nest in the major groove (blue: K120, S121, C277, and R280) and the bases of the response element with which they directly interact (black). As a general example, Figure 2.8A depicts two half-sites with no intervening spacer base pairs, highlighting the importance of low redox potential guanines at the 5′-RRRG-3′ site in direct p53 contact for responsiveness. The p53 response element is known to contain a 0-13 base pair linker region between the two p53 half sites; certain p53 binding sites may conform to these designated constraints but contain low redox potential sites that are not in direct contact with p53. Figure 2.8B depicts p53 binding to a response element with a 10 base linker between the two half sites. Guanine triplets located within such a linker region would be favorable locations for electron hole localization, but the electron holes would be funneled away from the direct p53 contact sites and the overall responsiveness of that site

FIGURE 2.8 — Response element DNA–p53 interaction. All diagrams are representations modeled from the 3KMD crystal structure by Chen *et al.*[23] A. p53 tetramer (green) bound to canonical response element represented by letters. The contacting p53 residues are shown in blue and the nucleobases that they hydrogen bond with are noted by black letters. B. Representation of a p53 tetramer bound to a response element with a 10 nucleobase linker between the two half sites C. Representative binding of a p53 tetramer to the Gadd45 response element. The orange circles indicate anticipated locations for an electron hole to localize within direct contact of a p53 monomer. D. Representative binding of a p53 tetramer to the p21 response element. The expected location of electron hole localization is denoted by the orange circle and located between the two half sites and away from direct p53 contact.

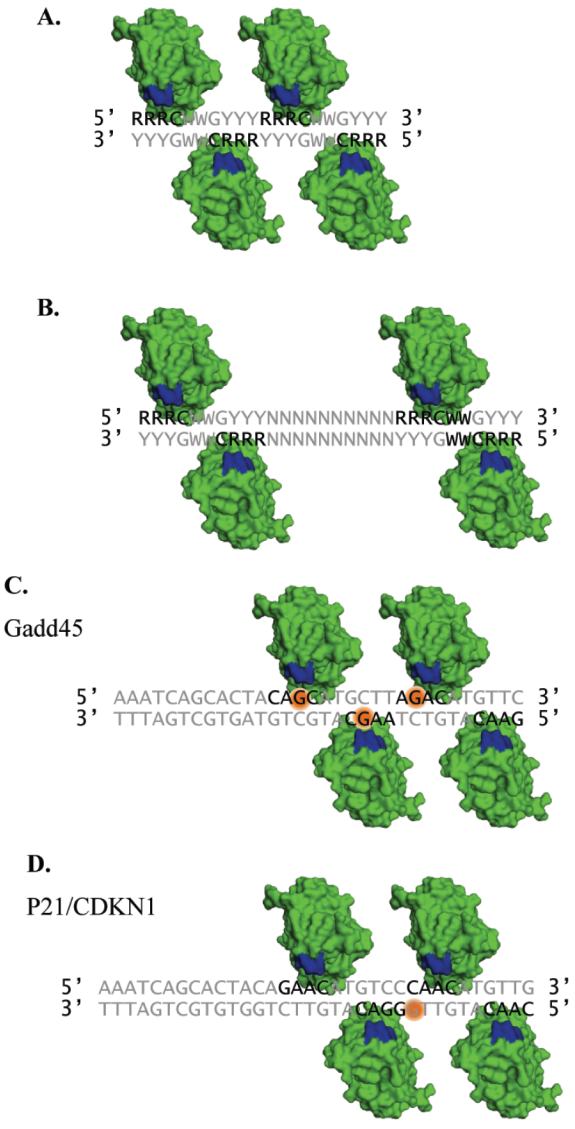

would therefore be decreased. The response element sequence for Gadd45 is shown to be responsive by gel shift assay *in vitro*.[9] Figure 2.8C illustrates that the p53 response element for Gadd45 indeed has guanines directly aligned with the p53 contact residues, and these guanines enable the overall responsiveness of this p53 binding site. The recognition sequence for p21 is shown in Figure 2.8D. This p53 binding site contains a low redox potential guanine triplet in the complement strand, but the 5′ guanine is located at the interface of the two half sites, away from the contacting p53 residues in the major groove. Upon oxidation, an electron hole would preferentially localize to the 5′ location of the guanine triplet at the interface of the two half sites, out of direct p53 contact, decreasing the opportunity for oxidation of p53, rendering the sequence non-responsive.

These results enable us to make predictions regarding the responsiveness of other human p53 response elements to DNA CT. Out of more than 200 known human p53 binding sites, we focused on sequences containing the canonical 5′-CWWT-3′ in both half-sites. An illustrative set of sequences, 21 which we felt confident in making predictions, is provided in Table 2.2.[24-27] Here, we highlight several interesting p53 response element predictions. Non-responsive p53 binding sites include chromosome 12 open reading frame 5 (C12orf5) and matrix metallopeptidase 2 (MMP2).[27,28] For both of these genes, p53 serves as an activator. Under conditions of oxidative stress, we predict p53 binding should not be affected by DNA CT and there should be no significant change in the regulation of that gene. C12orf5 will continue to be promoted, directing the glycolysis pathway into the pentose phosphate shunt, while also protecting the cell from reactive oxygen species.[27] MMP2, also predicted to be non-responsive, is involved in the

TABLE 2.2 — Predictions of p53 responsiveness to oxidative DNA CT on human response elements.

Gene	First quarter site	Second quarter site	Linker	Third quarter site	Fourth quarter site	Predicted Responsiveness	p53 Activity	Predicted CT Response of p53	Δ gene regulation	Ref.
AIFM2	AGGCA	TGAGC	CACCGTGCCT	GGCCA	AGCCC	**AIFM2**	Activator	Dissociation	Downregulation	32
	Yes	Yes	Traps	Yes	Yes	**Yes**				
APAF1	AGACA	TGTCT	GGAGACCCTAGGA	CGACA	AGCCC	**APAF1**	Activator	Dissociation	Downregulation	33
	No	No	Traps	No	Yes	**No**				
BBC3	CTGCA	AGTCC		TGACT	TGTCC	**BBC3**	Activator	Dissociation	Downregulation	34
	Yes	Yes		No	Yes	**Yes**				
C12orf5	AGACA	TGTCC	AC	AGACT	TGTCT	**C12orf5**	Activator	Dissociation	Downregulation	35
	No	Yes		No	No	**No**				
CCNK	AAACT	AGCTT	GC	AGACA	TGCTG	**CCNK**	Activator	Dissociation	Downregulation	36
	No	Yes		No	Yes	**Yes**				
CDKN1A	GAACA	TGTCC		CAACA	TGTTG	**CDKN1A**	Activator	Remains Bound	No Change	37
	No	Yes		No	No	**No**				
DDB2	GAACA	AGCCC	T	GGGCAT	TGTTT	**DDB2**	Activator	Dissociation	Downregulation	38
	No	Yes		Yes	No	**Yes**				
FAS	GGACA	AGCCC		TGACA	AGCCA	**FAS**	Activator	Dissociation	Downregulation	39
	Yes	Yes		No	Yes	**Yes**				
GADD45A	GAACA	TGTCT		AAGCAT	TGCTG	**GADD45A**	Activator	Dissociation	Downregulation	40
	No	No		Yes	Yes	**Yes**				
IGFBP3	AAACA	AGCCA	C	CAACA	TGCTT	**IGFBP3**	Repressor	Dissociation	Upregulation	41
	No	Yes		No	Yes	**Yes**				
MMP2	AGACA	AGCCT		GAACT	TGTCT	**MMP2**	Activator	Dissociation	Downregulation	42
	No	Yes		No	No	**No**				
PERP	AGGCA	AGCTC		CAGCT	TGTTC	**PERP**	Activator	Dissociation	Downregulation	43
	Yes	Yes		Yes	No	**Yes**				
PLK2	AAACA	TGCCT		GGACT	TGCCC	**PLK2**	Activator	Dissociation	Downregulation	44
	No	Yes		Yes	Yes	**Yes**				
PPM1J	GAACA	TGCCT		GAGCA	AGCCC	**PPM1J**	Activator	Dissociation	Downregulation	45
	No	Yes		Yes	Yes	**Yes**				
PTEN	GAGCA	AGCCC	CAGGCAGCTACACT	GGGCA	TGCTC	**PTEN**	Activator	Dissociation	Downregulation	46
	Yes	Yes (No)	Traps	Yes	Yes	**Yes**				
RRM2B	TGACA	TGCCC		AGGCA	TGTCT	**RRM2B**	Activator	Dissociation	Downregulation	47
	No	Yes		Yes	No	**Yes**				
SCARA3	GGGCA	AGCCC		AGACA	AGTTG	**SCARA3**	Activator	Dissociation	Downregulation	48
	Yes	Yes		No	No	**Yes**				
TP63	TAACT	TGTTA	TTG	AAACA	TGCTC	**TP63**	Activator	Remain Bound	No Change	49
	No	No		No	Yes	**No**				
TSC2	TAACA	AGCTC	G	GGGCT	AGCCC	**TSC2**	Activator	Dissociation	Downregulation	50
	No	Yes	Trap	(No) Yes	Yes	**Yes**				
VCAN	AGACT	TGCCA	C	AGACA	AGTCC	**VCAN**	Activator	Dissociation	Downregulation	51
	No	Yes		No	Yes	**Yes**				
VDR	TAACT	AGTTT		GAACA	AGTTG	**VDR**	Activator	Remains Bound	No Change	52
	No	No		No	No	**No**				

breakdown of extracellular matrix, which is useful for apoptotic processes.[28] In contrast, responsive p53 binding sequences that have been found include damage-specific DNA binding protein 2 (DDB2), polo-like kinase 2 (PLK2), and protein phosphatase, Mg^{2+}/Mn^{2+} dependent, 1J (PPM1J).[29-31] In all of these cases, p53 binding promotes the expression of these genes. As these sequences appear to be responsive based on the purine pattern, we predict p53 oxidative dissociation by DNA CT, which will decrease p53 occupancy and cause an overall downregulation of the corresponding gene products. DDB2 is necessary for the repair of DNA damage induced by ultraviolet light within the nucleotide excision repair pathway.[29] PLK2 is a member of the polo family of serine/threonine protein kinases, playing a primary role in normal cell division, and is necessary for the G1/S transition.[30] PPM1J encodes a serine/threonine protein phosphatase of unknown overall function.[31] In all of these cases, oxidation should lead to overall gene downregulation, leading to lowered MMR pathway activity and tuning of cell cycle control.

The pattern and location of bases in the p53 binding site have been shown to play a critical role in how p53 may regulate the expression of different genes under conditions of oxidative stress. DNA sequences with triplet guanine sites that make contact with p53 protein binding sites are particularly prone to activate oxidation of the bound protein under conditions of oxidative stress. This protein oxidation offers another layer of regulatory control and a means of modifying specific proteins post-translationally to respond to an environmental signal. The fact that this modification can occur from a distance through DNA CT is more powerful still in permitting a host of regulatory effects on the genome that respond specifically and chemically to the guanine radicals generated

with oxidative stress. Indeed, these results illustrate another unique role to consider for long range CT within the cell.

REFERENCES

1. Miled, C., Pontoglio, M., Garbay, S., Yaniv, M., and Weitzman, J. (2005) A genomic map of p53 binding sites identifies novel p53 targets involved in an apoptotic network. *Cancer Research 65*, 5096-5104.

2. Vousden, K., and Prives, C. (2009) Blinded by the light: The growing complexity of p53. *Cell 137*, 413-441.

3. Fischer, M., Steiner, L., and Engeland, K. (2014) The transcription factor p53: Not a repressor, solely an activator. *Cell Cycle 13*, 3037-3058.

4. O'Keefe, K., Li, H., and Zhang, Y. (2003) Nucleocytoplasmic shuttling of p53 is essential for MDM2-mediated cytoplasmic degradation but not ubiquitination. *Mol. Cell. Biol. 23*, 6396-6405.

5. el-Deiry, W., Kern, S., Pietenpol, J., Kinzler, K., and Vogelstein, B. (1992) Definition of a consensus binding site for p53. *Nat. Genet. 1*, 45-59.

6. Kraiss, S., Quaiser, A., Oren, M., and Montenarh, M. (1988) Oligomerization of oncoprotein p53. *J. Virol. 62*, 4737-4744.

7. Weinberg, R. A. (1991) Tumor suppressor genes. Science 254, 1138-1146.

8. Cho, Y., Gorina, S., Jeffrey, P. D., and Pavletich, N. P. (1994) Crystal-structure of a p53 tumor-suppressor DNA complex: Under- standing tumorigenic mutations. *Science 265*, 346-354.

9. Augustyn, K., Merino, E., and Barton, J. K. (2007) A role for DNA-mediated charge transport in regulating p53: Oxidation of the DNA-bound protein from a distance. *Proc. Natl. Acad. Sci. U. S. A. 104*, 18907-18912.

10. Armitage, B., Yu, C., Devadoss, C., and Schuster, G. B. (1994) Cationic anthraquinone derivatives as catalytic DNA photonucleases: Mechanisms for DNA damage and quinone recycling. *J. Am. Chem. Soc. 116*, 9847-9859.

11. Gasper, S. M. and Schuster, G. B. (1997) Intramolecular photoinduced electron transfer to anthraquinones linked to duplex DNA: The effect of gaps and traps on long-range radical cation migration. *J. Am. Chem. Soc. 119*, 12762-12771.

12. el-Deiry, W., Tokino, T., Velculescu, V., Levy, D., Parsons, R., Trent, J., Lin, D., Mercer, W., Kinzler, K., and Vogelstein, B. (1993) WAF1, a potential mediator of p53 tumor suppression. *Cell 75*, 817-825.

13. Sugiyama, H., and Saito, I. (1996) Theoretical studies of GG-specific photoclevage of DNA via electron transfer: significant lowering of ionization potential and 5′ localization of HOMO of stacked GG bases from B-form DNA. *J. Am. Chem. Soc. 118*, 7063-7068.

14. Saito, I., Nakamura, T., Nakatani, K., Yoshioka, Y., Yamaguchi, K., and Sugiyama, H., (1998) Mapping of the hot spots for DNA damage by one-electron oxidation: Efficacy of GG doublets and GGG triplets as a trap in long-range hole migration. *J. Am. Chem. Soc. 120*, 12686-12687.

15. Nikolova, P.V., Henckel, J., Lane, D. P., and Fersht, A. R. (1998) Semirational design of active tumor suppressor p53 DNA binding domain with enhanced stability. *Proc. Natl. Acad. Sci. U. S. A. 95*, 14675-14680.

16. Vallejo, A. N., Pogulls, R. J., and Pease, L. R. (2008) DNA-mediated oxidation of p53. *Cold Spring Harb. Protoc.* 2008.

17. Veprintsev, D. B., Freund, S. M., Andreeva, A., Rutledge, S. E., Tidow, H., Cañadillas, J. M., Blair, C. M., and Fersht, A. R. (2006) Core domain interactions in full-length p53 in solution. *Proc. Natl. Acad. Sci. U. S. A. 103*, 2115-2119.

18. Zeglis, B. M. and Barton, J. K. (2007) DNA base mismatch detection with bulky rhodium intercalators: synthesis and applications. *Nat. Protoc. 2*, 357-371.

19. Maxam, A. M., and Gilbert, W. (1977) A new method for sequencing DNA. *Proc. Natl. Acad. Sci. U. S. A. 74*, 560-564.

20. Gupta, S., Radha, V., Furukawa, Y., and Swarup, G. (2001) Direct transcriptional activation of human caspase-1 by tumor suppressor p53. J. *Biol. Chem. 276*, 10585-10588.

21. Wicki, R., Franz, C., Scholl, F. A., Heizmann, C. W., and Schäfer, B. W. (1997) Repression of the candidate tumor suppressor gene S100A2 in breast cancer is mediated by site-specific hypermethylation. *Cell Calcium 22*, 243-254.

22. Cao, L. Y., Yin, Y., Li, H., Jiang, Y., and Zhang, H. F. (2009) Expression and clinical significance of S100A2 and p63 in esophageal carcinoma. *World J. Gastroenterol. 15*, 4183-4188.

23. Chen, Y., Dey, R., and Chen, L. (2010) Crystal structure of the p53 core domain bound to a full consensus site as a self-assembled tetramer. *Structure 18*, 246-256.

24. Riley, T., Sontag, E., Chen, P., and Levine, A. (2008) Transcriptional control of human p53-regulated genes. *Nat. Rev. Mol. Cell Biol. 9*, 402-412.

25. Geer, L. Y., Marchler-Bauer, A., Geer, R. C., Han, L., He, J., He, S., Liu, C., Shi, W., and Bryant, S. H. (2010) The NCBI BioSystems database. *Nucleic Acids Res. D492-6*, 137939.

26. Wilson, D., Charoensawan, V., Kummerfeld, S., and Teichmann, S. (2008) DBD—taxonomically broad transcription factor predictions: new content and functionality. *Nucl. Acids Res. 36,* D88-D92.

27. Madan, E., Gogna, R., Bhatt, M., Pati, U., Kuppusamy, P., and Mahdi, A. (2011) Regulation of glucose metabolism by p53: emerging new roles for the tumor suppressor. *Oncotarget 2,* 948-957.

28. Werb, Z. (1997) ECM and cell surface proteolysis: regulating cellular ecology. *Cell 91*, 439-442.

29. Sun, N. K., Kamarajan, P., Huang, H., and Chao, C. (2002) Restoration of UV sensitivity in UV-resistant HeLa cells by antisense-mediated depletion of damaged DNA-binding protein 2 (DDB2). *FEBS letters 512*, 168-172.

30. Burns, T., Fei, O., Scata, K., Dicker, D., and el-Deiry, W. (2003) Silencing of the novel p53 target gene Snk/Plk2 leads to mitotic catastrophe in Paclitaxel (Taxol)-exposed cells. *Mol. Cell. Biol. 23*, 5556-5571.

31. Zolnierowicz, S. (2000) Type 2A protein phosphatase, the complex regulator of numerous signaling pathways. *Biochem. Pharmacol. 60*, 1225-1235.

32. Wu, M., Xu, L. G., Su, T., Tian, Y., Zhai, Z., and Shu, H. B. (2004) AMID is a p53-inducible gene downregulated in tumors. *Oncogene 23,* 6815-6819.

33. Robles, A., Bemmels, N., Foraker, A., and Harris, C. (2001) APAF-1 is a transcriptional target of p53 in DNA damage-induced apoptosis. *Cancer Res. 61*, 6660-6664.

34. Nakano, K. and Vousden, K. H. (2001) PUMA, a novel proapoptotic gene, is induced by p53. *Mol. Cell 7*, 683-694.

35. Bensaad, K., Tsuruta, A., Selak, M., Vidal, M., Nakano, K., Bartrons, R., Gottlieb, E., and Vousden, K. (2006) TIGAR, a p53-inducible regulator of glycolysis and apoptosis. *Cell 126*, 107-120.

36. Mori, T., Anazawa, Y., Matsui, K., Fukuda, S., Nakamura, Y., and Arakawa, H. (2002) Identification of the interferon regulatory factor 5 gene (IRF-5) as a direct target for p53. *Neoplasia 4,* 268-274.

37. Saramäki, A., Banwell, C., Campbell, M., and Carlberg, C. (2006) Regulation of the human p21(waf1/cip1) gene promoter via multiple binding sites for p53 and the vitamin D3 receptor. *Nucleic Acids Res. 34*, 543-554.

38. Tan, T. and Chu, G. (2002) p53 binds and activates the xeroderma picmitosa DDB2 gene in humans but not mice. *Mol. Cell. Biol. 22*, 3247-3254.

39. Müller, M., Wilder, S., Bannasch, D., Israeli, D., Lehlbach, K., Li-Weber, M., Friedman, S., Galle, P., Stremmel, W., Oren, M., and Krammer, P. (1998) p53 activates the CD95 (APO-1/Fas) gene in response to DNA damage by anticancer drugs. *J. Exp. Med. 188*, 2033-2045.

40. Tamura, R., de Vasconcellos, J., Sarkar, D., Libermann, T., Fisher, P., and Zerbini, L. (2012) GADD45 proteins: central players in tumorigenesis. *Curr. Mol. Med. 12*, 634-651.

41. Buckbinder, L., Talbott, R., Velasco-Miguel, S., Takenaka, I., Faha, B., Seizinger, B. R., and Kley, N. (1995) Induction of the growth inhibitor IGF-binding protein 3 by p53. *Nature 377*, 646-649.

42. Bian, J. and Sun, Y. (1997) Transcriptional activation by p53 of the human type IV collagenase (gelatinase A or matrix metalloproteinase 2) promoter. *Mol. Cell. Biol. 17*, 6330-6338.

43. Reczek, E. E., Flores, E. R., Tsay, A. S., Attardi, L. D., and Jacks, T. (2003) Multiple response elements and differential p53 binding control Perp expression during apoptosis. *Mol. Cancer Res. 1*, 1048-1057.

44. Burns, T. F. (2003) Silencing of the novel p53 target gene Snk/Plk2 leads to mitotic catastrophe in Paclitaxel (Taxol)-exposed cells. *Mol. Cell. Biol. 23*, 5556-5571.

45. Shiio, Y., Yamamoto, T., and Yamaguchi, N. (1992) Negative regulation of Rb expression by the p53 gene product. *Proc. Natl. Acad. Sci. U. S. A. 89*, 5206-5210.

46. Stambolic, V., MacPherson, D., Sas, D., Lin, Y., Snow, B., Jang, Y., Benchimol, S., and Mak, T. W. (2001) Regulation of PTEN transcription by p53. *Mol. Cell 8,* 317-325.

47. Kuo, M. L., Sy, A., Xue, L., Chi, M., Lee, M., Yen, T., Chiang, M.-I., Chang, L., Chu, P., and Yen, Y. (2012) RRM2B suppresses activation of the oxidative stress pathway and is up-regulated by p53 during senescence. *Sci. Rep. 2,* 822.

48. Herzer, K., Falk, C. S., Encke, J., Eichhorst, S. T., Ulsenheimer, A., Seliger, B., and Krammer, P. H. (2003) Upregulation of major histocompatibility complex class I on liver cells by hepatitis C virus core protein via p53 and TAP1 impairs natural killer cell cytotoxicity. *J. Virol. 77*, 8299-8309.

49. Harmes, D. C., Bresnick, E., Lubin, E. A., Watson, J. K., Heim, K. E., Curtin, J. C., Suskind, A. M., Lamb, J., and DiRenzo, J. (2003) Positive and negative regulation of ΔN-p63 promoter activity by p53 and ΔN-p63-α contributes to differential regulation of p53 target genes. *Oncogene 22*, 7607-7616.

50. Feng, Z., Hu, W., de Stanchina, E., Teresky, A. K., Jin, S., Lowe, S., and Levine A. J. (2007) The regulation of AMPK β1, TSC2, and PTEN expression by p53: Stress, cell and tissue specificity, and the role of these gene products in modulating the IGF-1-AKT-mTOR pathways. *Cancer Res. 67*, 3043-3053.

51. Yoon, H., Liyanarachchi, S., Wright, F. A., Davuluri, R., Lockman, J. C., de la Chapelle, A., and Pellegata, N. S. (2002) Gene expression profiling of isogenic cells with different TP53 gene dosage reveals numerous genes that are affected by TP53 dosage and identifies CSPG2 as a direct target of p53. *Proc. Natl. Acad. Sci. U. S. A. 99*, 15632-15637.

52. Maruyama, R., Aoki, F., Toyota, M., Sasaki, Y., Akashi, H., Mita, H., Suzuki, H., Akino, K., Ohe-Toyota, M., Maruyama, Y., Tatsumi, H., Imai, K., Shinomura, Y., and Tokino, T. (2006) Comparative genome analysis identifies the vitamin D receptor gene as a direct target of p53-mediated transcriptional activation. *Cancer Res. 66*, 4574-4583.

CHAPTER 3

In cellulo investigations of transcription factor p53 during genomic oxidative stress

Genomic sequencing conducted by the Millard and Muriel Jacobs Genetics and Genomics Laboratory at the California Institute of Technology.

INTRODUCTION

Gene regulation is the primary, and most well studied, role of transcription factor p53 in the human cell. It is generally accepted that gene regulation is initiated in a p53-dependent manner through the specific binding to defined response elements in the upstream regulatory region of certain genes. However, it currently remains unknown how p53 binding precisely results in the activation of certain genes, while simultaneously acting as a repressor for others.[1,2] Not only does p53 regulate protein production of well over a hundred confirmed genes, an emerging body of data also indicates that it may also play a pivotal role in genome-wide and cell type-specific changes in microRNA expression.[3]

Since we determined that p53 dissociates from DNA via oxidative DNA-mediated CT and that this dissociation is dependent upon guanine bases within the response element *in vitro*, we asked whether this response correlates to p53 activity during genomic stress *in cellulo*.[4] Preliminary research was conducted to determine whether this response correlated *in cellulo* by monitoring the levels of gene transcripts under p53 regulatory control via reverse transcription (RT) quantitative polymerase chain reaction (qPCR). For these experiments HCT116N cells were used since they contain a wild-type p53; genomic oxidative stress was induced through treatment with $Rh(phi)_2(bpy)^{3+}$ and subsequent irradiation.[5] During these experiments, three p53-regulated gene products were monitored which had formerly been characterized *in vitro* by EMSA: Caspase1A (CASP), S100A2 (S100A), and ornithine decarboxylase (ODC).[6]

Caspase1A is a cysteine-dependent aspartate-directed protease that plays essential roles in apoptosis, necrosis, and inflammation.[7] The binding of p53 to this response

element promotes the production of caspase. The response element of Caspase1A is very similar to the synthetic AAA sequence, with an adenine triplet within the purine region and no guanine doublets or triplets in either of the complementary strands.[4,7] Through EMSA analysis, it was determined that p53 does not readily oxidatively dissociate from this response element, with a maximum of 6.4% dissociation upon 30 minutes of irradiation, as shown in Figure 3.1.[4]

Conversely, the S100A2 protein is intimately involved in cell cycle progression, cellular differentiation, and may function as a tumor suppressor.[8,9] When p53 is bound to this guanine-rich response element, production of the S100A2 protein is promoted. The S100A2 response element is very similar to the synthetic GGG sequence, containing two guanine triplets within the purine regions.[4] Through EMSA analysis it was observed that p53 does oxidatively dissociate from the response element, with a maximum of 14% dissociation upon 30 minutes of irradiation, as depicted in Figure 3.1.

Ornithine Decarboxylase (ODC) is the rate-limiting enzyme in the decarboxylation of ornithine, a product of the urea cycle, to form putrescine.[10,11] In healthy cells, putrescine is synthesized in small quantities since it is a necessary polyamine that acts as a growth factor for cell division; however, high levels of putrescine are cytotoxic. When p53 is bound to the ODC response element the production of ornithine decarboxylase is repressed. This response element is similar to the GGG/GGG synthetic sequence, containing guanine doublets and triplets in both complementary strands of the response element. We experimentally observed in EMSA analysis that p53 oxidatively dissociates from this sequence, around 14.2% but with a drastically wide range of error, as seen in Figure 3.1.

FIGURE 3.1 — EMSA analysis (above) and corresponding preliminary RT-qPCR (below) of $Rh(phi)_2(bpy)^{3+}$-treated HCT116N cells to determine changes in p53 gene regulation. RT-qPCR Samples were normalized to the untreated control and the data represents the fold change in mRNA levels with respect to the control. The p53 response element sequences are located below the plots.[4,5]

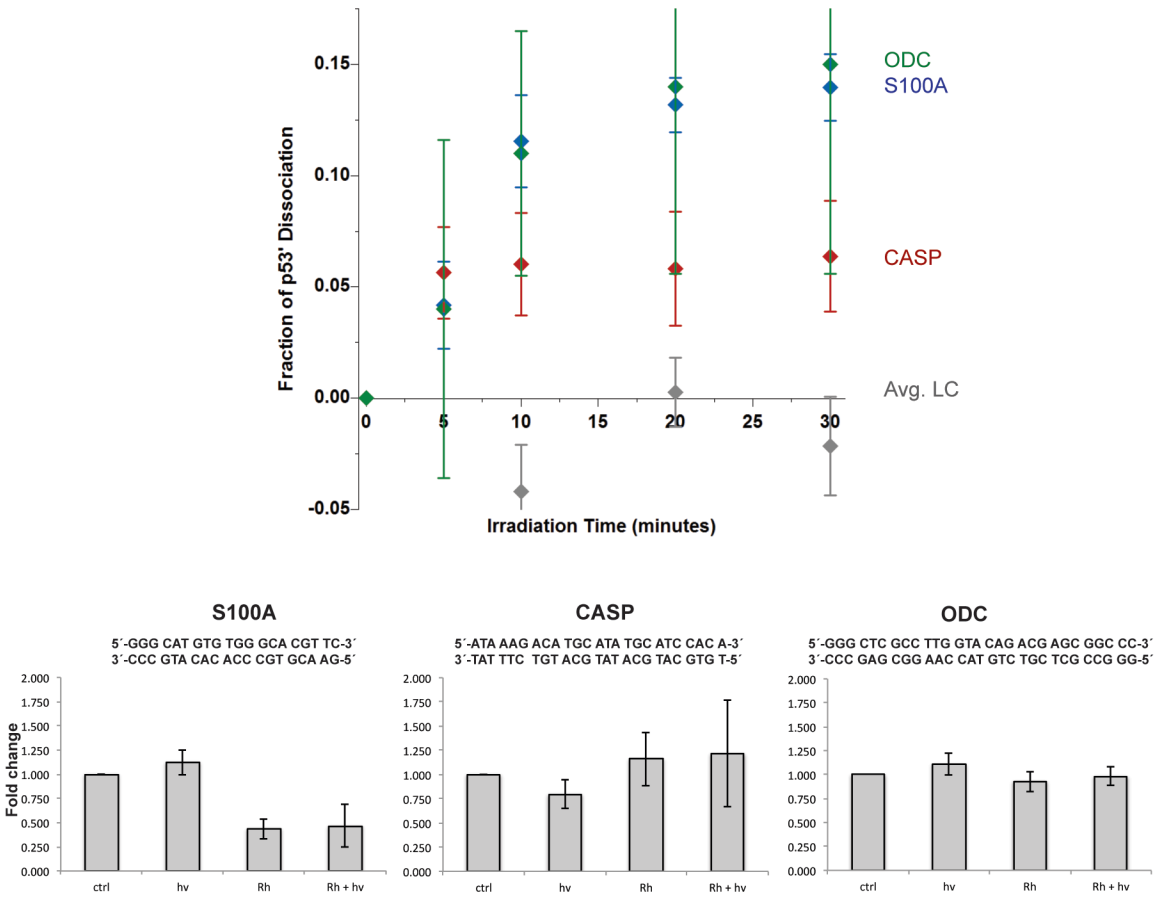

To examine the parallels of these EMSA data *in cellulo*, preliminary RT-qPCR trials were conducted.[5] The RT-qPCR results for S100A, as depicted in Figure 3.1, display a slight increase in gene product with irradiation without Rh treatment (-Rh). However, the Rh treated (+Rh) samples both showed a marked attenuation in the S100A gene product, even without irradiation. This indicates that the addition of Rh may be interfering with other cellular processes, leading to an overall decrease in S100A production solely due to the presence of Rh intracellularly. Since we did observe oxidative dissociation from the S100A response element *in vitro,* and p53 acts as a promoter for this gene, a correlating decrease in S100A gene product was anticipated for the +Rh-irradiated sample. The +Rh-irradiated samples for S100A showed attenuation within error of the +Rh-unirradiated samples, indicating no significant change in gene regulation occurred by inducing oxidative DNA CT.

In the case of Caspase1A, since p53 does not readily dissociate from this sequence *in vitro,* we would anticipate a continued or upregulated production of this gene transcript under conditions of oxidative genomic stress. The RT-qPCR results indicated a slight decrease in mRNA levels in the -Rh-irradiated samples, and a slight increase in the +Rh-unirradiated samples. When oxidative DNA CT was induced in the +Rh-irradiated samples, we observed a slight increase over the +Rh-unirradiated sample, and a much larger margin of variability.

With respect to ODC, which p53 dissociated from *in vitro* and functions as a repressor intracellularly, we would anticipate the dissociation of p53 to lead to an increase of ODC production. However, all experimental conditions were within error of

one another. Thus, despite thorough experimentation, no conclusions could be drawn by RT-qPCR.

To more directly probe the changes in p53 binding in response to oxidative DNA CT *in cellulo*, we decided to investigate the changes of p53 binding more directly through chromatin immunoprecipitation (ChIP). This technique allows the isolation of genomic fragments in direct contact with p53, which are then quantified through qPCR. This technique allows us to determine the occupancy of p53 at specific genomic locations in HCT116N cells under varied conditions. To gain more insight into p53 binding *in cellulo* during oxidative genomic stress, the isolated ChIP chromatin fragments were sequenced (ChIP-Seq) and aligned to the human genome. Lastly, from this ChIP-Seq data we were able to return to our former sets of ChIP DNA and explore other genomic sites showing p53 occupancy by qPCR.

MATERIALS AND METHODS

HCT116N cell growth. HCT116N cells were cultured at 37 °C with 5% carbon dioxide in RPMI medium 1640 supplemented with 10% FBS, 2 mM L-glutamine, 0.1 mM nonessential amino acids, 1 mM sodium pyruvate, 100 units/mL penicillin, 100 μg/mL streptomycin, and 400 μg/mL Geneticin. Two 75 cm^2 flasks of HCT116N cells were grown in complete HCT116 media, seeded from 1 million cells from cryostorage. The cells were grown until nearly confluent, harvested by trypsonization, combined, and split among four 500 cm^2 plates with 100 ml of complete media in each. Growth was allowed to continue for about two more days, until a confluence of about 30% was reached.

Rhodium photooxidant. [$Rh(phi)_2bpy]^{3+}$ (phi= 9,10-phenanthrenequinone diimine) was used in the following experiments to induce oxidative genomic stress within the HCT116N cells. The complex was made as previously described and synthesized by Ariel Furst for use in the ChIP experiments.[12]

$[Rh(phi)_2bpy]^{3+}$ treatment of HCT116N cells. Dry $Rh(phi)_2bpyCl_3$ was solvated in PBS buffer, sonicated to ensure a homogenous solution, and the concentration determined through UV-Visible spectroscopy (ε_{365} = 26300 nm). The HCT116N cells in a 500 cm^2 plate at 30% confluence were then dosed with 10 μM $[Rh(phi)_2bpy]^{3+}$ (+Rh) and 100 μl of DMSO in a total volume of 100 ml. The plates that were not treated with $[Rh(phi)_2bpy]^{3+}$ (-Rh) were treated with the same amount of PBS and DMSO as the +Rh samples. The cells were allowed to incubate at 37 °C for 16 h to internalize the complex.

Nutlin-3 treatment of HCT116N cells. Nutlin-3 was used to promote the upregulation of p53 through inhibiting MDM2 interaction. Following incubation with +Rh or -Rh, all four 500 cm^2 plates were washed twice with PBS, dosed with 50 mL 10 μM Nutlin-3 (Cayman Chemicals) in media, and allowed to incubate for 3 h at 37 °C. An example western blot depicting p53 upregulation is located in Appendix Figure 3.1. Treatment of the plates was staggered so that the +Rh treated samples were dosed with Nutlin-3 an hour prior to the -Rh samples. After 3 h of incubation in 10 μM Nutlin-3, the cells were washed twice with PBS and switched to 100 ml of 2.5 μM Nutlin-3 in PBS.

Irradiation. Samples were then irradiated for 45 minutes using a Solar Simulator (Oriel Instruments) equipped with a 1000W Hg/Xe lamp and an internal and external UVB/UVC cut-off filter. The corresponding unirradiated sample sat underneath the

irradiated sample, wrapped in foil to protect it from light, with the irradiated samples placed at a distance of 21.5 cm from the light source.

2-step cellular fixation. 50 mg of disuccinimidyl glutarate (DSG, Thermo Scientific) solvated in DMSO was freshly made and added to PBS about 10 min prior to completion of the cellular irradiation. Upon completion of irradiation, the solution of 2.5 μM Nutlin-3 in PBS was decanted from each 500 cm^2 plate and the cells were washed once with 4 °C PBS; caution was taken to ensure that the plates did not dry out at any point of the procedure. After removing the wash PBS from the plates, 60 mL of 3 mM DSG in PBS at 4 °C was added to each plate and fixation was allowed to proceed for 2 h at 4 °C. During this incubation, the plates sat directly on the metal bench-top in the cold room, covered with foil to prevent further light exposure, and covered with bags of ice. After 2h, the DSG solution was decanted and the plates were washed twice with ambient temperature PBS. The cells were subsequently fixed with 70 mL of 1% formaldehyde (16% formaldehyde single use methanol-free ampule, Thermo Scientific) for 15 minutes at ambient temperature while gently shaking. Formaldehyde crosslinking was quenched by the addition glycine in molar excess, and allowed to shake for 5 min.

The doubly fixed cells were then washed twice with 4 °C PBS, followed by 10 ml of 0.5 mM phenylmethanesulfonylfluoride (PMSF) in 4 °C PBS, made from a 100 mM PMSF in isopropanol stock solution.[13] The cells were then harvested by scraping and isolated by centrifugation. The plates were treated once more with 10 ml of 0.5 mM PMSF, scraped, and combined with the fist pellet. After a second centrifugation, the pelleted cells were frozen in liquid nitrogen, and stored at -80 °C.

Coupling of antibody to magnetic beads. The following procedures were all preformed at 4 °C. Dynabeads goat-anti-mouse IgG magnetic beads (Invitrogen), 50 µL per experiment, were prepared simultaneously for all replicates. The desired amount of Dynabeads was placed in a 15 ml falcon tube and the volume adjusted to 15 ml with sterile filtered 5 mg/ml BSA in PBS. The beads were then mixed by gentle rotation for 5 min, magnetically collected for 5 min, and the supernatant carefully decanted. This wash procedure was then repeated twice more. The beads were then treated with 10 µl of monoclonal DO-7 antibody per 50 µl of Dynabeads in a total volume of 10 ml PBS with 5 mg/ml BSA. The antibody conjugation was allowed to precede overnight at 4 °C while gently rotating.

Chromatin isolation and sonication. The cells were removed from storage at -80 °C and allowed to thaw on ice in 10 ml of Farnham lysis buffer (5 mM PIPES, pH 8.0, 85 mM KCl, 0.5% NP-40, with one complete protease inhibitor tablet per 50 ml (Roche)) and allow to gently rotate for 15 min.[13] To isolate the nuclear pellet, the solution was centrifuged for 5 min at 2000 RPM, and supernatant decanted. The nuclear pellet was then suspended 1.0 ml of RIPA buffer (1x PBS, 1% NP-40, 0.5% sodium deoxycholate, 0.1% SDS, with one complete protease inhibitor tablet per 50 mL) and transferred to a 1.7 ml flat bottom eppendorff tube.[13] To shear the chromatin, the solution was then sonicated with a QSonica sonifier with microtip at 45% power for 30 sec on and 59 sec off for 20 rounds. To prevent heating of the sample, the sample was held within a -20 °C ethanol bath. The sonicated was cleared by centrifugation in a tapered 1.5 ml eppendorff tube at 14,000 rpm for 15 minutes. The supernatant was then transferred to a clean tube, without disturbing the pellet, and the protein concentration determined via

BCA assay as per manufacturer protocol. This will yield enough sample for 3 or 4 replicates per condition, and at least 100 µl of this solution is to be saved for input analysis and sonication control.

Chromatin immunoprecipitation. As the BCA assay incubated, the DO-7 treated Dynabeads were washed three times, as described above, with 5 mg/ml BSA in PBS. At this point, the beads are to be equally divided into 1.5 mL eppendorf tubes respective to the number of samples and replicates in preparation. To each sample, 100 µl of 5 mg/ml BSA in PBS, 1 mg total protein content of chromatin sonicate (as determined by BCA), and RIPA buffer up to 1 ml total volume were added and incubated while rotating at 4 °C for 16-24 h.

To ensure equivalent sonication among all samples, 50 µl of each sample condition chromatin was treated with 150 µl of elution buffer (1% SDS in 0.1 M $NaHCO_3$) and incubated at 65 °C overnight for crosslink reversal.[13] These samples were purified with the Qiagen DNeasy kit, dried, and run on a 1% agarose gel in 1% TBE and ethidium bromide for visualization.

Chromatin washing and elution. Due to overnight rotation, magnetic beads may stick to the eppendorf cap. The samples are briefly centrifuged and washed 5 times with 1 ml of LiCl wash buffer (100 mM Tris, 500 mM LiCl, 1% NP-40, and 1% deoxycholate) with 10 min rotational mixing, and 5 min magnetic isolation.[13] After the final wash, the beads were suspended in TE buffer (10 mM Tris, pH 8.0, 1 mM EDTA) and transferred to O-ring screw cap tubes.[13] The beads were then magnetically isolated once more and suspended in 200 µl IP Elution buffer (1% SDS in 0.1 M $NaHCO_3$) and incubated at 65 °C for 16 h, vortexing intermittently.[13]

Purification of immunoprecipitated DNA. To isolate and purify the immunoprecipitated chromatin, the solution was extracted once with 200 µl of phenol/$CHCl_3$ /isoamyl alcohol (Sigma). The mixture was vortexed thoroughly and centrifuged at 14,000 RPM for 10 min for phase separation. The aqueous phase was then transferred to a clean eppendorf tube. The remaining organic phase was then back-extracted once with 100 µl of elution buffer, as above, and pooled the first aqueous phase. The isolated chromatin was then purified using the Qiagen PCR cleanup kit as per manufacturer protocol, with the final sample eluted twice with 100 µl of buffer EB.

Quantitative PCR reactions. qPCR was conducted on a Bio-Rad CFX 96 real time PCR platform. Individual reactions were carried out at a total reaction volume of 20 µl per well, in a 96 well low-profile PCR plate. Samples were composed of 2x SybreGreen Supermix (Roche), 50 µM primers, 2.0 µL of ChIP DNA isolate, and the respective amount of water. A two-step amplification method was used, followed by melting curve determination. The qPCR procedure used was as follows: 10 min denaturing at 95 °C, followed by 45 cycles of 10 sec for denaturing at 95 °C, and 30 sec for annealing and amplification at 63 °C, reading the plate fluorescent intensity after each cycle. The melting curve was determined over a range of 65 °C to 95 °C with plate reads taken at 0.5 °C intervals.

Quantitation of qPCR data. These data are first analyzed by the comparative Ct method (ΔΔCt), determining the fold change in p53 occupancy of each sample with respect to its non-immmunoprcipitated control.

$$\Delta Ct = Ct\ (ChIP\ sample) - Ct\ (Input\ sample)$$

$$\Delta\Delta Ct = [Ct\ (ChIP\ sample, Dark) - Ct\ (Input\ sample, Dark)] - [Ct\ (ChIP\ sample, Light) - Ct\ (Input\ sample, Light)]$$

Samples: (-Rh Dark) — no photooxidant treatment and uniradiated.

(-Rh Light) — no photooxidant treatment and irradiated.

(+Rh Dark) — treated with $[Rh(phi)_2(bpy)]^{3+}$ and uniradiated.

(+Rh Light) — treated with $[Rh(phi)_2(bpy)]^{3+}$ and iradiated.

Once the ΔΔCT values are determined, the ratio of the target p53 site relative to the untreated sample can be determined by taking $2^{\Delta\Delta Ct}$. The overall change in p53 occupancy induced by DNA CT is determined, where positive values indicate an increase in p53 occupancy at the response element site and negative values indicate decreased p53 occupancy, as described below:

$$2^{[\Delta\Delta Ct\ (+Rh)]} - 2^{[\Delta\Delta Ct\ (-Rh)]} = change\ in\ p53\ occupancy\ under\ oxidative\ DNA\ CT$$

Genetic sequencing of genome wide p53 occupancy by chromatin immunoprecipitation of $[Rh(phi)_2bpy]^{3+}$ treated HCT116N cells. Samples were prepared as described above, but the majority of the isolated chromatin sample was not subject to qPCR. The concentrations of the samples were determined through Qubit fluorescent analysis. The purified samples were subsequently made into Illumina sequencing libraries (TruSeq ChIP Sample Prep Kit, Illumina), and sequenced on the

Illumina Next-Gen sequencing platform using the C23KDACXX 50 base pair single ended flowcell.[14] The determined reads were mapped to the hg19 human genome using the Bowtie program to create genome coverage plots.[15] The data were then imported to and visualized through the UCSC genome browser.[16] The program MACS2 was used for model-based Analysis for ChIP-Seq, which called peaks of statistical significance.[17] Overall, 18489 peaks were called. Of those peaks, the top 20 were chosen to be further investigated by qPCR. Digital resources for the sequencing data are located in Appendix 3.2 and 3.3.

RESULTS

ChIP-qPCR.

The raw data obtained by qPCR were analyzed using the ΔΔCT method over ten experimental replicates. Since the addition of the Rh photooxidant influences p53 binding, the data were first normalized to the respective irradiated controls for both the –Rh and +Rh sample pairs. Once each sample set was normalized to their respective unirradiated control, the change in p53 occupancy due to oxidative DNA CT can be determined through the difference observed between the –Rh sample set and the +Rh sample set. It was found that the results were widely variable among all ten sample sets, including both increased and decreased p53 occupancy at the three investigated response elements. The determined change in p53 occupancy is depicted graphically in Figure 3.2 and corresponding values are listed in Table 3.1. The floating bar depiction of the ChIP-qPCR data in Figure 3.2 depicts the 25th and 75th percentiles of the observed data in the boxed region, while the whiskers represent the 5th and 95th percentiles, and the solid bar

FIGURE 3.2 — Floating bar plot of ChIP-qPCR experimental results. The floating bar depiction of the column of boxed data represents the 25th and 75th percentiles, while the whiskers represent the 5th and 95th percentiles. The solid bar within the box represents the median value.

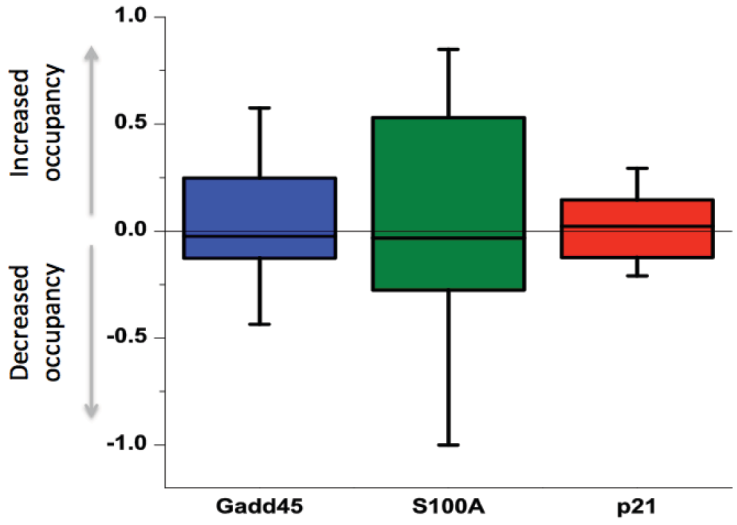

TABLE 3.1 — Change in p53 occupancy for the +Rh–irradiated samples as determined by the ΔΔCT method.

Exp. Date	Gadd45	S100A	p21
20130325	-0.125	-0.651	0.164
20130301	0.326	0.213	0.352
20130204	0.575	0.529	0.294
20121217	-0.041	-0.276	-0.124
20121126	-0.262	-0.269	-0.209
20121106	0.332	0.849	0.007
20121031	-0.009	-0.046	-0.018
20121021	-0.437	-1.001	-0.147
20120911	-0.126	-0.021	0.039
20121204	0.247	0.619	0.146
Avg.	0.048	-0.005	0.050

within each box represents the median value.

In the case of the p21 response element (red in Figure 3.2), we anticipated to observe minimal p53 dissociation based upon results observed in EMSA assays, corresponding to a minimal change in p53 occupancy. As normalized to the -Rh-unirradiated control, we observe p53 dissociation in the +Rh unirradiated sample, and both increased and decreased p53 occupancy within the -Rh irradiated control. When determining the overall fold change in occupancy with respect to oxidative DNA CT, we observe what appears to be a reasonable average of the two controls, with the majority of the samples being within limits of the dark and untreated control. The maximum fold decrease for p21 was determined at -0.209 and a maximum increase at +0.35, giving a total range of change of 0.559.

With respect to the Gadd45 response element (blue in Figure 3.2), we anticipated observing a large trend toward decreased p53 occupancy, since p53 readily dissociates from this response element *in vitro*. Overall, with respect to the unirradiated controls, the change in p53 occupancy based upon oxidative DNA CT was a dramatically varied distribution of both increased and decreased p53 occupancy. However, it appears that the majority of the replicates displayed decreased p53 occupancy. The maximum fold decrease for Gadd45 was determined at -0.437 and a maximum increase at +0.575, giving a total range of change of 1.048.

For the S100A response element (green), we anticipated a large trend toward decreased p53 occupancy, since p53 dissociation was observed *in virto.* Overall, an extraordinarily variable change in occupancy is observed, with both increased and

decreased occupancy. The maximum fold decrease for Gadd45 was determined at -1.001 and a maximum increase at +0.849, giving a total range of change of 1.85.

ChIP-Sequencing.

One set of ChIP samples were run on the Illumina Nex-Gen sequencing platform, comparing the four samples conditions against input, not immunoprecipitated, samples. The determined fragments were correspondingly mapped to the hg19 human genome, allowing us to observe density reads, as well as fold enrichment.[15-17] Links to these data are located in Appendix 3.2. Using a Model-based Analysis for ChIP-Seq, 18489 peaks of statistically significant chromatin enrichment were called. Of those peaks, the top 20 were investigated, p53 response elements determined, and then p53 occupancy investigated by qPCR in our former sets of ChIP isolates. For the genomic locations of interest, the response elements within them are located in Table 3.2. qPCR analysis was conducted upon four ChIP chromatin sets. The results for these enriched sequences also displayed significant variations in p53 occupancy, both increased and decreased. These data and variability determined are depicted in Table 3.3, and the corresponding primer sequences used in this analysis are located in Appendix table 3.1. These results led us to conclude that using ChIP qPCR to determine p53 occupancy *in cellulo* is a difficult task with inherent variability too large to successfully achieve our desired goal of monitoring p53 function in response to oxidative genomic stress.

DISCUSSION

Although the ChIP-qPCR result for Gadd45, S100A, and p21 were highly variable, and showed increased p53 occupancy on the response element sites

when only decreased p53 occupancy was anticipated, one interesting trend did emerge. In the case of S100A and Gadd45, the two response elements from which oxidative dissociation was observed *in vitro*, we observed a wide range of decreased and increased p53 occupancy. For Gadd45, we observed change in p53 occupancy from -0.437 to +0.575; a range of change of 1.048. For S100A, we observed even wider changes in p53 occupancy from -1.001, and the maximum and median values determined over the ten experimental replicates were both negative values, suggesting a slight preference toward p53 dissociation. However, on the sequence that we did not anticipate dissociation from, p21, we observed a much more narrow range than in the change of p53 occupancy. For p21, we observed change in p53 occupancy from -0.209 to +0.35, a range of change of 0.559. For the p21 response element, the determined median value was positive, suggesting p53 does not preferentially dissociate from this sequence. Although a well-defined response of p53 to genomic oxidative stress has yet to be observed *in cellulo*, our results via ChIP-qPCR may suggest that our predications about responsiveness based on response element DNA sequence may be valid. We can correlate the predicted responsiveness of a p53 response element to an increased amount of variability of p53 occupancy *in cellulo* during oxidative genomic stress. As for the response elements we would anticipate to be not responsive, substantially less variability in p53 occupancy will be observed at those response elements under oxidative genomic stress. However, determining whether an increase or a decrease in p53 occupancy will occur remains elusive.

TABLE 3.2 — Significant peaks as determined by ChIP-Seq and evaluated by ChIP-qPCR. p53 response elements located within most significant peaks as determined by ChIP-Seq.analysis. qPCR was used to determined the relative p53 occupancy determined for the +Rh–irradiated samples as calculated by the ΔΔCT methods with green indicating increased occupancy and red indicating decreased occupancy.

Peak Rank	Response Element (5'-3')	Genomic Location	A	B	C	D
1	AGACATGCCTGAACATGCCCAGGCATGTCCCAGCTTGCAG	chr17: 37,203,119-37,203,158	1.90	0.27	0.02	1.33
2	GAACATGCCCAGGCATGTCT	chr2: 70,824,222-70,824,241	0.97	0.09	-0.33	0.70
3	GGGCATGCCCAGACAAGCCC	chr7: 40,757,090-40,757,109	1.34	0.57	-0.47	0.40
4	GGACATGTCTGGGCATGTCC	chr6: 31,305,110-31,305,129	0.81	0.08	-0.19	-0.04
5	AGGCATGCCCGGGCATGTCT	chr1: 181,104,278-181,104,297	-0.08	1.39	-0.41	-1.75
6	GGACATGTTGGGACATGCCA	chr8: 29,628,142-29,628,161	1.34	-0.14	0.25	0.15
7	GAACATGTCC	chr18: 3,305,487-3,305,496	n/a	0.44	-1.88	0.87
8	GGGCATGTTGGGACATGCCT	chr4: 41,146,994-41,147,013	0.15	2.54	-0.22	-1.65
9	AGGCATGTCTGGACATGTCT	chr7: 121,151,349-121,151,368	1.19	0.11	-0.36	-0.02
10	AGACATGTTCAGACATGCCT	chr21: 34,739,689-34,739,708	2.08	0.03	-0.21	1.18
11	GAACATGTCTGGGACATGTTC	chr7: 123,886,643-123,886,663	n/a	0.12	0.29	0.96
12	ATACATGTCCAAACATGCCC	chr16: 20,877,270-20,877,289	n/a	0.51	0.16	1.02
13	AAACATGTCAGGACATGCCT	chr1: 234,754,327-234,754,346	1.49	-0.08	0.23	0.81
15	GGACATGCCTGGGCATGTCC	chr6: 151,178,483-151,178,502	4.14	0.29	1.28	-0.43
17	GGGCATGCCTGGGCATGCCT	chr9: 114,907,243-114,907,262	0.02	2.74	0.07	-0.08
19a	GGGCTTGTCTAAGACATGCCC	chr1: 244,898,865-244,898,885	-0.11	2.36	1.25	0.90
19b	GACTTGCCCCAGACATGCCC	chr1: 244,898,918-244,898,936	0.10	1.17	0.13	0.43
20	AGGCTAGCCCAGGCATGTTC	chr9: 84,636,327-84,636,346	1.90	0.27	0.02	1.33
21b	ACACATGCCTGGACATGCCC	chr4: 84,092,282-84,092,301	2.01	0.04	1.40	0.57

The genomic sequencing of one set of ChIP DNA samples revealed to us a large pool of information about the DNA to which p53 binds. Overall, more than 18,000 genomic locations were found to be enriched by anti-p53 ChIP. Aligning the data to the human genome (hg19), we were able to compare the overall enrichment, over the non-immunoprecipitated input sample, of the four sample conditions in comparison to one another. It was evident in these profiles that increases in genomic material around certain response elements also occurs in the +Rh-irradiated samples, as compared to the respective controls. This finding confirms that the increased occupancy observed in the ChIP-qPCR experiments is a real phenomenon.

From the best peaks determined through the MACS2 program, most were found to contain p53 response element DNA patterns within those genomic locations, and primers were designed to conduct qPCR on these new sites of interest. Of the samples determined through sequencing and re-evaluated in the ChIP samples, we again observed large ranges of variability among the four sample sets tested, and continued testing was felt to be futile.

These results highlight the intricacies of transcription factor p53 gene regulation and the level of complexity and variation that can occur *in cellulo*. The study of p53 *in cellulo* has been complex, extensive, and left us with more questions than answers. There is much still to be learned about the role of p53 in response to genomic oxidative stress and how it interacts with DNA. Before further *in cellulo* experiments are undertaken, a cleaner approach to inducing DNA CT must be devised. These studies merely confirm the eloquently stated

words by Karen H. Vousden and Carol Prives: “If genius is the ability to reduce the complicated to the simple, then the study of p53 makes fools of us all.”[18]

REFERENCES

1. Riley, T., Sontag, E., Chen, P., and Levine, A. (2008) Transcriptional control of human p53-regulated genes. *Nat. Rev. Mol. Cell Biol. 9*, 402-412.

2. Wei, C. L., Wu, Q., Vega, V.B., Chiu, K. P., Ng, P., Zhang, T., Shahab, A., Yong, H. C., Fu, Y., Weng, Z., Liu, J., Zhao, X. D., Chew, J. L., Lee, Y. L., Kuznetsov, V. A., Sung, W. K., Miller, L. D., Lim, B., Liu, E. T., Yu, Q., Ng, H. H., and Ruan, Y. (2006) A Global Map of p53 Transcription-Factor Binding Sites in the Human Genome. *Cell 124*, 207-219.

3. Hattori, H., Janky, R., Nietfeld, W., Aerts, S., Madan Babu, M., and Venkitaraman, A. R. (2014) p53 shapes genome-wide and cell type-specific changes in microRNA expression during the human DNA damage response. *Cell Cycle 13*, 2572-2586.

4. Schaefer, K. N., and Barton, J. K. (2014) DNA-mediated oxidation of p53. *Biochemistry 53*, 3467-3475.

5. Geil, W. M. (2012) Regulation of wild-type and mutant p53 through DNA-mediated charge transport. Dissertation Ph.D., California Institute of Technology.

6. Fischer, M., Steiner, L., and Engeland, K. (2014) The transcription factor p53: Not a repressor, solely an activator. *Cell Cycle 13*, 3037-3058.

7. Gupta, S., Radha, V., Furukawa, Y., and Swarup, G. (2001) Direct Transcriptional Activation of Human Caspase-1 by Tumor Suppressor p53. *J. Biol. Chem. 276*, 10585-10588.

8. Wicki, R., Franz, C., Scholl, F. A., Heizmann, C. W., and Schäfer, B. W. (1997) Repression of the candidate tumor suppressor gene S100A2 in breast cancer is mediated by site-specific hypermethylation. *Cell Calcium 22*, 243-254.

9. Cao, L. Y., Yin, Y., Li, H., Jiang, Y., and Zhang, H. F. (2009) Expression and clinical significance of S100A2 and p63 in esophageal carcinoma. *World J. Gastroenterol. 15*, 4183-4188.

10. Mirza, A., Wu, Q., Wang, L., McClanahan, T., Bishop, W. R., Gheyas, F., Ding, W., Hutchins, B., Hockenberry, T., Kirschmeier, P., Greene, J. R., and Liu, S. (2002) Global transcriptional program of p53 target genes during the process of apoptosis and cell cycle progressions. *Oncogene*. *22*, 3645-3654.

11. Liu, S., Mirza, A., and Wang, L. (2004) Generation of p53 target database via integration of microarray and global p53 DNA-binding site analysis. *Methods Mol. Biol. 281*, 33-54.

12. Hall, D., Holmlin, R., and Barton, J. (1996) Oxidative DNA damage through long-range electron transfer. *Nature 382*, 731-735.

13. Wells, J., and Farnham, P. J. (2002) Characterizing transcription factor binding sites using formaldehyde crosslinking and immunoprecipitation. *Methods 26*, 48-56.

14. Sequencing Methods Review, a review of publications featuring Illumina Technology. http://www.illumina.com/content/dam/illumina-marketing/documents/products/research_reviews/sequencing-methods-review.pdf

15. Langmead, B., Trapnell, C., Pop, M., and Salzberg, S. L. (2009) Ultrafast and memory-efficient alignment of short DNA sequences to the human genome. *Genome Biol 10*, R25.

16. Kent, W. J., Sugnet, C. W., Furey, T. S., Roskin, K. M., Pringle, T. H., Zahler, A. M., and Haussler, D. (2002) The human genome browser at UCSC. *Genome Res. 12*, 996-1006.

17. Zhang, Y., Liu, T., Meyer, C., Eeckhoute, J., Johnson, D., Bernstein, B., Nusbaum, C., Myers, R., Brown, M., Li, W., and Liu, X. (2008) Model-based Analysis of ChIP-Seq (MACS). *Genome Biol. 9*, R137.

18. Vousden, K., and Prives, C. (2009) Blinded by the Light: The Growing Complexity of p53. *Cell 137*, 413-431.

Appendix 3.1 — Example gel shift of upregulation of p53 via Nutlin-3 treatments (top). Example of sonication gel of chromatin prepared for ChIP (bottom).

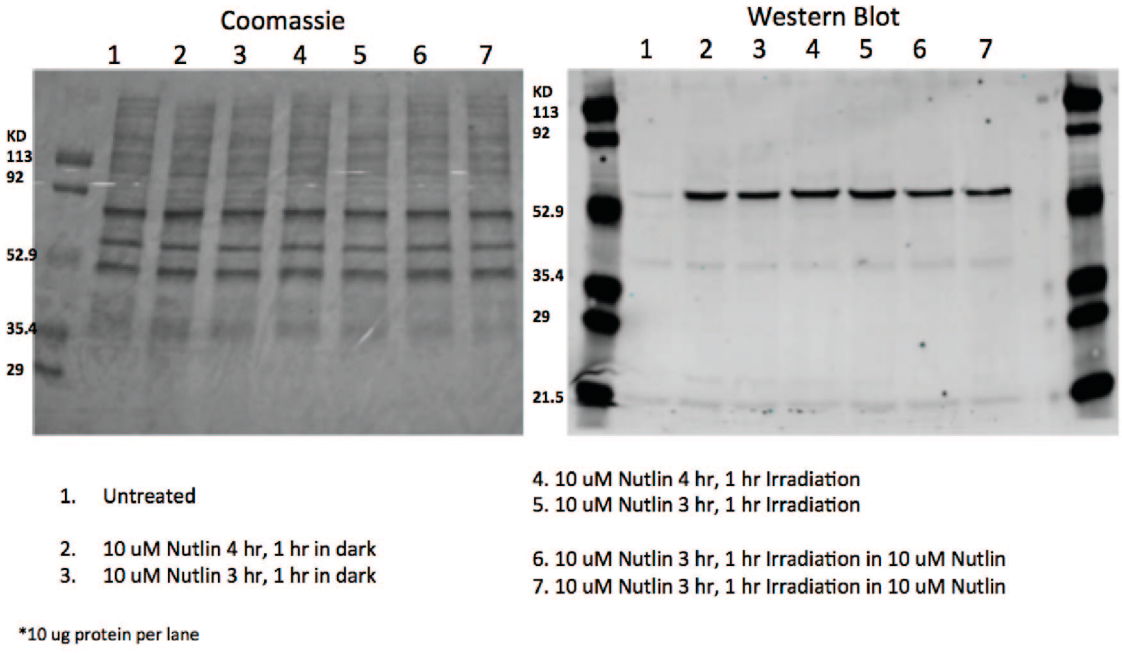

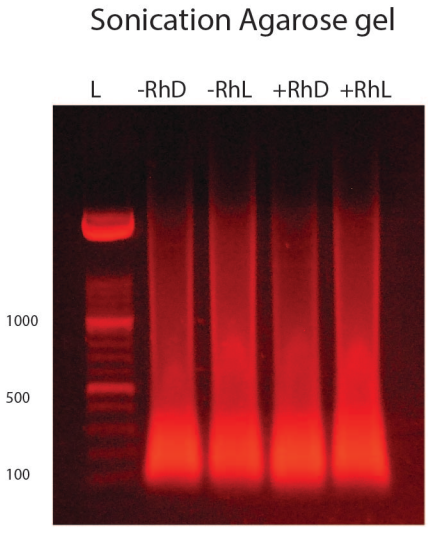

Appendix 3.2

The following libraries are on the flowcell C23KDACXX, which is a 50 base pair single ended flowcell:

Lane : (Library Id) Library Name (Cluster Estimate)

Lane #4 : (13682) index # 10 Rh Dark HCT116N p53 (None)

https://jumpgate.caltech.edu/library/13682

Lane #4 : (13683) Index #11 Rh Light HCT116N p53 (None)

https://jumpgate.caltech.edu/library/13683

Lane #4 : (13679) Index # 4 Input of HCT116N ChIP (None)

https://jumpgate.caltech.edu/library/13679

Lane #4 : (13680) Index #5 Untreated Dark HCT116N p53 (None)

https://jumpgate.caltech.edu/library/13680

Lane #4 : (13681) Index #7 Untreated Light HCT116N p53 (None)

https://jumpgate.caltech.edu/library/13681

Appendix 3.3

Genome browser data:

http://genome.ucsc.edu/cgi-bin/hgTracks?db=hg19&hgct_customText=track%20type=bigWig%20name=%22Input%22%20visibility=full%20color=64,64,64%20bigDataUrl=http://cheget.caltech.edu/~igor/tempHtml/KatieSchaefer/13679_input.wig.bigWig

http://genome.ucsc.edu/cgi-bin/hgTracks?db=hg19&hgct_customText=track%20type=bigWig%20name=%22Untreated_dark%22%20visibility=full%20color=128,0,128%20bigDataUrl=http://cheget.caltech.edu/~igor/tempHtml/KatieSchaefer/13680_untreated_dark.wig.bigWig

http://genome.ucsc.edu/cgi-bin/hgTracks?db=hg19&hgct_customText=track%20type=bigWig%20name=%22Untreated_light%22%20visibility=full%20color=128,0,0%20bigDataUrl=http://cheget.caltech.edu/~igor/tempHtml/KatieSchaefer/13681_untreated_light.wig.bigWig

http://genome.ucsc.edu/cgi-bin/hgTracks?db=hg19&hgct_customText=track%20type=bigWig%20name=%22Rh_dark%22%20visibility=full%20color=0,128,0%20bigDataUrl=http://cheget.caltech.edu/~igor/tempHtml/KatieSchaefer/13682_rh_dark.wig.bigWig

http://genome.ucsc.edu/cgi-bin/hgTracks?db=hg19&hgct_customText=track%20type=bigWig%20name=%22Rh_light%22%20visibility=full%20color=0,0,128%20bigDataUrl=http://cheget.caltech.edu/~igor/tempHtml/KatieSchaefer/13683_rh_light.wig.bigWig

Fold enrichment tracks:

http://genome.ucsc.edu/cgi-bin/hgTracks?db=hg19&hgct_customText=track%20type=bigWig%20name=%22Untreated_dark_FE%22%20visibility=full%20color=128,0,128%20bigDataUrl=http://cheget.caltech.edu/~igor/tempHtml/KatieSchaefer/untreated_dark_gb_FE.bigWig

http://genome.ucsc.edu/cgi-bin/hgTracks?db=hg19&hgct_customText=track%20type=bigWig%20name=%22Untreated_light_FE%22%20visibility=full%20color=128,0,0%20bigDataUrl=http://cheget.caltech.edu/~igor/tempHtml/KatieSchaefer/untreated_light_gb_FE.bigWig

http://genome.ucsc.edu/cgi-bin/hgTracks?db=hg19&hgct_customText=track%20type=bigWig%20name=%22Rh_dark_FE%22%20visibility=full%20color=0,128,0%20bigDataUrl=http://cheget.caltech.edu/~igor/tempHtml/KatieSchaefer/rh_dark_gb_FE.bigWig

http://genome.ucsc.edu/cgi-bin/hgTracks?db=hg19&hgct_customText=track%20type=bigWig%20name=%22Rh_light_FE%22%20visibility=full%20color=0,0,128%20bigDataUrl=http://cheget.caltech.edu/~igor/tempHtml/KatieSchaefer/rh_light_gb_FE.bigWig

Appendix 3.4 — qPCR primers for peaks determined through ChIP-Seq.

Peak	Forward Primer (5´-3´)	Reverse Primer (5´-3´)
1	ATGCCCAGGCATGTCCCAGCTT	ACGCACTGGGCTTCTACTGCTGTGT
2	ACGTGCGTGGTAGCAGGTGGTCTGCTT	ACGTGCGTGGTAGCAGGTGGTCTGCTT
3	TCCTCCCGTGCACAAGGCGTGAACT	GCAAATGAGGGAACCTGCCCAGGGCTT
4	TCCTGTCTCCATTGGCTGGAACTGGACC	CCTAGTCTGCCTGGATCTGCCTGGACA
5	TGTCCCTGGGTGTCTGCATCTGCGT	ACTCGGGCGTTCTCTCCATGCCTCAGA
6	TGGTAATGCCTTCTCTGGAACTTTGCCTGC	TGCTGGCATGTCCCAACATGTCCCAA
7	GCCTATGTGTGTAGGAGGCTAGACCATCTAGGTTT	TGCACGGGCTGCATTCATGCCTCA
8	CCAGACGTTCAAGACCAGCCTGGGCAA	ATAGCTGGGCCCACAGGCATGTCCCAA
9	TCCCTGTGTCTAGGGTTGGACTGCACA	TCCAGCCTGCCAACAACTCTCCCACT
10	TCCGCTCTGATTGTGCCCTGACATGC	CCCGCATGCAGCTTCTGTTCCTGTGT
11	AGACGAGACTAAGGGTTCATATAATGGGTCAGGGT	ACCAGTCAGCAGCACCACAAAGGTACGCA
12	CCCTTCTCCACCCGCAAAGAGAGCA	CCCTTGTACCATGGTCTTCCAAGAATTAACCC
13	AGCCTGGAATGCTGAAACCCTCTTAGACTGAA	AGTACGGAATGTGGAATTCTGAGCCTAAACCGT
15	TCCATTGGCTGGAGCCAGACCTCACA	TCCTTGTACCTTAGTCAGAATATTCGTGCTGGACA
17	ATGCCTGGGCATGCCTATGGTCCCAGT	CCTCCTGCCTCAGCCTCTTGAGCAACT
19A	AATCCGGTCAGGCAGGCAGTTAGGGTG	TCCATTGCGGGCATGTCTGGGCAAGT
19B	GCCCACAGCTGCACAGACAAGAAAGCC	ATTGCGGGCATGTCTGGGCAAGTCACC
20	TGTTTGTCTGGAGCTTTGCCTGGGACAC	CATGGACCCTTGCAACCTGCTTAGCCA
21B	GCTGCATGCGCCCTTTGGTGGTTGA	GGAGACTTCTTGACTTGTGGGCAACAACTTCCT

CHAPTER 4

Oxidation of p53 through DNA charge transport involves a network of disulfides within the DNA-binding domain

Adapted from Schaefer, K. N., Geil, W. M., Sweredoski, M. J., Moradian, A., Hess, S., and Barton, J. K. (2015) Oxidation of p53 through DNA Charge Transport Involves a Network of Disulfides within the DNA-Binding Domain. *Biochemistry* 54, 932–941.

KNS and WMG produced the protein mutants and conducted EMSA experiments; KNS conducted mass spectrometry sample preparation; MJS, AM, and SH conducted mass spectrometry on QTRAP 6500 and acquired data; and KNS analyzed data.

INTRODUCTION

Transcription factor p53 is one of the most heavily studied human proteins due to its marked prevalence of mutation in human cancer. Over half of all human cancers display mutations in the p53 gene, with the vast majority of these mutations localized to the DNA-binding domain, as seen in Figure 4.1.[1-3] Although much research has been conducted on this protein and its many roles within the cell, the precise mechanisms by which p53 senses cellular stresses and influences cellular fate are still largely unknown. We have previously shown that DNA-mediated charge transport (CT) can sequence selectively promote the oxidative dissociation of p53 bound to DNA.[4,5] Here, we examine the mechanisms by which DNA-mediated oxidation is sensed by p53 and how the resulting dissociation from DNA occurs.

A major focus of our laboratory has been the characterization of long-range charge transport through DNA.[6-10] We have found that oxidative damage to DNA can occur from a distance because of the migration of electron holes through the π-stacked bases. Ground state CT has been observed to occur over 100 base pairs (34 nm) through DNA, and oxidative damage products have been observed over 200 Å away from a DNA tethered photooxidant.[11,12] However, perturbations in the intervening base pair stack, such as abasic sites and base mismatches, severely attenuate DNA CT. In a cellular environment, oxidative damage can occur by reactive oxygen species attacking DNA, and we have found that oxidative DNA damage can also occur from a distance *in vivo*.[6,7] The one-electron oxidation potential of guanine is the lowest of the bases (+1.29 V), therefore making it the most readily oxidized base.[13-16] Thus a known hallmark of DNA CT oxidation is the formation of DNA damage products at 5′ guanines of guanine

doublets and triplets.[17] However, certain amino acid functional groups possess lower 1-electron oxidation potentials than guanine and could thermodynamically be oxidized in DNA-bound proteins, behaving as mild reducing agents.[13] The residues and their corresponding one-electron oxidation potentials at pH7 are as follows: cysteine (+0.9 V), tyrosne (+0.9 V), tryptophan (+1.0 V), and histidine (+1.2).[13] Notably, the oxidation of cysteine residues within close proximity can lead to the formation of a disulfide bond, which may induce a substantial conformational change within proteins.

To determine whether the chemistry of thiol groups near DNA could be modulated via DNA CT, thiols and disulfides located near the DNA base stack were investigated. Electrochemistry experiments on a graphite surface have shown that disulfide moieties covalently modified into the backbone of surface-bound oligonucleotides can be reduced to the corresponding thiol groups through the application of a reducing potential.[18] Additionally, DNA CT induced by a distally bound anthraquinone (AQ) photooxidant is able to promote the oxidation of neighboring thiol groups incorporated into the backbone of an oligonucleotide into a corresponding disulfide bond.[19]

DNA-mediated oxidation via AQ excitation leads to the dissociation of p53 from its response element DNA. Unlike other redox active proteins studied in the Barton group, p53 does not contain an FeS cofactor and its redox activity appears to be conferred through a network of cysteine residues within the DNA binding domain. An intriguing feature of p53 is that it contains 10 cysteine residues within the DNA-binding domain, nine of which are highly conserved.[2] These cysteines are purported to play a variety of roles, including tetramer formation, Zn^{2+} binding, and sequence-specific interaction with

FIGURE 4.1 — The frequency of p53 point mutations observed in cancer. The cysteine residues within p53 are noted in red. The numbers corresponding with each residue note the number of cancer observed with point mutations at that codon, and the percent of which these mutations constitute the observed p53 point mutations.[3] A representation of the p53 structural domains are depicted below the plot, giving a general idea of the location of these mutations.

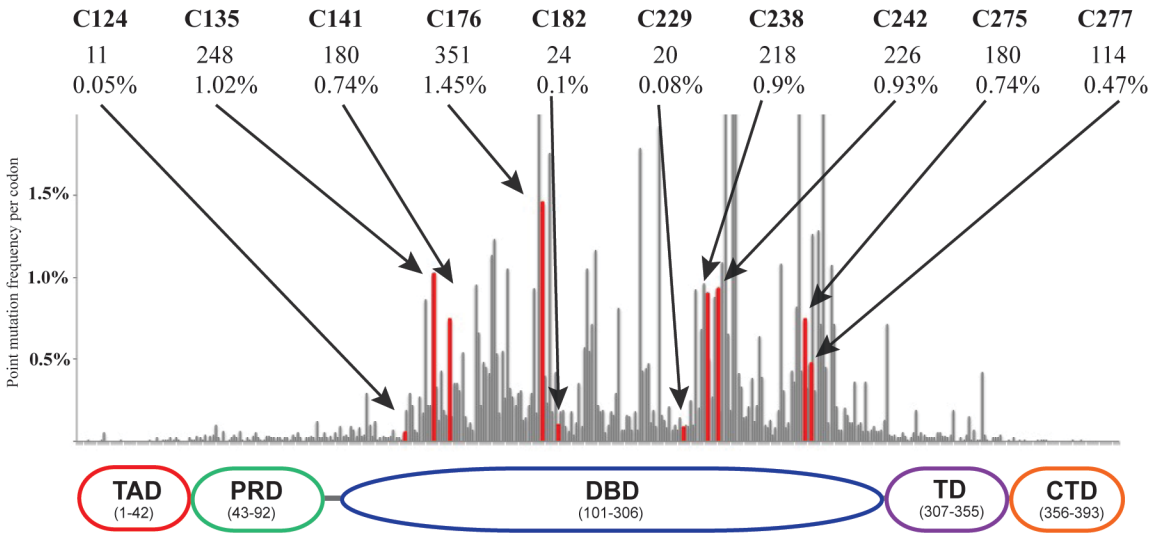

the p53 response element, as depicted in Figure 4.2. Each orange sphere represents the sulfur atom of the cysteine residues present within the protein. Within each p53 monomer, three cysteine residues (C176, C238, and C242) and one histidine (H179) coordinate a zinc ion that is believed to be structurally necessary for DNA binding.[2, 20-22] Located close to the Zn^{2+}, but not participating in metal binding, is C182. Closer to the DNA-p53 interface are the remaining conserved residues of interest: C124, C135, C141, C275, and C277. Nestled into the major groove, C277 is capable of forming a hydrogen bond within the purine region of the p53 response element quarter site.[20-22] C275 is located 7.0 Å away from C277, from sulfur atom to sulfur atom. Residues C124, C135, and C141 are found as a cluster situated deeper into the core of the DNA binding domain, with C275 7.0 Å away from C135. Chen and coworkers have reported these residues as reduced in their structural characterizations of the p53 DNA binding site; however, disulfide formation is plausible based on the proximity of these residues with respect to one another.[21-22]

One can imagine these conserved cysteine residues electronically coupling to promoter site DNA and playing a role in the redox modulation of p53. A model of p53 oxidation in response to DNA CT is illustrated in Figure 4.2. Oxidation of p53 is initiated at a distance by the photoexcitation of AQ covalently tethered to DNA, injecting an electron hole into the DNA base stack.[4,5,23] This oxidizing equivalent is then shuttled through the π-stacked base pairs and localizes to sites of low redox potential. If the electron hole localizes to a site to which protein is bound, such as the p53 response element, the hole can oxidize the lower redox potential amino acid residues within close proximity to the DNA. This oxidation of p53 leads to dissociation from the DNA,

FIGURE 4.2 — Schematic illustration of p53 oxidation through DNA-mediated charge transport. Oxidation is initiated by AQ excitation, causing it to abstract an electron from DNA. This electron hole equilibrates among the π-stacked bases, ultimately localizing to a low redox potential guanine site. If the trapped electron hole localizes to the DNA-p53 interface the bound p53 protein may be oxidized, due to amino acids with lower one-electron oxidations potentials than guanine. The oxidation of DNA-bound p53 causes the formation of a disulfide bond and leads to the dissociation from DNA. The orange spheres represent the sulfur atoms of each cysteine residue within the p53 DNA-binding domain, making them candidates for oxidation via DNA CT and subsequent disulfide formation. The DNA-p53 interface is examined in greater detail in the corresponding boxed region to the right. This diagram depicts the nine conserved cysteine residues within a DNA-bound p53 monomer in relation to one another and the DNA based on the 3KMD crystal structure.[21]

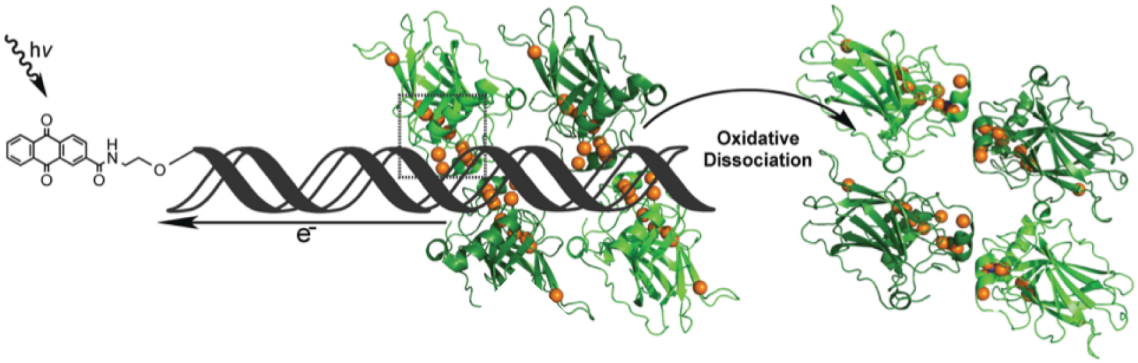

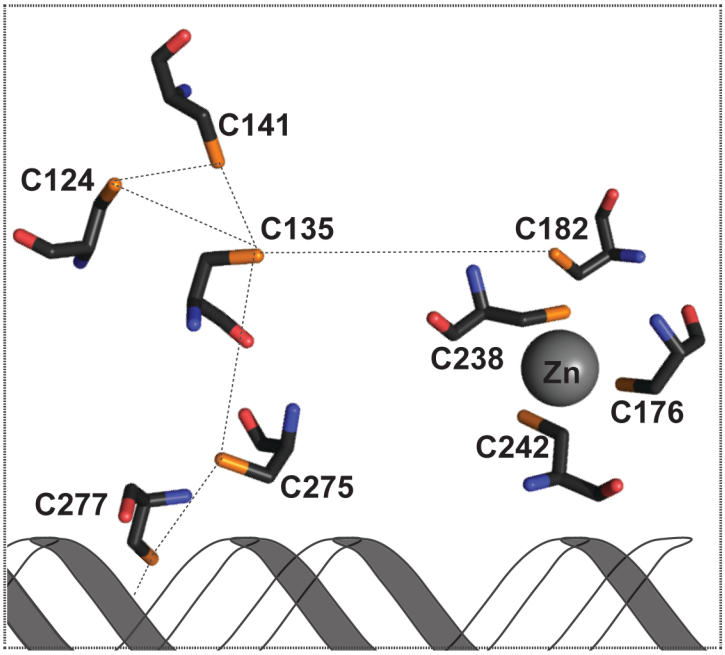

ultimately altering gene regulation in response to genomic stress while leaving the DNA undamaged.[5]

Experiments using electrophoretic mobility shift assays (EMSA) have determined that p53 responds selectively to oxidation via DNA CT, causing the protein to dissociate from various promoter sites. We have determined that the location of the guanine residues within a p53 response elements is what dictates whether DNA-bound p53 can be oxidized through DNA CT.[5] This sequence selectivity in DNA-mediated oxidation of p53 indicates an element of control, causing oxidative dissociation of p53 when bound to certain promoter sites but not to others. This selectivity in response to DNA CT seemingly correlates with the biological regulation of genes controlled by p53 under conditions of oxidative stress.

Several groups have worked to investigate the intricacies of p53 oxidation at a molecular level, an area of which little information is known after more than 30 years of research. The idea of redox modulation of p53 first arose in work showing that p53 can bind promoter sites selectively under reducing conditions, but not under oxidizing conditions.[24] More recently, Fersht and coworkers investigated the reactivity of cysteine residues by alkylation in an effort to stabilize mutant p53 observed in cancer.[25] Using nanospray ionization (nESI) mass spectrometry, they determined that C141 and C124 react first with alkylating agents and are therefore the most reactive cysteine residues, followed by C135, C182, and C277. Landridge-Smith and coworkers have utilized top-down and middle-down Fourier transform ion cyclotron resonance (FT ICR) mass spectrometry to determine the reactivity of cysteine residues within p53 oxidized by H_2O_2.[26] They determined that C182 and C277 exhibit significant modification with N-

ethylmaleimide and were deemed the most reactive residues. However, the high reactivity of these residues was determined to be primarily due to their high solvent accessibility, which may not be the dominant factor in DNA-bound p53 oxidation *in vivo*. Work has also been done to map oxidized cysteine residues in H_2O_2-treated p53 by nESI FT ICR mass spectrometry.[27] This work showed that oxidation of the p53 core domain by H_2O_2 caused a loss of Zn^{2+} binding within p53, with corresponding formation of two disulfide bonds among C176, C182, C238, and C242. Our laboratory found using MALDI-TOF mass spectrometry that DNA-mediated oxidation of p53 might proceed via formation of a disulfide bond involving C141 and an undetermined second cysteine.[4]

Here, we continue to investigate p53 cysteine oxidation promoted at a distance through DNA CT. Specifically, we aim to resolve the interplay of cysteine oxidation within the p53 DNA-binding domain through the study of p53 mutants. Using EMSA, we investigate the effect of select p53 mutations on DNA binding affinity as well as the ability to undergo oxidative dissociation from the Gadd45 promoter site. The Gadd45 promoter site was chosen since p53 is known to readily bind this sequence and also readily dissociates upon oxidation via DNA CT.[4] To determine if oxidative dissociation of p53 occurs concurrently with disulfide bond formation and probe the specific residues involved, we employed a differential thiol labeling technique targeting cysteine residue oxidation states through the use of isotopically distinct iodoacetamide labels. The sequentially labeled samples were proteolytically digested, and labeled peptide fragment intensities were examined on a QTRAP 6500 LC-MS/MS and directly compared. Through this methodology, we are able to characterize the redox states of individual cysteine residues and observe disulfide formation within p53 oxidized at a distance

through DNA CT.

MATERIALS AND METHODS

Synthesis and modification of oligonucleotides. DNA was synthesized using standard solid phase automated synthesis, modified with anthraquinone (AQ), and radiolabeled as described previously.[4,5,23,28] The DNA used in the following experiments contains the Gadd45 promoter site (underlined) with a 12 base 5′ linker. Constructs both without photooxidant (light control, LC) and with AQ were made. AQ: 5′-AQ- AAA TCA GCA CTA CAG CAT GCT TAG ACA TGT TC-3′. LC: 5′- AAA TCA GCA CTA CAG CAT GCT TAG ACA TGT TC-3′. Complement: 5′- GAA CAT GTC TAA GCA TGC TGT AGT GCT GAT TT -3′.

Protein preparation. The p53′ protein is a full-length human p53 containing three stabilizing mutations: M133L, V203A, and N268D.[29] All subsequent mutants studied are in addition to the p53′ mutations and incorporated by site-directed mutagenesis (QuikChange II, Agilent) with resulting sequences verified by Laragen (primer sequences are Appendix Table 4.1). The p53′ protein and subsequent mutants were purified as previously described.[5, 30]

Electrophoretic mobility shift assay of p53′ and mutants. For the determination of apparent K_D values for each mutant, varied concentrations of each p53′ mutant were added to 25 nM Gadd45 response element DNA in the presence of 5 μM competitor DNA (5′-GGAAAAAAAAAAAAAAAAACC-3′) (IDT), 0.1% NP-40 (Surfact-Amps NP-40, Thermo Scientific), 0.1 mg/mL BSA in p53 buffer (20 mM Tris-HCl, pH 8.0, 20% glycerol, 100 mM KCl, 0.2 mM EDTA). Samples were prepared at

ambient temperature, allowed to incubate for 20 minutes, and electrophoresed on a 10% TBE polyacrylamide native gel (Bio-Rad) in 0.5 x TBE buffer at 4 °C and 50 V for 1.5 h. DNA from the gel was transferred to Amersham Hybond-N nucleotide blotting paper (GE Healthcare) with a semidry electroblotter (Owl HEP-1) for 1 h at 175 mA in transfer buffer (25 mM Tris-HCl, pH 8.5, 200 mM glycine, 10% methanol). The blots were exposed to a phosphorimaging screen (GE Healthcare), imaged with a STORM 820 or Typhoon FLA 9000 scanning system (GE Healthcare), and analyzed using ImageQuant TL and OriginPro.

Samples prepared for p53 oxidation assays contained 25 nM p53 tetramer in the same conditions as listed above for the majority of the mutants. Two mutants were assayed at higher p53 concentrations due to their higher apparent K_D values: Y236F-p53′ at 50 nM tetramer and C275S-p53′ at 125 nM tetramer. Samples were made at 4 °C and irradiated in an ice bath for varying lengths of time (0, 5, 15, 30, 45, and 60 min) by solar simulator (ORIEL Instruments) with a UVB/UVC long-pass filter. These samples were then analyzed by EMSA as described above and data were normalized to the corresponding unirradiated control. The change in p53 binding was determined by monitoring the free DNA signal over the total DNA signal in each lane. Data are an average of a minimum of three assay replicates, and the error is reported as the standard error of the mean.

Selective cysteine labeling with iodoacetamide tags. Proteins p53′, C275S-p53′, and C141S-p53′ were studied to observe changes in cysteine oxidation state in DNA-bound p53 upon long range DNA CT. An overview of the reaction scheme is depicted in Figure 4.3. Each sample consisted of 100 µl 1.0 µM Gadd45 DNA (LC or

AQ), 2.0 μM p53′ monomer, 0.1% NP-40, 5.0 μM competitor DNA, in p53 buffer. Samples were prepared at 4 °C and allowed to incubate for 20 min prior to aliquoting. Samples for irradiation were aliquoted into a low profile 96-well PCR plate (Bio-Rad) at 10 μL each, placed in an ice-water bath, and irradiated for 1 h by solar simulator with a UVB/UVC long-pass filter. Unirradiated samples remained in the dark at 4 °C for the duration of the other irradiations. Samples were adjusted to 6 M guanidine hydrochloride (GdmCl), by the addition of 8 M GdmCl in 20 mM Tris, 100 mM KCl, 0.2 mM EDTA, at pH 7.75. The samples were transferred to Amicon Ultra 0.5 ml 30 KDa cutoff centrifugal filter units (Millipore) and centrifuged at 13,000 x G for 15 min. The concentrated samples, ~30 μl, were then treated with a 100-fold molar excess of iodoacetamide (Single-Use, Thermo Scientific) with respect to the number of cysteine residues present. The reaction was allowed to continue for 1 h in the dark, shaking at 250 rpm. Samples were diluted with 6 M GdmCl and centrifuged, repeatedly, until the concentration of remaining iodoacetamide within the sample was at least 100-fold below the number of cysteine residues, and concentrated to ~30 μL. Dithiothreitol (DTT) was added at a 10-fold molar excess than the reactive species present in the sample, cysteine and remaining iodoacetamide, to reduce disulfides. This reduction was allowed to incubate for 20 min at ambient temperature in the dark, shaking at 250 rpm. The same molar concentration of Tris(2-carboxyethyl)phosphine (TCEP-Neutral, Calbiochem) as DTT was then added to further ensure disulfide reduction and allowed to incubate, as above, for another 20 min. Samples were diluted with 6 M GdmCl and centrifuged, repeatedly, until the concentration of remaining DTT and TCEP were at a molar concentration 1000-fold below the number of cysteine residues present and the total volume concentrated to ~30

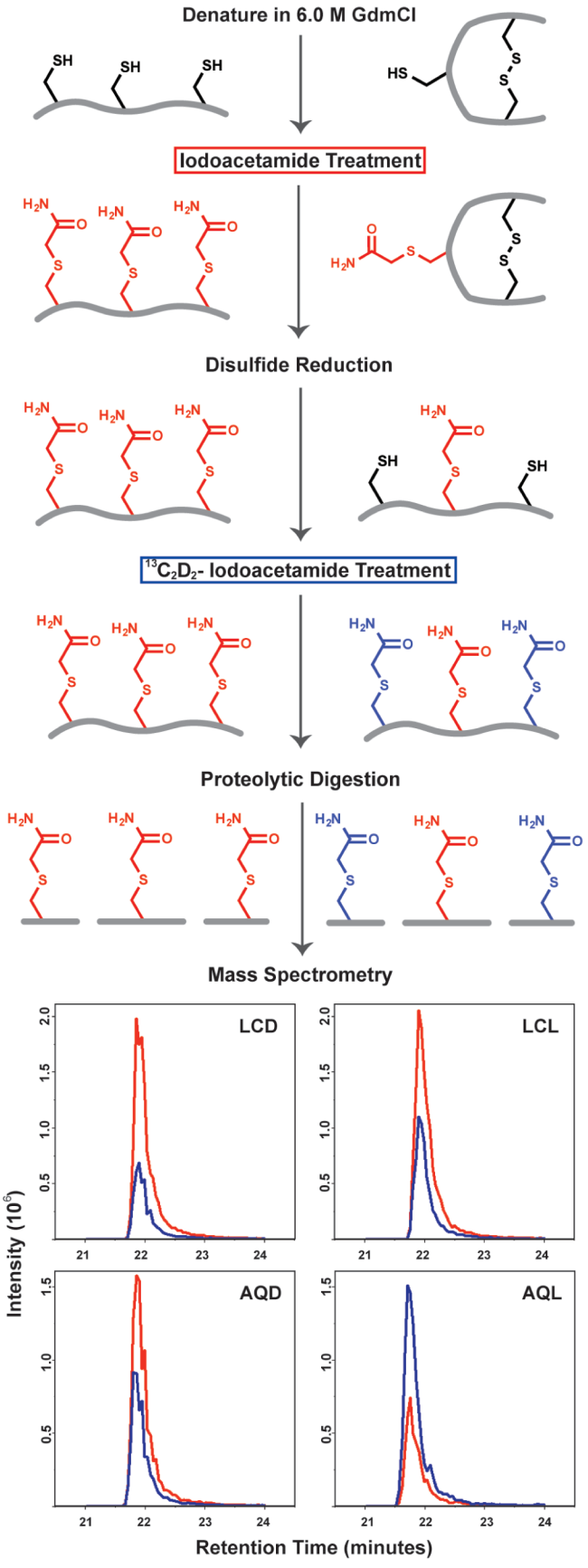

FIGURE 4.3 — Procedure for differential thiol labeling of cysteine residues. Examples of the labeling procedure are depicted for a fully reduced protein (Left) and its corresponding oxidized, disulfide-containing counterpart (Right). After oxidation from a distance through DNA CT, the protein sample is denatured in 6 M GdmCl and treated with iodoacetamide. Cysteine residues in a reduced state will react with iodoacetamide (red), while cysteine residues participating in disulfide bonds remain chemically unavailable. Removal of excess iodoacetamide followed by reduction of all disulfide bonds allow for accessibility of newly reduced thiol groups to react with the second $^{13}C_2D_2$-iodoacetamide label (blue). The protein is then proteolytically digested, peptide fragments are analyzed on a QTRAP 6500 LC-MS/MS, and peak areas are integrated in Skyline. Representative chromatograms of the C124 containing SVTCTYSPALNK peptide fragment from a p53′ sample set are shown as relative intensities of iodoacetamide (red) and $^{13}C_2D_2$IAA (blue) peptides detected. The four traces represent LCD—light control dark, LCL—light control light, AQD—anthraquinone dark, and AQL—anthraquinone light.

μL. To each sample $^{13}C_2D_2$-iodoacetamide (Aldrich) in H_2O was added at a 100-fold molar excess with respect to the cysteine residues and remaining reducing agents present. This reaction was allowed to continue for 4 h at ambient temperature, shaking at 250 rpm, in the dark. The samples were diluted using 100 mM Tris, pH 8.5, to lower the GdmCl concentration. The sample was repeatedly diluted and centrifuged until the final GdmCl concentration was below 0.1 M GdmCl in a final sample volume of ~30 μL and dried *in vacuo*. The dry sample pellet was dissolved in 40 μL of 8 M urea in 100 mM Tris-HCl, pH 8.5. 1 μL of 0.1 μg/μL of lysyl endopeptidase (WAKO) dissolved in 100 mM Tris-HCl pH 8.5 was added to each sample and allowed to incubate for 4 h at ambient temperature in the dark. The samples were subsequently diluted with 100 mM Tris-HCl, pH 8.5, to a final concentration of 2 M urea and adjusted to 1 mM $CaCl_2$. Trypsin (1 μL of 0.5 μg/μL)(Promega) in water was added to each sample and allowed to incubate in the dark overnight at ambient temperature. The following morning, each sample was adjusted to 5% formic acid to simultaneously inhibit protease activity and protonate tryptic peptides; samples were then dried *in vacuo*. Dry samples were suspended into 50 μL of 0.1% TFA and sonicated for 5 min. Stagetips were made in-house with Empore Extraction disk C-18 membranes (3M) for desalting the peptide samples.[31] The stagetip was washed once with 100 μL of 80% acetonitrile in 0.1% TFA and twice with 100 μL 0.1% TFA prior to sample loading, centrifuging for 3 min at 3000 rpm between each round. Samples were loaded to the stagetip by centrifugation and then washed twice with 100 μL 0.1% TFA. The sample was eluted with 100 μL of 80% acetonitrile in 0.1% TFA into fresh collection tube. The eluent was dried *in vacuo* and stored at -20 °C until analysis.

Multiple reaction monitoring (MRM) mass spectrometry. Each protein sample, 500 fmol per injection, was dissolved in 2% acetonitrile with 0.2% formic acid (FA). To ensure consistency among sample sets and to help validate proper peak assignment by retention time, iRT peptide standards (BIOGNOSYS) were added. Samples were examined on the ABSciex QTRAP 6500 LC-MS/MS system, equipped with an Eksigent ekspert nanoLC 425 pump, ekspert nanoLC400 autosampler, ekspert cHiPLC, and Analyst software. Samples were separated on a cHiPLC Chrom XP C18-CL 3 μm trap column, 120Å (200 μm * 0.5 mm), inline with a cHiPLC Chrom XP C18-CL 3 μm column, 120Å (75 μm * 150 mm) using a 45 min linear gradient of acetonitrile in 0.2% FA at a flow rate of 300 nL/min. An unscheduled transition list of cysteine-containing peptides with both respective iodoacetamide labels, as well as iRT peptide standards, was generated by Skyline and exported to the QTRAP for quantitation and are located in Appendix Table 4.2.[32] Raw data files generated by the QTRAP were imported back into Skyline, where peak areas were then integrated and exported for further processing. Observable and quantifiable peptide fragments include: C124—[121, 132] SVTCTYSPALNK, C135—[133, 138] LFCQLAK, C141—[140, 156] TCPVQLWVDSTPPPGTR, C182—[182, 196] CSDSDGLAPPQHLIR, and C275 and C277—[274, 280] VCACPGR. Two cysteine-containing peptide fragments were unobservable in our methods due to unfavorable mass/charge of the fragments: C175—[174, 180] RCPHHER, and C229, C238, and C242—[213, 248] HSVVVPYEPPEVGSDCTTIHYNYMC-NSSCMGGMNRR. Various proteases were evaluated; however, this large peptide fragment could not be further cleaved due to the inherent amino acid sequence of p53′.

RESULTS

Mutant p53′ affinity for the Gadd45 response element.

To understand the chemistry of p53 oxidation from a distance through DNA CT, individual residues within the DNA-binding domain were selectively mutated. We used a pseudo-wild-type p53, termed p53′, that incorporates three stabilizing mutations (M133L, V203A, and N268D) while remaining redox active.[29] All other mutants studied were created by site directed mutagenesis of the p53′ plasmid. The following cysteine residues were mutated to similarly sized but redox-inactive serine: C124, C135, C141, C182, C275, and C277. Two other mutations studied include Y236F and N239Y. These mutations were chosen since they are within close proximity to the cysteine residues in question and involve the addition or deletion of a similarly redox-active tyrosine (+0.9 V).[13] This cohort of p53 mutants was studied by EMSA to determine if any changes in binding affinity to the Gadd45 promoter site were evident without photooxidation.

Each mutant protein was evaluated by EMSA and the apparent K_D values were determined using varied concentrations of the p53′ mutants in the presence of 25 nM Gadd45 DNA (LC or AQ) in p53 buffer with 5 μM competitor DNA, 0.1% NP-40, and 0.1 mg/mL BSA. The determined apparent K_D values are listed in Table 1. The majority of the chosen mutations did not significantly change the binding affinity of these proteins to the Gadd45 promoter site as compared to p53′, with or without AQ. The baseline of binding affinity is shown by p53′ with K_D values of 1.6 ± 0.6 nM and 2.4 ± 1.1 nM of p53 tetramer for LC and AQ, respectively. C124S-p53′, C135S-p53′, C141S-p53′, and C277S-p53′ all share similar values as p53′ with apparent K_D values below 5 nM p53′ tetramer. Two mutants exhibited a slight decrease in affinity, at 9.7 ± 4.3 nM (LC)

TABLE 4.1 — Relative dissociation constants of mutant p53 bound to Gadd45 response element.

Mutant of p53 [a]	**K_D LC DNA** (nM tetramer)[b]	**K_D AQ DNA** (nM tetramer)[b]
p53′	1.6 ± 0.6	2.4 ± 1.1
C124S	3.7 ± 0.5	4.29 ± 0.04
C135S	4.4 ± 2.8	3.1 ± 1.2
C141S	4.6 ± 1.2	3.7 ± 0.3
C182S	15.1 ± 1.8	13.7 ± 4.4
Y236F	9.7 ± 4.3	8.2 ± 4.7
N239Y	1.2 ± 0.4	1.0 ± 0.1
C275S	56 ± 13	54 ± 8
C277S	3.0 ± 0.8	2.3 ± 0.5

a. All mutants contain the stabilizing mutations M133L, V203A, and N268D.

b. The apparent K_D of p53′ (in tetramer units) was determined at 25 nM duplex, 5 μM dAdT, 0.1% NP-40, 0.1 mg/mL BSA in 20 mM Tris-HCl (pH 8.0), 20% glycerol, 100 mM KCl, and 0.2 mM EDTA at ambient temperature and the sample electrophoresed at 50 V on a 10% polyacrylamide gel in 0.5 × TBE at 4 °C.

and 8.2 ± 4.7 nM (AQ) tetramer for Y236F-p53′ and 15.1 ± 1.8 nM (LC) and 13.7 ± 4.4 nM (AQ) tetramer for C182S-p53′. Notably, the C275S-p53′ mutant displays severely attenuated affinity for the Gadd45 promoter site with apparent K_D values of 56 ± 13 nM (LC) and 54 ± 8 nM (AQ).

Oxidative dissociation of p53′ mutants through DNA CT.

Additional EMSAs were employed to determine if any of these mutations altered the ability of p53′ to oxidatively dissociate from the Gadd45 promoter site. Changes in p53′ binding to the Gadd45 promoter site with respect to irradiation time for each mutant were quantified and the results are shown in Figure 4.4, along with representative EMSA autoradiograms of C135-p53′ and C275S-p53′. Most samples were composed of 25 nM p53′ tetramer and 25 nM Gadd45 DNA in the presence of 5 μM competitor DNA, 0.1% NP-40, 0.1 mg/mL BSA in p53 buffer. Y236F-p53′ and C275S-p53′ were assayed at higher protein concentrations, 50 nM tetramer and 125 nM tetramer, respectively, to ensure protein-DNA binding due to their higher apparent K_D values. The fraction change in p53′ binding is determined as the free DNA signal divided by the sum of the free DNA and p53-bound DNA signals, normalized to the unirradiated control. Each mutant was analyzed over a minimum of three replicates, with the error bars reflecting the standard error of the mean. Previous experiments with the same construct, although with an intervening mismatch, showed an inhibition of oxidative dissociation, demonstrating that oxidation of p53 is DNA-mediated as opposed to involving a direct AQ-protein interaction.[4] The behavior of p53′ is the standard to which each mutant is compared in Figure 4.4. The EMSAs of p53′ oxidation reveal minimal oxidative dissociation from the

FIGURE 4.4— Representative autoradiogram of the C135S-p53′ EMSA for the evaluation of mutant p53 activity on Gadd45-response element DNA. The LC samples do not contain a photooxidant, while the AQ samples contain a 5′ covalently tethered anthraquinone. The band intensities of free DNA and p53-bound-DNA are quantified with ImageQuant to determine changes in p53 occupancy upon irradiation. EMSA analysis to determine the activity of mutant p53 bound to the Gadd45 promoter site upon distally induced DNA-mediated oxidation. Solid markers represent AQ samples, while hollow markers represent LC samples. The data are representative of the average of a minimum of three replicates, with the error as the standard error of the mean. Samples contained 25 nM mutant p53′ tetramer and 25 nM Gadd45 DNA in the presence of 5 μM competitor DNA, 0.1% NP-40, and 0.1 mg/mL BSA in p53 buffer [20 mM Tris-HCl, pH 8.0, 20% glycerol, 100 mM KCl, and 0.2 mM EDTA]. Two mutants were assayed at higher protein concentrations due to their higher apparent K_D values: Y236F-p53′ at 50 nM tetramer and C275S-p53′ at 125 nM tetramer.

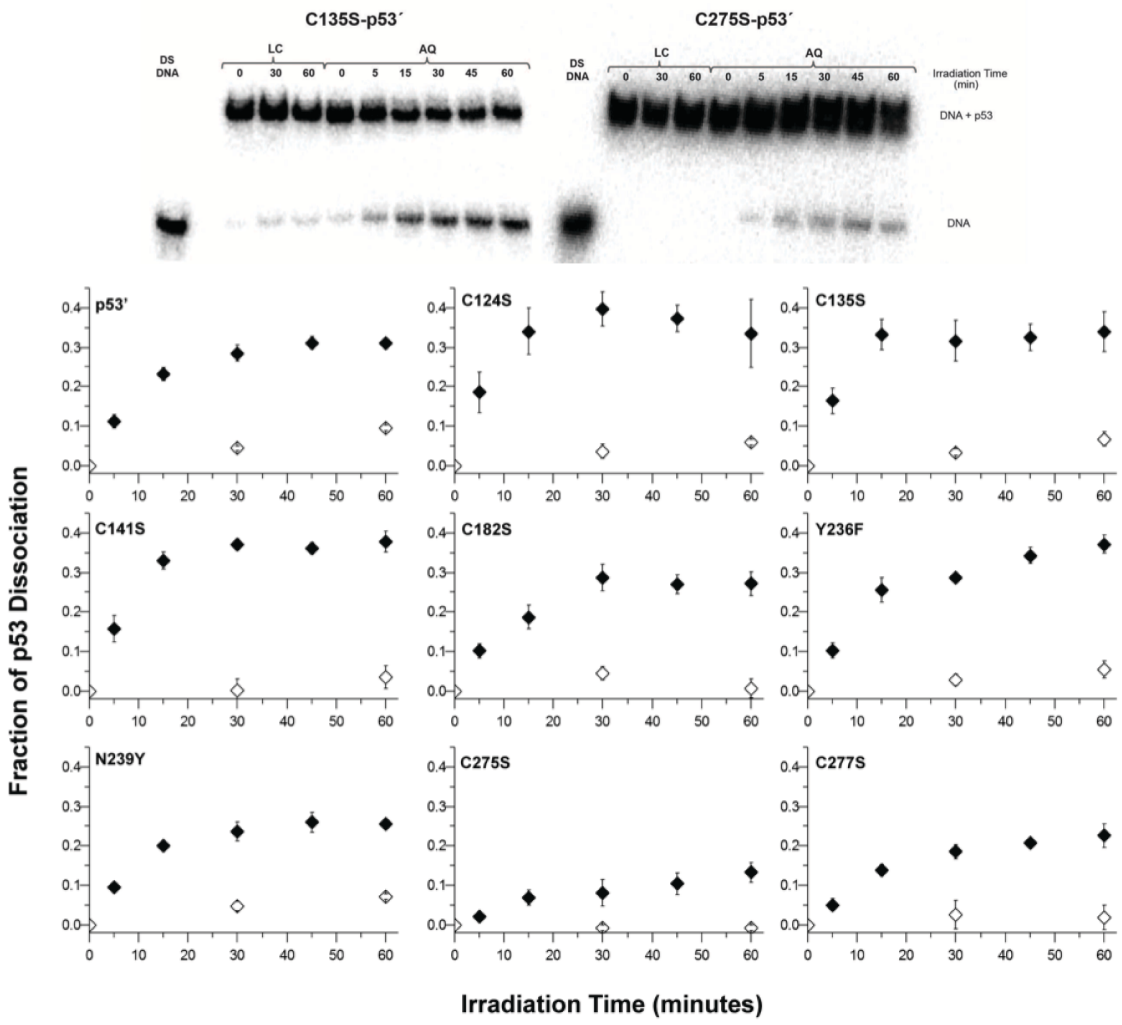

LC-Gadd45 DNA (white), lacking the pendant AQ photooxidant. However, the p53′ protein readily dissociated from the AQ-Gadd45 DNA (black), with 31.0 ± 1.2 % total p53′ dissociation upon 60 minutes of irradiation. The LC-Gadd45 DNA samples across all of the mutants behave similarly, with minimal dissociation upon irradiation irrespective of additional mutations. As compared to the p53′ protein, several mutants displayed a slight increase in the amount of dissociation from the AQ-Gadd45 DNA upon irradiation: C141S-p53′ (37.9 ± 2.7%), Y236F-p53′ (37.2 ± 2.3%), C135S-p53′ (34.0 ± 5.0%), and C124S-p53′ (33.4 ± 8.6%). Conversely, several mutants displayed a slight attenuation in the oxidative dissociation of p53 upon irradiation: C182S-p53′ (27.2 ± 3.0%), N239Y-p53′ (25.5 ± 0.9%), and C277S-p53′ (22.6 ± 2.9%). The most notable difference is observed with C275S-p53′, which reaches a maximum of only 13.3 ± 2.5% protein dissociation upon irradiation and is not within error of any other mutant.

Analysis of cysteine oxidation in p53′ by mass spectrometry.

Using multiple reaction monitoring (MRM) through sensitive analytical mass spectrometry, we directly examined the formation of disulfide bonds within p53′ and mutants from a distance through DNA CT. An overview of the cysteine labeling protocol used to differentially label cysteine residues within p53 respective to oxidation state is shown in Figure 4.4. Using this methodology, one can distinguish whether individual cysteine residues in the protein are participating in a disulfide bond. After protein oxidation is induced from a distance by irradiation of the AQ-DNA, the protein is denatured in 6 M GdmCl and treated with iodoacetamide. Reduced cysteine residues in p53′ will react with iodoacetamide (red), while oxidized cysteine residues participating in

disulfide bonds remain chemically unavailable. Removal of excess iodoacetamide and subsequent reduction of all disulfide bonds allow for accessibility of the newly reduced cysteine residue thiol groups to react with the isotopically heavy $^{13}C_2D_2$-iodoacetamide (blue). The protein is then proteolytically digested, desalted by C18 stagetip, and analyzed on a QTRAP 6500 LC-MS/MS. Representative chromatograms of the acquired data for the peptide fragment containing C124 from a p53′ sample set are shown at the bottom of Figure 4.3. The peak areas for both the iodoacetamide (red) and $^{13}C_2D_2$-iodoacetamide (blue) labeled fragments were analyzed in Skyline, then directly compared.[32] These data clearly show the trend toward the $^{13}C_2D_2$-iodoacetamide label with the AQL sample, whereas (LCD, LCL, and AQD, see Figure 4.3) were predominated by the isotopically light iodoacetamide label.

Proteins p53′, C275S-p53′, and C141S-p53′ were studied by mass spectrometry to observe changes in cysteine oxidation in DNA-bound p53′ promoted at a distance through DNA CT. We monitored the changes of cysteine residues in p53′ as our standard of comparison. We also examined C275S-p53′ since it displayed the least oxidative dissociation by EMSA, and C141S-p53′ since C141 was previously implicated in potential disulfide formation through DNA CT.[4] The floating-bar plots for each peptide fragment depict the fraction of the total signal of heavy and light modified species, totaling 1.0, as depicted in Figure 4.5 for p53′, Figure 4.6 for C141S-p53′, and Figure 4.7 for C275S-p53′. The fraction of $^{13}C_2D_2$-iodoacetamide labeled species is represented in positive values (black) and the fraction of iodoacetamide labeled species is represented in negative values (white). These cumulative data sets are represented with individual protein mutants located in rows, and corresponding cysteine-containing peptide

fragments in columns. Each sample set per mutant is composed of 4 variants, corresponding to DNA used (LC or AQ) and irradiation (D-dark, L-light). The data represent the average of three replicates for C124, C135, C141, and C182 peptide fragments. The data for C275 and C277 represent the average of two replicates. The error is represented as the standard error of the mean. Peptide fragments corresponding to C176, C229, C238, and C242 could not be observed due to an unfavorable mass/charge ratio.

A shift toward increased $^{13}C_2$-D_2-iodoacetamide labeling indicates that the cysteine of interest has become oxidized and is participating in a disulfide bond. For p53′ and C141S-p53′ sample sets, the AQL samples show a marked increase in $^{13}C_2D_2$-iodoacetamide labeling over the LCD, LCL, and AQD control samples. The value (white) located within the AQL floating bar represents the percent change in heavy labeling of AQL sample with respect to the average of the corresponding LCD, LCL, and AQD controls. The protein p53′ does indeed undergo chemical oxidation through DNA-mediated DNA CT. Interestingly, the C275S-p53′ sample set depicts a different interplay of oxidation states than observed for p53′ and C141S-p53′. The overall baseline of $^{13}C_2D_2$-iodoacetamide corresponding to the C135 and the C182 peptides are significantly higher across all four samples. The C124, C141, and C277 peptides in C275S-p53′ behave more similarly to the other sample sets with a distinct, albeit a less intense, increase in the AQL samples as compared to the controls.

FIGURE 4.5 — Determination of cysteine oxidation states by MRM mass spectrometry of p53′ to observe changes in cysteine oxidation induced through DNA CT. Cumulative data are depicted with individual mutant proteins localized in rows, and the corresponding cysteine-containing peptide fragments in columns. The floating-bar plots for each peptide fragment are depicted as the fraction of the total signal of both heavy and light modified species, totaling 1.0. The fraction of $^{13}C_2$-D_2-iodoacetamide labeled species is represented in positive values (black) and the fraction of iodoacetamide labeled species is represented in negative values (white). Each plot is composed of four samples: LCD—light control dark, LCL—light control light, AQD—anthraquinone dark, and AQL—anthraquinone light. The value (white) located within the AQL floating bar represents the percent change in heavy labeling of the AQL sample with respect to the average of the corresponding LCD, LCL, and AQD controls.

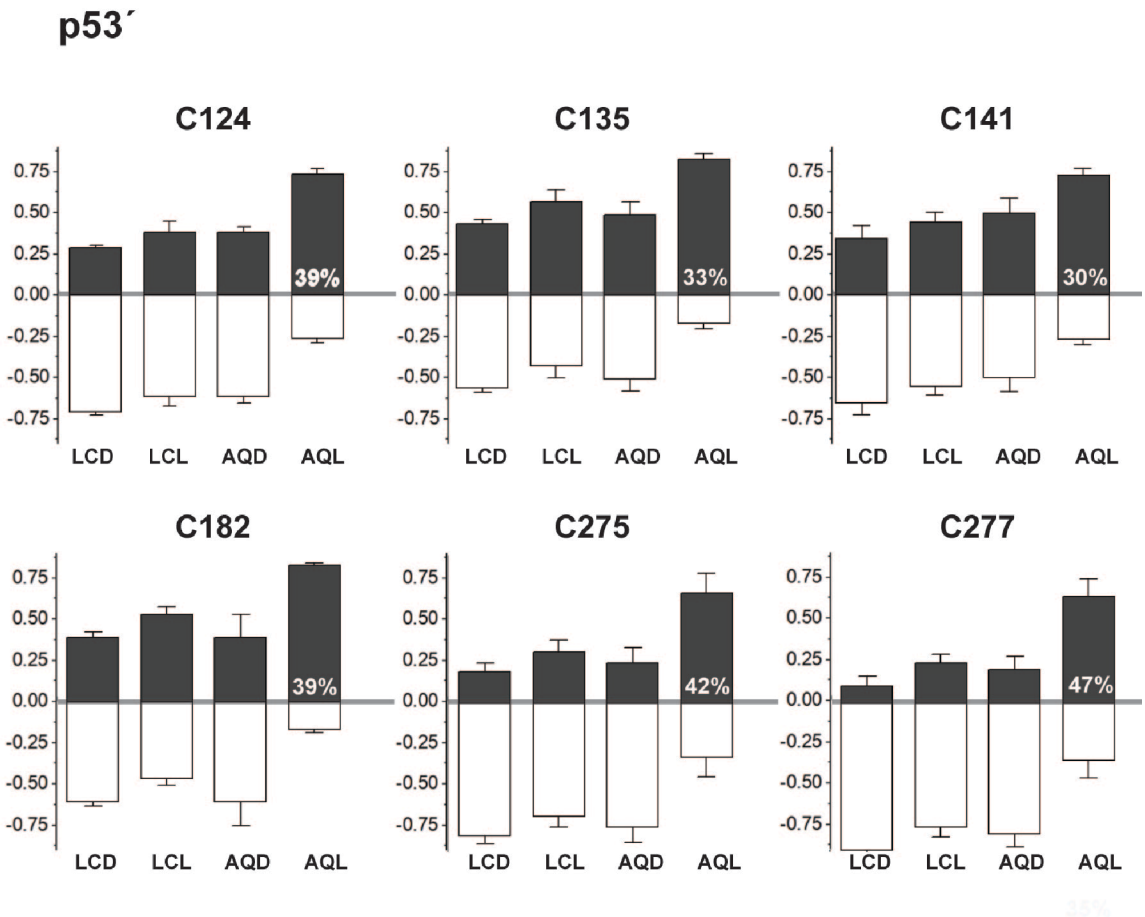

FIGURE 4.6 — Determination of cysteine oxidation states by MRM mass spectrometry of C141S-p53′ to observe changes in cysteine oxidation induced through DNA CT. Cumulative data are depicted with individual mutant proteins localized in rows, and the corresponding cysteine-containing peptide fragments in columns. The floating-bar plots for each peptide fragment are depicted as the fraction of the total signal of both heavy and light modified species, totaling 1.0. The fraction of $^{13}C_2$-D_2-iodoacetamide labeled species is represented in positive values (black) and the fraction of iodoacetamide labeled species is represented in negative values (white). Each plot is composed of four samples: LCD—light control dark, LCL—light control light, AQD—anthraquinone dark, and AQL—anthraquinone light. The value (white) located within the AQL floating bar represents the percent change in heavy labeling of the AQL sample with respect to the average of the corresponding LCD, LCL, and AQD controls.

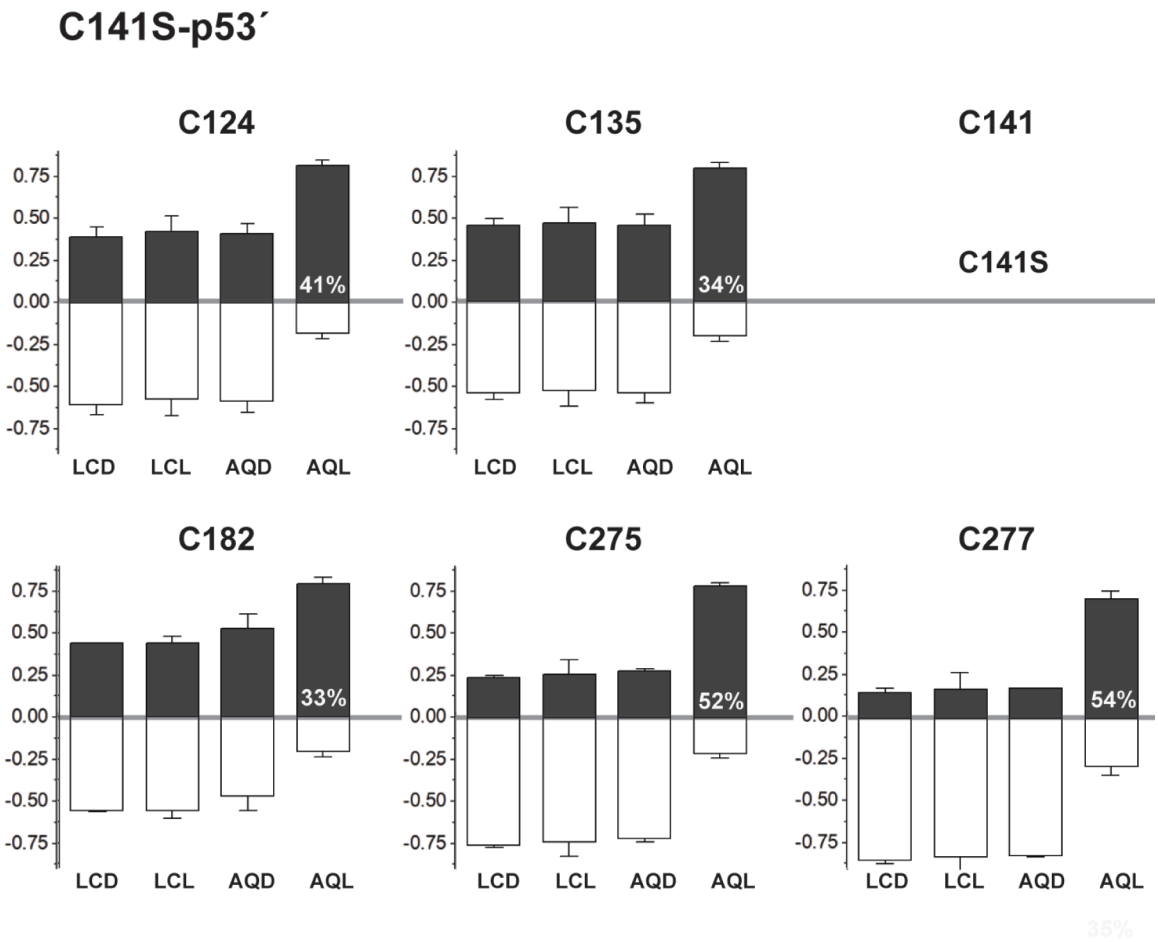

FIGURE 4.7 — Determination of cysteine oxidation states by MRM mass spectrometry of C275S-p53′ to observe changes in cysteine oxidation induced through DNA CT. Cumulative data are depicted with individual mutant proteins localized in rows, and the corresponding cysteine-containing peptide fragments in columns. The floating-bar plots for each peptide fragment are depicted as the fraction of the total signal of both heavy and light modified species, totaling 1.0. The fraction of $^{13}C_2$-D_2-iodoacetamide labeled species is represented in positive values (black) and the fraction of iodoacetamide labeled species is represented in negative values (white). Each plot is composed of four samples: LCD—light control dark, LCL—light control light, AQD—anthraquinone dark, and AQL—anthraquinone light. The value (white) located within the AQL floating bar represents the percent change in heavy labeling of the AQL sample with respect to the average of the corresponding LCD, LCL, and AQD controls.

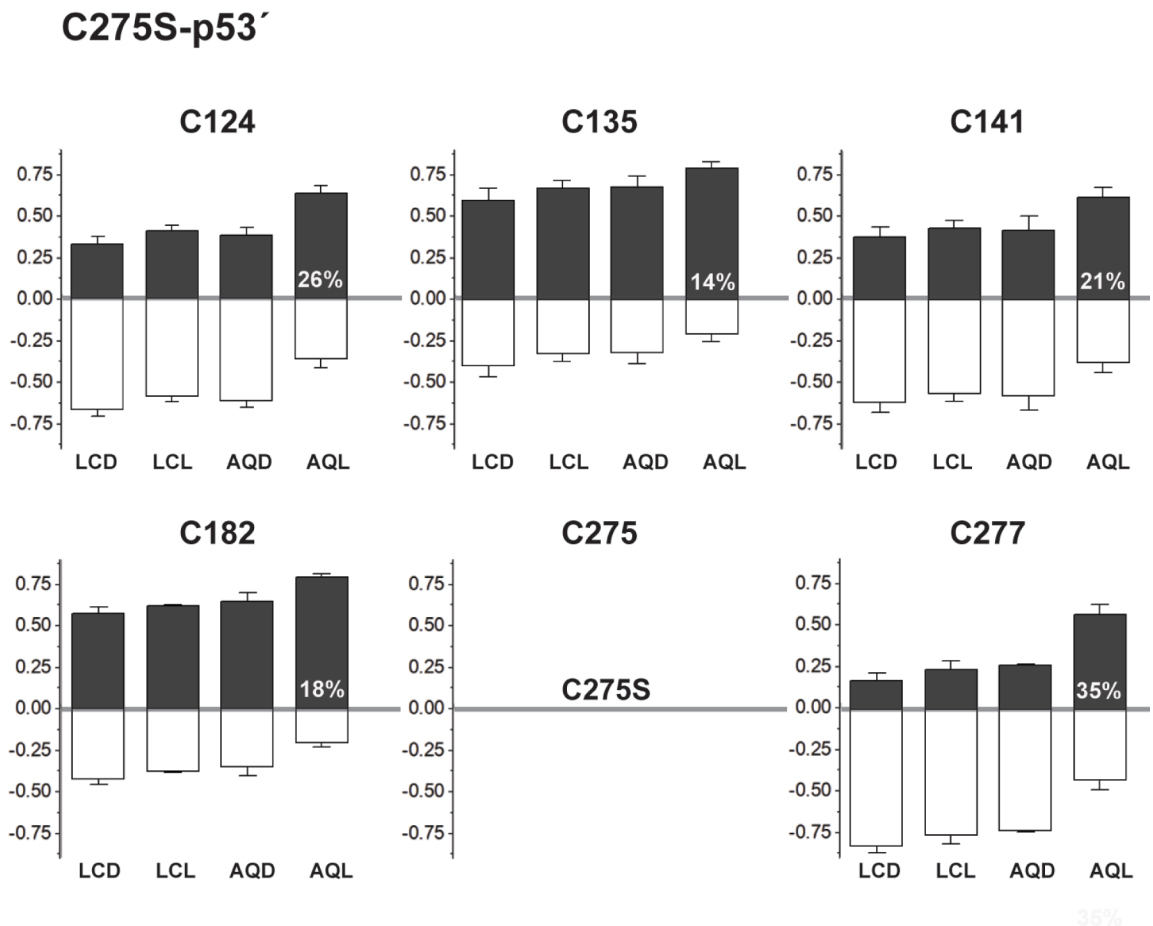

DISCUSSION

Although much work has been done elucidating the redox-dependent binding of p53 to different promoter sites, relatively little is known about the chemistry of p53 oxidation at a molecular level. We are particularly interested in how the protein may be coupled into a charge transport pathway with DNA and how DNA-mediated oxidation of p53 may affect the affinity of p53 for individual promoter sites. The conserved cysteine residues not involved in Zn^{2+} binding are of particular interest due to their biologically accessible oxidation potential, close proximity to DNA, and ability to form disulfide bonds. In our studies, we sought to determine the role of various cysteine residues (C124, C135, C141, C182, C275, and C277) within the DNA-binding domain of p53 through mutagenesis. The cysteine-to-serine mutation was chosen, since serine is structurally similar to cysteine but does not contain the redox-active sulfur atom. Two other mutations involving redox-active tyrosine residues (Y236F and N239Y) were investigated as well, as tyrosine has the same one-electron oxidation potential as cysteine (+0.9 V), also making it accessible to photooxidation by DNA-bound AQ.[13]

Effect of select mutations on p53′ binding affinity.

Each mutant of p53′ was first evaluated by determining changes in affinity for the Gadd45 promoter site. All comparisons were made against the observed affinity of p53′ tetramer for Gadd45 DNA, which was determined to be 1.6 ± 0.6 nM and 2.4 ± 1.1 nM of tetramer for LC and AQ, respectively. The majority of our chosen mutations did not significantly alter the binding affinity of these proteins to the Gadd45 promoter site. C124S-p53′, C135S-p53′, C141S-p53′, N239Y-p53′, and C277S-p53′ all share similar

affinities as p53′, with apparent K_D values below 5 nM p53′ tetramer, indicating that C124, C135, C141, N239, and C277 do not play a significant role in modulating p53 binding affinity to DNA. Y236F-p53′ and C182S-p53′ both exhibited a slight decrease in affinity, with corresponding apparent K_D values between 8-15 nM p53 tetramer. This indicates that the integrity of Y236 and C182 within the protein may contribute to binding affinity through necessary DNA-protein contacts or protein-protein interactions in tetramer formation. Notably, the C275S-p53′ mutant displays severely attenuated affinity for the Gadd45 promoter site with K_D values of 56 ± 13 (LC) and 54 ± 8 nM (AQ). This finding demonstrates that the integrity and likely positioning of C275 is necessary for the high affinity binding of p53 to promoter site DNA.

Effect of select mutations on oxidative dissociation.

How do these mutations affect the oxidative dissociation of DNA-bound p53? The behavior of p53′ is the standard to which each mutant was compared. For p53′, 31% p53′ dissociation is seen relative to controls after 60 minutes of irradiation of DNA-tethered AQ. Oxidative dissociation from the AQ-Gadd45 DNA is equal to or slightly increased for C124S-p53′, C135S-p53′, C141S-p53′, and Y236F-p53′ upon irradiation. Slightly increased dissociation suggests that the integrity of these residues is not essential. In contrast, several mutants did cause attenuation in oxidative dissociation. The C182S-p53′ mutation appears to slightly decrease oxidative dissociation. The N239Y-p53′ mutation also shows a slight decrease in dissociation; since tyrosine has the same redox potential as cysteine and is within close proximity of the DNA, the added tyrosine residue may become oxidized, preventing electron hole migration to other

cysteine residues.[12] Interestingly, while known to be a stabilizing mutation within p53, N239Y has been observed in colorectal cancer somatic cell mutations.[29, 33, 34] It is noteworthy that the C277-p53′ mutant binds Gadd45 DNA with comparable affinity as p53′ but does not to dissociate as readily at 22% and not within error of p53′. This result indicates that C277 may be a necessary element for the oxidative dissociation of p53, perhaps through coupling into the DNA CT pathway and initiating disulfide formation with the nearby C275. Indeed, the most significant difference observed with the mutants is the severe attenuation of oxidative dissociation of C275S-p53′, with a maximum of only 13% dissociation. Thus it is evident that C275 plays a critical role in the affinity of p53 for its promoter site as well as enabling oxidative dissociation. Interestingly, the mutation of C275 has been observed in lung cancer.[35] The attenuation of oxidative dissociation in both C275S and C277S suggests the possibility that these residues form a key disulfide bond upon oxidation. The formation of a disulfide between C275 and C277 would also remove DNA contacts, lowering DNA affinity overall, and enabling p53 dissociation. The observed amounts of oxidative dissociation of C275S-p53′ and C277S-p53′ are not equivalent, indicating that these two residues are not phenocopies. This variation is due to the location of the cysteine residues with respect to the DNA bases conveying the electron hole.

Mass spectrometry results to characterize cysteine oxidation states.

Mass spectrometry studies were carried out to understand the chemistry of DNA-mediated p53 oxidation. A differential-thiol labeling method was devised to determine the oxidation state of specific cysteine residues within p53. The sequential use of

iodoacetamide, reducing agents, and isotopically distinct $^{13}C_2D_2$-iodoacetamide enables us to label cysteine residues depending on their respective oxidation state. A shift toward greater $^{13}C_2D_2$-iodoacetamide labeling in comparison to controls, as monitored through MRM mass spectrometry, indicates oxidation of that residue and its disulfide participation. We were able to study six of the ten cysteine residues present within the DNA-binding domain through this technique. We were unable to detect C176 since it is located in a very small and highly charged peptide fragment [RCPHHER], resulting in an unfavorable mass/charge ratio. Three cysteine residues (C229, C238, and C242) all reside within one extraordinarily large peptide fragment that [HSVVVPYEPPEVGSDCTTIHYNYMCN-SSCMGGMNRR] could not be further digested proteolytically and could therefore not be detected within the limits of our instrumentation. The remaining six cysteine residues are readily detected and quantifiable. However, C275 and C277 reside within the same peptide fragment, so secondary ion intensities were utilized to deconvolute mixed species containing both iodoacetamide and $^{13}C_2D_2$-iodoacetamide.

It is important to note that these mass spectrometry data indicate directly that the DNA-bound p53′ protein can be oxidized from a distance through DNA-mediated CT. Residues bound to the DNA, and not those most accessible to solution, are oxidized, funneling oxidative damage from the DNA helix and into the protein. This DNA-mediated process promotes p53′ dissociation from the Gadd45 promoter site.

The mass spectrometry data furthermore establish which cysteine residues are being oxidized from a distance through DNA CT. In most cysteine residues observed for both the p53′ and the C141S-p53′ sample sets, the AQL samples show a marked increase

in $^{13}C_2D_2$-iodoacetamide labeling samples as compared to the LCD, LCL, and AQD controls. Thus, cysteine oxidation resulting in disulfide bond formation is occurring among all observable cysteine residues within p53′ and C141S-p53′. However, we are unable to determine whether the disulfide formation is occurring intramolecularly or intermolecularly through our methodologies. Both p53′ and C141S-p53′ show very similar profiles of oxidation with a significant AQL-$^{13}C_2D_2$-iodoacetamide increase in all observable cysteine residues: C124, C135, C141, C182, C275, and C277. It should be noted that across all of the samples there is a baseline level of oxidation, indicating some disulfide presence in the protein prior to DNA CT. Nonetheless it appears that the majority of the cysteines are in the reduced state. Importantly, the fraction of $^{13}C_2D_2$-iodoacetamide labeling is greatly increased upon oxidation, resulting from DNA CT. Removal of C141 through the C141S mutation does not appear to alter the DNA binding affinity, oxidative dissociation, or the ability to oxidize any other cysteine residues. This suggests that oxidation of C141 may occur, but its presence is not necessary for modulation of p53′ binding affinity through DNA-mediated oxidation.

The C275S-p53′ sample set depicts a different interplay of oxidation states than observed in either p53′ or C141S-p53′, however. The overall baseline of $^{13}C_2D_2$-iodoacetamide labeling for C135 and C182 peptide controls are high across all four samples, greater than 60%, and only show a slight increase in the AQL samples over the controls. The C124, C141, and C277 peptides in C275S-p53′ behave more similarly to the other sample sets with a distinct, albeit less intense, increase in the AQL samples with respect to the controls. The smaller shift toward $^{13}C_2D_2$-iodoacetamide labeling in the

AQL samples relative to the controls suggests that the absence of C275 disrupts the ability of oxidation to be transferred to the more internal residues.

Oxidative dissociation of p53′ by disulfide formation.

By applying the observed data to the network of cysteine residues within p53, we can consider how DNA-mediated oxidation of p53 may occur and how it may lead to changes in protein conformation that decrease affinity for DNA. Reduced p53 binds as a tetramer to the Gadd45 promoter site. Upon DNA oxidation, an electron hole will migrate through the π-stacked bases and localize to DNA sites of low redox potential, such as guanine. This CT occurs on a timescale that is fast compared to irreversible reaction of guanine radicals.[36] In the case of the Gadd45 promoter site, the low oxidation potential guanine sites are located within the purine region of the response element in close proximity to the p53 residue C277. Since the redox potential of cysteine (+0.9 V) is lower than guanine (+1.29 V), the C277 residue tucked in the major groove near guanine can accept the electron hole, become oxidized, and lose its hydrogen bond to the major groove of DNA.[13-16] Due to the solvent accessibility of C277 and its close proximity to C275, further oxidation of C277 by molecular oxygen would allow for loss of a second electron and result in disulfide formation between C277 and C275, located 7.0 Å away. Disulfide formation between these two residues would result in the loss of essential p53-DNA binding contacts, leading to a significant decrease in affinity, causing the dissociation of the oxidized p53 monomer, as is schematically depicted in Figure 4.8.

Disulfide bonds are known to rearrange among other cysteine residues within close proximity of one another within proteins.[37,38] Upon formation of the C277-C275

FIGURE 4.8 — Proposed disulfide formation within p53 via DNA CT based on the 3KMD crystal structure.[21] Formation of the disulfide bond between C275 and C277 results in the loss of DNA response element contacts and is therefore most likely responsible for the loss of DNA binding affinity upon oxidation through DNA CT.

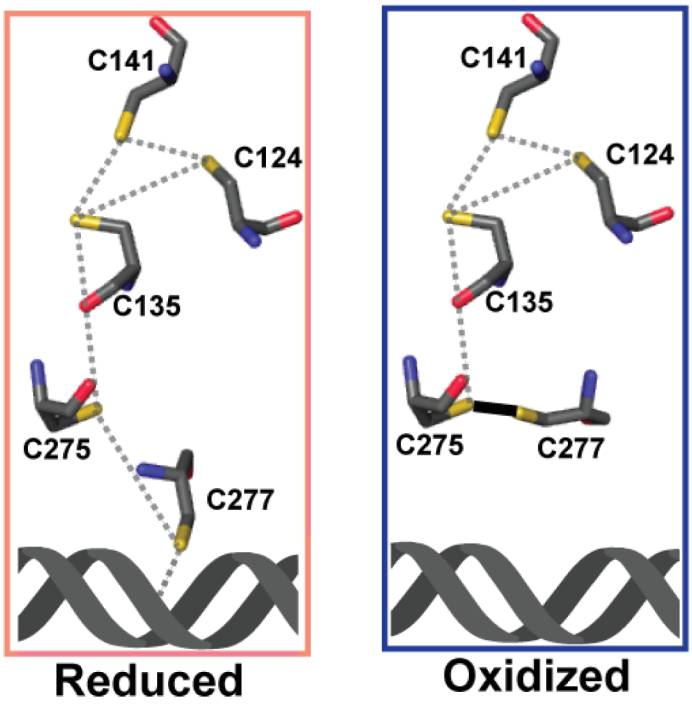

disulfide bond, a subsequent rearrangement could occur given the presence of many other reduced cysteine residues within close proximity. If this were to occur, C275 would most likely form a disulfide with C135 (7 Å away). This bond rearrangement would funnel the disulfide bond deeper into the protein and enable C277 to become reduced and possibly reestablish its H-bond to DNA. The disulfide bond could then rearrange once more, resulting in one disulfide bond potentially residing among the inner triad of cysteine residues: C124, C135, and C141.

Thus, well conserved cysteine residues of p53 provide a chemical platform through which genomic oxidative stress can be directly sensed. Since p53 is a transcription factor presiding over the regulation of hundreds of human genes, the oxidative dissociation of p53 allows for a direct response in p53 gene regulation during times of genomic stress. The extent of oxidative dissociation of p53 depends on the DNA sequence of the promoter site to which it is bound.[5] Low redox potential guanine bases located in the purine region of the p53 promoter site allow for electron holes to localize at the DNA-protein interface and concomitantly oxidize p53. The variability of bases within the promoter site, while fully conforming to the response element constraints, allows for a tuning of the redox potential at the DNA-protein interface. The DNA sequence of the promoter site determines whether DNA-bound p53 will be able to accept an electron hole and respond to genomic stress. The cysteine residues in the protein create a network, which is coupled to DNA, capable of accepting electron holes via DNA CT. It is through p53 oxidation and disulfide formation that the affinity of p53 for DNA is decreased, leading to the observable oxidative dissociation of DNA-bound p53.

These results thus indicate that DNA-mediated oxidation of p53 is a chemically distinct mechanism for the cell to respond specifically to oxidative damage to the genome. The oxidation of p53 through DNA CT resulting in disulfide formation within a protein is an exciting new chapter in the study of cellular signaling of oxidative stress and the response of p53.

REFERENCES

1. Paveletich, N. P., Chambers, K. A., and Pabo, C. O. (1993) The DNA-binding domain of p53 contains the four conserved regions and the major mutation hot spots. *Genes Dev. 7*, 2256-2564.

2. Joerger, A. C., and Fersht, A. R. (2007) Structure-function-rescue: The diverse nature of common p53 cancer mutants. *Oncogene 26*, 2226-2242.

3. Petitjean, A., Mathe, E., Kato, S., Ishioka, C., Tavtigian, S. V., Hainaut, P., and Olivier, M. (2007) Impact of mutant p53 functional properties on TP53 mutation patterns and tumor phenotype: lessons from recent developments in the IARC TP53 database. *Hum Mutat. 28*, 622-629. Version R17.

4. Augustyn, K. E., Merino, E., and Barton, J. K. (2007) A role for DNA-mediated charge transport in regulating p53: Oxidation of the DNA-bound protein from a distance *Proc. Natl. Acad. Sci. USA 104*, 18907-18912.

5. Schaefer, K. N., and Barton, J. K. (2014) DNA-mediated oxidation of p53. *Biochemistry* 53, 3467-3475.

6. Hall, D., Holmlin, R., and Barton, J. K. (1996) Oxidative DNA damage through long-range electron transfer. *Nature 382*, 731-735.

7. Delaney, S., and Barton, J. K. (2003) Long-range DNA charge transport. *J. Org. Chem. 68*, 6475-6483.

8. Muren, N. B., Olmon, E.D., and Barton, J. K. (2012) Solution, surface, and single molecule

platforms for the study of DNA-mediated charge transport *Phys. Chem. Chem. Phys. 14*, 13754-13771.

9. Sontz, P. A., Muren, N. B., and Barton, J. K. (2012) DNA charge transport for sensing and signaling. *Acc. Chem. Res. 45*, 1792-1800.

10. Genereux, J., Boal, A., and Barton, J. K. (2010) DNA-mediated charge transport in redox sensing and signaling. *J. Am. Chem. Soc. 132*, 891-905.

11. Slinker, J., Muren, N., Renfew, S. E., and Barton, J. K. (2011) DNA charge transport over 34 nm. *Nat. Chem. 3*, 228-233.

12. 9. Núñez, M. E., Hall, D. B., and Barton, J. K. (1999) Long-range oxidative damage to DNA: Effects of distance and sequence. *Chem. Biol. 6*, 85-97.

13. Milligan, J. R., Tran, N. Q., Ly, A., and Ward, J. F. (2004) Peptide repair of oxidative DNA damage. *Biochemistry 43*, 5102-5108.

14. Steenken, S., Jovanovic, S. V., Bietti, M., and Bernhard, K. (2000) The Trap Depth (in DNA) of 8-Oxo-7,8-dihydro-2´deoxyguanosine as Derived from Electron-Transfer Equilibria in Aqueous Solution. *J. Am. Chem. Soc. 122*, 2373-2374.

15. Milligan, J. R., Aguilera, J. A., Nguyen, J. V., and Ward, J. F. (2001) Redox reactivity of guanyl radicals in plasmid DNA. *Int. J. Radiat. Biol.* 77, 281-293.

16. Steenken, S. and Jovanovic, S. V. (1997) How easily oxidizable is DNA? One electron reduction potentials of adenosine and guanosine radicals in aqueous solution. *J. Am. Chem. Soc. 119*, 617-618.

17. Sugiyama, H., and Saito, I. (1996) Theoretical studies of GG specific photocleavage of DNA via electron transfer: Significant lowering of ionization potential and 5′-localization of HOMO of stacked GG bases in B-form DNA. *J. Am. Chem. Soc. 118*, 7063-7068.

18. Gorodetsky, A. A., and Barton, J. K. (2007) DNA-mediated electrochemistry of disulfides on graphite. *J. Am. Chem. Soc. 129*, 6074-6075.

19. Takada, T., and Barton, J. K. (2005) DNA charge transport leading to disulfide bond formation. *J. Am. Chem. Soc. 127*, 12204-12205.

20. Cho, Y., Gorina, S., Jeffrey, P. D., and Pavletich, N. P. (1994) Crystal-structure of a p53 tumor-suppressor DNA complex: Understanding tumorigenic mutations. *Science 265*, 346-354.

21. Chen, Y., Dey, R., and Chen, L. Crystal structure of the p53 core domain bound to a full consensus site as a self-assembled tetramer. (2010) *Structure 18*, 246-256.

22. Chen, Y., Zhang, X., Dantas Machado, A. C., Ding, Y., Chen, Z., Qin, P. Z., Rohs, R., and Chen, L. (2013) Structure of p53 binding to the BAX response element reveals DNA unwinding and compression to accommodate base-pair insertion. *Nucleic Acids Research*, *41*, 8368-8376.

23. Parks, D., Bolinger, R., and Mann, K. (1997) Redox state regulates binding of p53 to sequence-specific DNA, but not to non-specific or mismatched DNA. *Nucleic Acids Research 25*, 1289-1295.

24. Kaar, J. L., Basse, N., Joerger, A. C., Stephens, E., Rutherford, T. J., and Fersht, A.R. (2010) Stabilization of mutant p53 via alkylation of cysteines and effects on DNA binding. *Prot. Sci. 19*, 2267-2278.

25. Scotcher, J., Clarke, D. J., Weidt, S. K., Mackay, C. L., Hupp, T. R., Sadler, P. J., and Langridge-Smith, P. R. (2011) Identification of two reactive cysteine residues in the tumor suppressor protein p53 using top-down FT ICR mass spectrometry. *J. Am. Soc. Mass Spectrom. 22*, 888-897.

26. Scotcher, J., Clarke, D. J., Mackay, C. L., Hupp, T., Sadler, P. J., and Langridge-Smith, P. R. (2013)) Redox regulation of tumour suppressor protein p53: identification of the sites of hydrogen peroxide oxidation and glutathionylation. *Chemical Science 4*, 1257-1269.

27. Armitage, B., Yu, C., Devadoss, C., and Schuster, G. B. (1994) Cationic anthraquinone derivatives as catalytic DNA photonucleases: Mechanisms for DNA-damage and quinone recycling. *J. Am. Chem.Soc. 116*, 9847-9859.

28. Gasper, S. M. and Schuster, G. B. (1997) Intramolecular photoinduced electron transfer to anthraquinones linked to duplex DNA: The effect of gaps and traps on long-range radical cation migration. *J. Am. Chem. Soc. 119*, 12762-12771.

29. Nikolova, P. V., Henckel, J., Lane, D. P., and Fersht, A. R. (1998) Semirational design of active tumor suppressor p53 DNA binding domain with enhanced stability. *Proc. Natl. Acad. Sci. USA 95*, 14675-14680.

30. Veprintsev, D. B., Freund, S. M., Andreeva, A., Rutledge, S. E., Tidow, H., Cañadillas, J. M., Blair, C. M., and Fersht, A. R. (2006) Core domain interactions in full-length p53 in solution *Proc. Natl. Acad. Sci. USA 103*, 2115-2119.

31. Graham, R. L. J., Kalli, A., Smith, G. T., Sweredoski, M. J., Hess, S. (2011) Avoiding pitfalls in proteomics sample preparation. *Biomacromol. Mass Spectrom. 2*, 273-284.

32. MacLean, B., Tomazela, D. M., Shulman, N., Chambers, M., Finney, G. L., Frewen, B., Kern, R., Tabb, D. L., Liebler, D. C., and MacCoss, M. J. (2010) Skyline: an open source document editor for creating and analyzing targeted proteomics experiments. *Bioinformatics 26*, 966-968.

33. Rebischung, C., Gerard, J. P., Gayet J., Thomas, G., Hamelin, R., and Laurent-Puig, P. (2002) Prognostic value of P53 mutations in rectal carcinoma. *Int. J. Cancer 100*, 131-135.

34. Webley, K. M., Shorthouse, A. J., and Royds, J. A. (2000) Effect of mutation and conformation on the function of p53 in colorectal cancer. *J. Pathol. 191*, 361-367.

35. Gao, H. G., Chen, J. K., Stewart, J., Song, B., Rayappa, C., Whong, W. Z., and Ong, T. (1997) Distribution of p53 and K-ras mutations in human lung cancer tissues. *Carcinogenesis 18*, 473-478.

36. Arkin, M. R., Stemp, E. D. A., Pulver, S. C., and Barton, J. K. (1997) Long-range oxidation of guanine by Ru(III) in duplex DNA. *Chemistry & Biology 4*, 389-400.

37. Gilbert, H.F. (1995) Thiol/disulfide exchange equilibria and disulfide bond stability. *Methods in Enzymology 215*, 8-28.

38. Kadokura, H., Katzen, F., and Beckwith J. (2003) Protein disulfide bond formation in prokaryotes. *Annu. Rev. Biochem. 72*, 111-135.

Appendix 4.1: Primer sequences for site directed mutagenesis of the p53′ plasmid.

Mutation	Direction	Primer Sequence (5′ to 3′)
N239Y	Original plasmid of stabilized p53 quadruple mutant from Fersht Lab containing M133L, V203A, N268D, and N239Y.[1]	
Reversion on the N239Y mutation was used to create the p53′ plasmid		
Y239N	Forward	CCA CTA CAA CTA CAT GTG TAA CAG TTC CTG CAT GG
	Reverse	CCA TGC AGG AAC TGT TAC ACA TGT AGT TGT AGT GG
C124S	Forward	GTC TGT GAC TTC CAC GTA CTC CCC
	Reverse	GGG GAG TAC GTG GAA GT CACA GAC
C135S	Forward	CAA GCT GTT TAG CCA ACT GGC C
	Reverse	GGC CAG TTG GCT AAA CAG CTT G
C141S	Forward	CCA ACT GGC CAA GAC CTC CCC TGT GC
	Reverse	CAG CTG CAC AGG GGA GGT CTT GGC C
C182S	Forward	GGC GCT GCC CCC ACC ATG AGC GCA GC
	Reverse	GGA GGG GCC AGA CCA TCG CTA TCT GA
Y236F	Forward	CCA TCC ACT ACA ACT TCA TGT GTA AC
	Reverse	CTG TTA CACA TG AAG TTG TAG TGG AT
C275S	Forward	GTG CGT GTT AGT GCC TGT CCT
	Reverse	AGG ACA GGC ACT AAC ACG CAC
C277S	Forward	GTG CGT GTT TGT GCC AGT CCT GGG
	Reverse	CCC AGG ACT GGC ACA AAC ACG CAG

1. Nikolova, P. V., Henckel, J., Lane, D. P., and Fersht, A. R. (1998) Semirational design of active tumor suppressor p53 DNA binding domain with enhanced stability. *Proc. Natl. Acad. Sci. USA 95*, 14675−14680.

Appendix 4.2: QTRAP 6500 LC-MS/MS Peptide Transitions.

Peptide	Q1 (amu)	Q3 (amu)	Dwell Time (msec)	Declustering Potential (V)	Collision energy (V)
C141S.TSPVQLWVDSTPPPGTR.+2y10.light	919.475782	1026.52145	20	98.1	42
C141S.TSPVQLWVDSTPPPGTR.+2y9.light	919.475782	927.453036	20	98.1	42
C141S.TSPVQLWVDSTPPPGTR.+2y8.light	919.475782	812.426093	20	98.1	42
C141S.TSPVQLWVDSTPPPGTR.+2y6.light	919.475782	624.346386	20	98.1	42
p53_3X.TC[CAM]PVQLWVDSTPPPGTR.+2y11.light	955.975092	1212.600763	20	100.8	43.3
p53_3X.TC[CAM]PVQLWVDSTPPPGTR.+2y10.light	955.975092	1026.52145	20	100.8	43.3
p53_3X.TC[CAM]PVQLWVDSTPPPGTR.+2y8.light	955.975092	812.426093	20	100.8	43.3
p53_3X.TC[CAM]PVQLWVDSTPPPGTR.+2y6.light	955.975092	624.346386	20	100.8	43.3
p53_3X.TC[CAM]PVQLWVDSTPPPGTR.+2y11.heavy	957.984724	1212.600763	20	100.8	43.3
p53_3X.TC[CAM]PVQLWVDSTPPPGTR.+2y10.heavy	957.984724	1026.52145	20	100.8	43.3
p53_3X.TC[CAM]PVQLWVDSTPPPGTR.+2y8.heavy	957.984724	812.426093	20	100.8	43.3
p53_3X.TC[CAM]PVQLWVDSTPPPGTR.+2y6.heavy	957.984724	624.346386	20	100.8	43.3
p53_3X.TC[CAM]PVQLWVDSTPPPGTR.+2y11.light	927.46436	1212.600763	20	98.7	42.2
p53_3X.TC[CAM]PVQLWVDSTPPPGTR.+2y10.light	927.46436	1026.52145	20	98.7	42.2
p53_3X.TC[CAM]PVQLWVDSTPPPGTR.+2y8.light	927.46436	812.426093	20	98.7	42.2
p53_3X.TC[CAM]PVQLWVDSTPPPGTR.+2y6.light	927.46436	624.346386	20	98.7	42.2
p53_3X.VC[CAM]AC[CAM]PGR.+2y6.light	410.18364	720.29159	20	61	23.6
p53_3X.VC[CAM]AC[CAM]PGR.+2y5.light	410.18364	560.260942	20	61	23.6
p53_3X.VC[CAM]AC[CAM]PGR.+2y4.light	410.18364	489.223828	20	61	23.6
p53_3X.VC[CAM]AC[CAM]PGR.+2y3.light	410.18364	329.193179	20	61	23.6
p53_3X.VC[CAM]AC[CAM]PGR.+2y6.heavy	414.202903	728.330116	20	61	23.6
p53_3X.VC[CAM]AC[CAM]PGR.+2y5.heavy	414.202903	564.280205	20	61	23.6
p53_3X.VC[CAM]AC[CAM]PGR.+2y4.heavy	414.202903	493.243091	20	61	23.6
p53_3X.VC[CAM]AC[CAM]PGR.+2y3.heavy	414.202903	329.193179	20	61	23.6
p53_3X.VC[CAM]AC[CAM]PGR.+2y6.light	353.162176	606.248662	20	56.9	21.6
p53_3X.VC[CAM]AC[CAM]PGR.+2y5.light	353.162176	503.239478	20	56.9	21.6
p53_3X.VC[CAM]AC[CAM]PGR.+2y4.light	353.162176	432.202364	20	56.9	21.6
p53_3X.VC[CAM]AC[CAM]PGR.+2y3.light	353.162176	329.193179	20	56.9	21.6
p53_3X.VC[CAM]AC[CAM]PGR.+2y6.light	412.193272	724.310853	20	61.2	23.7
p53_3X.VC[CAM]AC[CAM]PGR.+2y5.light	412.193272	560.260942	20	61.2	23.7
p53_3X.VC[CAM]AC[CAM]PGR.+2y4.light	412.193272	489.223828	20	61.2	23.7
p53_3X.VC[CAM]AC[CAM]PGR.+2y3.light	412.193272	329.193179	20	61.2	23.7
p53_3X.VC[CAM]AC[CAM]PGR.+2y5.light	412.193272	564.280205	20	61.2	23.7
p53_3X.VC[CAM]AC[CAM]PGR.+2y4.light	412.193272	493.243091	20	61.2	23.7
p53_3X.VC[CAM]AC[CAM]PGR.+2y6.light	414.202903	728.330116	20	61.3	23.8
p53_3X.VC[CAM]AC[CAM]PGR.+2y5.light	414.202903	564.280205	20	61.3	23.8
p53_3X.VC[CAM]AC[CAM]PGR.+2y4.light	414.202903	493.243091	20	61.3	23.8
p53_3X.VC[CAM]AC[CAM]PGR.+2y3.light	414.202903	329.193179	20	61.3	23.8
C275S.VSAC[CAM]PGR.+2y6.light	373.68433	647.29297	20	58.4	22.3
C275S.VSAC[CAM]PGR.+2y5.light	373.68433	560.260942	20	58.4	22.3

C275S.VSAC[CAM]PGR.+2y4.light	373.68433	489.223828	20	58.4	22.3
C275S.VSAC[CAM]PGR.+2y3.light	373.68433	329.193179	20	58.4	22.3
C275S.VSAC[CAM]PGR.+2y6.heavy	375.693962	651.312233	20	58.4	22.3
C275S.VSAC[CAM]PGR.+2y5.heavy	375.693962	564.280205	20	58.4	22.3
C275S.VSAC[CAM]PGR.+2y4.heavy	375.693962	493.243091	20	58.4	22.3
C275S.VSAC[CAM]PGR.+2y3.heavy	375.693962	329.193179	20	58.4	22.3
C275S.VSAC[CAM]PGR.+2y6.light	345.173598	590.271506	20	56.3	21.3
C275S.VSAC[CAM]PGR.+2y5.light	345.173598	503.239478	20	56.3	21.3
C275S.VSAC[CAM]PGR.+2y4.light	345.173598	432.202364	20	56.3	21.3
C275S.VSAC[CAM]PGR.+2y3.light	345.173598	329.193179	20	56.3	21.3
iRT.LGGNETQVR.+2y8.light	487.256705	860.42207	20	66.6	26.4
iRT.LGGNETQVR.+2y4.light	487.256705	503.293622	20	66.6	26.4
iRT.AGGSSEPVTGLADK.+2y8.light	644.822606	800.451245	20	78.1	32.1
iRT.AGGSSEPVTGLADK.+2y6.light	644.822606	604.330067	20	78.1	32.1
iRT.VEATFGVDESANK.+2b8.light	683.827888	819.38831	20	81	33.5
iRT.VEATFGVDESANK.+2y9.light	683.827888	966.452701	20	81	33.5
iRT.YILAGVESNK.+2y8.light	547.298038	817.441408	20	71	28.6
iRT.YILAGVESNK.+2y6.light	547.298038	633.32023	20	71	28.6
iRT.TPVISGGPYYER.+2y9.light	669.838059	1041.499986	20	79.9	33
iRT.TPVISGGPYYER.+2y8.light	669.838059	928.415922	20	79.9	33
iRT.TPVITGAPYYER.+2y8.light	683.853709	956.447222	20	81	33.5
iRT.TPVITGAPYYER.+2y7.light	683.853709	855.399543	20	81	33.5
iRT.GDLDAASYYAPVR.+2y8.light	699.338423	926.473043	20	82.1	34
iRT.GDLDAASYYAPVR.+2y7.light	699.338423	855.435929	20	82.1	34
iRT.DAVTPADFSEWSK.+2y9.light	726.835713	1066.484001	20	84.1	35
iRT.DAVTPADFSEWSK.+2y9+2.light	726.835713	533.745639	20	84.1	35
iRT.TGFIIDPGGVIR.+2y7.light	622.853512	713.394064	20	76.5	31.3
iRT.TGFIIDPGGVIR.+2y6.light	622.853512	598.367121	20	76.5	31.3
iRT.GTFIIDPAAIVR.+2y8.light	636.869162	854.509428	20	77.5	31.8
iRT.GTFIIDPAAIVR.+2y6.light	636.869162	626.398421	20	77.5	31.8
iRT.FLLQFGAQGSPLFK.+2y10.light	776.929751	1051.557107	20	87.8	36.8
iRT.FLLQFGAQGSPLFK.+2y9.light	776.929751	904.488693	20	87.8	36.8
p53.ELNEALELK.+2y7.light	529.790046	816.446159	20	69.7	27.9
p53.ELNEALELK.+2y6.light	529.790046	702.403232	20	69.7	27.9
p53.ELNEALELK.+2y5.light	529.790046	573.360639	20	69.7	27.9
p53.ELNEALELK.+2y4.light	529.790046	502.323525	20	69.7	27.9
p53.SVTC[CAM]TYSPALNK.+2y8.light	670.829377	893.472708	20	80	33
p53.SVTC[CAM]TYSPALNK.+2y7.light	670.829377	792.42503	20	80	33
p53.SVTC[CAM]TYSPALNK.+2y6.light	670.829377	629.361701	20	80	33
p53.SVTC[CAM]TYSPALNK.+2y5.light	670.829377	542.329673	20	80	33
p53.SVTC[CAM]TYSPALNK.+2y8.heavy	672.839008	893.472708	20	80	33
p53.SVTC[CAM]TYSPALNK.+2y7.heavy	672.839008	792.42503	20	80	33
p53.SVTC[CAM]TYSPALNK.+2y6.heavy	672.839008	629.361701	20	80	33
p53.SVTC[CAM]TYSPALNK.+2y5.heavy	672.839008	542.329673	20	80	33

p53.SVTC[CAM]TYSPALNK.+2y8.light	642.318645	893.472708	20	77.9	32
p53.SVTC[CAM]TYSPALNK.+2y7.light	642.318645	792.42503	20	77.9	32
p53.SVTC[CAM]TYSPALNK.+2y6.light	642.318645	629.361701	20	77.9	32
p53.SVTC[CAM]TYSPALNK.+2y5.light	642.318645	542.329673	20	77.9	32
p53.LFC[CAM]QLAK.+2y6.light	440.241481	766.391622	20	63.2	24.7
p53.LFC[CAM]QLAK.+2y5.light	440.241481	619.323208	20	63.2	24.7
p53.LFC[CAM]QLAK.+2y3.light	440.241481	331.233982	20	63.2	24.7
p53.LFC[CAM]QLAK.+2y6+2.light	440.241481	383.699449	20	63.2	24.7
p53.LFC[CAM]QLAK.+2y6.heavy	442.251112	770.410885	20	63.2	24.7
p53.LFC[CAM]QLAK.+2y5.heavy	442.251112	623.342471	20	63.2	24.7
p53.LFC[CAM]QLAK.+2y3.heavy	442.251112	331.233982	20	63.2	24.7
p53.LFC[CAM]QLAK.+2y6+2.heavy	442.251112	385.70908	20	63.2	24.7
p53.LFC[CAM]QLAK.+2y6.light	411.730749	709.370158	20	61.1	23.7
p53.LFC[CAM]QLAK.+2y5.light	411.730749	562.301744	20	61.1	23.7
p53.LFC[CAM]QLAK.+2y3.light	411.730749	331.233982	20	61.1	23.7
p53.LFC[CAM]QLAK.+2y6+2.light	411.730749	355.188717	20	61.1	23.7
p53.C[CAM]SDSDGLAPPQHLIR.+3y7.light	555.938627	860.510097	20	71.6	27.8
p53.C[CAM]SDSDGLAPPQHLIR.+3y6.light	555.938627	763.457333	20	71.6	27.8
p53.C[CAM]SDSDGLAPPQHLIR.+3y8+2.light	555.938627	466.277243	20	71.6	27.8
p53.C[CAM]SDSDGLAPPQHLIR.+3y7+2.light	555.938627	430.758686	20	71.6	27.8
p53.C[CAM]SDSDGLAPPQHLIR.+3y7.heavy	557.278382	860.510097	20	71.6	27.8
p53.C[CAM]SDSDGLAPPQHLIR.+3y6.heavy	557.278382	763.457333	20	71.6	27.8
p53.C[CAM]SDSDGLAPPQHLIR.+3y8+2.heavy	557.278382	466.277243	20	71.6	27.8
p53.C[CAM]SDSDGLAPPQHLIR.+3y7+2.heavy	557.278382	430.758686	20	71.6	27.8
p53.C[CAM]SDSDGLAPPQHLIR.+3y7.light	536.931473	860.510097	20	70.3	26.8
p53.C[CAM]SDSDGLAPPQHLIR.+3y6.light	536.931473	763.457333	20	70.3	26.8
p53.C[CAM]SDSDGLAPPQHLIR.+3y8+2.light	536.931473	466.277243	20	70.3	26.8
p53.C[CAM]SDSDGLAPPQHLIR.+3y7+2.light	536.931473	430.758686	20	70.3	26.8